Strain-specific profiling of Amyloid-β in Alzheimer´s disease: functional and clinical signature

Dissertation
for the award of the degree
'Doctor rerum naturalium'
of the Georg-August-Universität, Göttingen within the doctoral program "Molecular Medicine"
of the Georg-August University School of Science (GAUSS)

Submitted by
ANEEQA NOOR
from Bahawalpur, Pakistan

Göttingen, 2020

THESIS COMMITTEE

Spervisor: Dr. rer. nat. Saima Zafar

Prion research group, Department of Neurology, University Medical Center, Göttingen.

First member of Thesis Committee: Prof. Dr. mult. Thomas Meyer

Department of Psychosomatic Medicine and Psychotherapy, University Medical Center, Göttingen.

Second member of Thesis Committee: Prof. Dr. Tiago Fleming Outeiro

Department of Neurodegeneration and Restorative Research, University Medical Center, Göttingen.

Third member of Thesis Committee: Prof. Dr. Inga Zerr

Department of Neurology, University Medical Center, Göttingen.

Further members of the Examination Board

Prof. Dr. Carolin Wichmann

Institute for Auditory Neuroscience & InnerEarLab, University Medical Center, Göttingen.

Prof. Dr. med. Christine Stadelmann-Nessler

Institute for Neuropathology, University Medical Center, Göttingen.

Dr. Dieter Klopfenstein

Third Institute of Physics, Department of Biophysics, Georg August University, Göttingen.

PD Dr. Michael Hoppert

Department of General Microbiology, Georg August University, Göttingen.

Date of the oral examination: 25th May 2020.

This project was funded by the Physics-to-Medicine Initiative Göttingen (LM der Niedersächsischen Vorab).

DECLARATION

I hereby declare that the PhD thesis entitled "Strain-specific profiling of Amyloid-β in Alzheimer´s disease: functional and clinical signature" is exclusively my own work and does not contain any published materials other than the ones quoted with references.

Aneeqa Noor

Göttingen, February 2020.

Dedicated to

My Grandparents

Table of Contents

Abbreviations:

1D-PAGE	One-dimensional polyacrylamide gel electrophoresis
2D-PAGE	Two-dimensional polyacrylamide gel electrophoresis
Å	Ångstrom
ADAM-10	A disintegrin and metalloprotease domain-containing protein 10
AD	Alzheimer's Disease
AFM	Atomic force microscopy
AICD	APP intracellular domain
AMPA	α-Amino-3-hydroxyl-5-methyl-4-isoxazole-propionate
APP	Amyloid precursor protein
AUC	Area under the curve
Aβ	Amyloid beta
BACE-1	β-site APP cleaving enzyme-1
CHAPS	3-[(3-Cholamidopropyl)-dimethylammonio]-1-propane sulfonate
CSF	Cerebrospinal fluid
DHB	Dihydroxybenzoic acid
DLB	Dementia with Lewy bodies
DMEM	Dulbecco's modified Eagle's medium
DTT	Dithiothreitol
ECE	Endothelial converting enzyme
ECL	Enhanced chemiluminescence
EDTA	Ethylenediaminetetraacetic acid
ELISA	Enzyme-linked immunosorbent assay
EOAD	Early onset Alzheimer's disease
ER	Endoplasmic reticulum
FA	Formic acid
fAD	Familial/autosomal dominant Alzheimer's disease
FBS	Fetal bovine serum
FTD	Frontotemporal dementia
GSS	Gerstmann-Sträussler syndrome
HCCA	α-Cyano-4-hydroxycinnamic acid
hr	Hours
HRP	Horseradish peroxidase
Hz	Hertz
IB	Immunoblot
IDE	Insulin-degrading enzyme
IEF	Isoelectric focusing
IP	Immunoprecipitation
kDa	Kilodaltons
LOAD	Late onset Alzheimer's disease
MALDI	Matrix-assisted laser desorption/ionization

MALDI-ToF MS	MALDI-Time of flight mass spectrometry
min	Minutes
MMPs	Matrix metalloproteases
MMSE	Mini-Mental State Examination
Nep	Neprilysin
NFTs	Neurofibrillary tangles
NMDA	N-methyl-d-aspartate
PBS	Phosphate-buffered saline
PD	Parkinson's disease
pI	Isoelectric pH
PrP^{C}	Cellular prion protein
PrP^{Sc}	Scrapie isoform of the cellular prion protein
PS	penicillin/streptomycin
PSEN-1	Presenilin-1
PSEN-2	Presenilin-2
p-tau	Phospho-tau
PVDF	Polyvinylidene fluoride
RAGE	Receptor for advanced glycation end products
ROS	Reactive oxidative species
rpAD	Rapidly progressive AD
rpm	Rotations per minute
RT-QuIC	Real-time quaking induced conversion
SA	Sinapinic acid
sAD	Sporadic Alzheimer's disease
sAPPα	Secreted APP alpha
sAPPβ	Secreted APP beta
sCJD	Sporadic Creutzfeldt–Jakob disease
SDS	Sodium dodecyl sulphate
SEM	Standard error of mean
S/N	Signal-to-noise ratio
TEMED	Tetramethylethylenediamine
TFA	Trifluoroacetic acid
Th-T	Thioflavin-T
w/v	Weight/volume

Abstract

The molecular culprits driving the atypical clinical variants of Alzheimer's disease (AD), including the recently discovered rapidly progressive AD (rpAD), are unknown to date. Of the several mechanisms being studied in this regard, the fibrillization of the amyloid-β (Aβ) peptide is most frequently targeted. The Aβ peptide can exist as multiple proteoforms that vary with respect to their sequences, post-translational modifications, capabilities to generate amyloids and mechanisms of toxicity. The current study was designed to target these variations in AD patients exhibiting classical and rapid progression, with the primary aim of establishing if these variants can constitute strains that underlie the phenotypic variability of AD.

The differences in sequences of pathophysiological proteoforms among sporadic AD (sAD), rpAD and non-demented controls were established using hybrid-immunoprecipitation followed by 2D gel electrophoresis and top-down MALDI mass spectrometry. A total of 33 Aβ proteoforms were identified. $A\beta_{40}$, $A\beta_{42}$, $A\beta_{4\text{-}42}$, $A\beta_{11\text{-}42}$ and pyroglutamate $A\beta_{11\text{-}42}$ were common in all AD cases however, several shorter N and C-terminally truncated proteoforms showed subtype-specific involvement. sAD showed a greater variety among monomeric species of proteoforms in comparison to rpAD. Although no significant differences were evident in the quantities of various Aβ-cleaving enzymes that were analyzed to explain the variations in the signature of proteoforms, the ratio of β-secretase/α-secretase was significantly higher in rpAD in comparison to sAD indicating higher cleavage of Aβ via the amyloidogenic pathway.

The aggregation of common sAD and rpAD-derived proteoforms and variations in the generated fibrils were assessed through a combination of RT-QuIC, Infrared spectroscopy and Atomic force microscopy. Although spectroscopy showed that the secondary structure of Aβ fibrils from both subtypes of AD was highly similar, the conversion of monomeric species to β-sheet rich fibrils was faster in sAD cases in comparison to rpAD. The latter group presented significantly larger aggregates highlighting the presence of more hydrophobic, albeit decelerated, Aβ seeds. Applications of these fibrils to neuronal cells resulted in no significant differences in the survival, implicating that Aβ from sAD and rpAD were equally toxic. Co-IP experiments, on the other hand, validated differences in Aβ-modulated toxic pathways in sAD and rpAD. Aβ proteoforms from

the former group mainly affected transcription and metabolism while Aβ proteoforms isolated from rpAD primarily modulated neurogenesis and neurotransmission.

This study gives a comprehensive insight into the constituents of Aβ proteome, their relative quantities and their generation in sAD and rpAD brains and, for the first time, establishes differences in aggregation kinetics and 3D morphologies of fibrils associated with distinct clinical variants of AD. Further validation of reported targets and mechanisms will aid in establishing potential points of intervention in the diagnosis and therapy of AD.

1. Introduction

1.1 The Amyloid-beta peptide

The Aβ peptide is one of the thirty amyloidogenic proteins that are known to cause diseases in humans (Knowles et al., 2014). It has been conventionally defined as a 42-residue peptide that is produced through the cleavage of amyloid precursor protein (APP). Since its first characterization in the 1980s, the genetic, transcriptomic and translational aberrations in APP and its subsequent products, especially Aβ, have been an active target of research (Glenner and Wong, 1984; Kang et al., 1987).

1.1.1 Pathophysiological generation of Aβ

APP undergoes a series of cleavage steps to attain its final conformation, generating several shorter functional peptides along the way that are believed to play a role in cell growth and differentiation (Clarris et al., 1995). After translation and post-translational processing, APP is trafficked to the plasma membrane where a combination of three proteases, the α, β and γ-secretases, modulates its processing. Two major routes can be employed for APP processing namely, the amyloidogenic and non-amyloidogenic pathway (Haass et al., 2012).

Under physiological conditions, most of the APP (~90%) is cleaved via the non-amyloidogenic pathway. It is initiated by cleavage of APP between residues 687 and 688 by α-secretase. Although several enzymes possess α-secretase activity, a disintegrin and metalloprotease domain-containing protein 10 (ADAM-10) is most active in the neurons (Kuhn et al., 2010). This cleavage step occurs within the Aβ domain of APP, thereby preventing the formation of Aβ. At this step, secreted APP alpha (sAPPα) is liberated from the membrane. The remaining 83-residue membrane-bound C-terminal fragment, C83, undergoes another cleavage via γ-secretase that results in the formation of p3 and APP intracellular domain (AICD). A complex containing presenilin-1 (PSEN-1), presenilin-2 (PSEN-2), nicastrin, anterior pharynx-defective-1 and presenilin enhancer-2 constitutes the γ-secretase. It has various cleavage sites, including residues 711 and 713 of APP, therefore the exact sizes of p3 and AICD fragments vary. sAPPα and AICD are known to function in neuronal survival and cell signaling, respectively, however, the function of p3 is not fully understood (Chow et al., 2010).

The cleavage of APP via the amyloidogenic pathway occurs more commonly in neurons in comparison to other tissues because of higher amounts of β-site APP cleaving enzyme-1 (BACE-1), the major β-secretase, in neuronal tissue. In this pathway, APP is initially cleaved between residues 671 and 672, releasing secreted APP beta (sAPPβ) and leaving the Aβ domain intact. C99, the remaining membrane-bound C-terminal fragment, is further cleaved by γ-secretase releasing Aβ and AICD in the cytosol and extracellular environment. sAPPβ plays a role in cell signaling and differentiation (Chow et al., 2010). Since only a small percentage of total APP reaches the cell membrane, there are several sites within the endosomal pathway and trans-Golgi network where the remnant APP is processed. The majority of Aβ is therefore generated intracellularly mainly in endoplasmic reticulum (ER), the Golgi apparatus and endosomes where β-secretase and γ-secretase are abundantly present (Haass et al., 2012; Zhang and Song, 2013). The pathways involved in the processing of membrane-bound and intracellular APP and the subsequent generation of Aβ are summarized in Figure 1.

Under physiological conditions, Aβ acts as an antimicrobial agent and has also been reported to attack oncoviruses and prevent tumors. Additionally, it repairs blood-brain barrier and neuronal tissues, thereby aiding in recovery from brain injury. There is also evidence for its role in synaptic function and memory consolidation (Brothers et al., 2018). In these cases, the balance between amyloidogenic and non-amyloidogenic pathway is strictly maintained and any excess Aβ is degraded by insulin-degrading enzyme (IDE), neprilysin (Nep), plasmin, matrix metalloproteases (MMPs) and endothelial-converting enzyme (ECE) on the plasma membrane or within lysosomes and proteasomes. The shorter fragments generated by these proteases are secreted into the cerebrospinal fluid (CSF) and lymph (Baranello et al., 2015). Other than neuronal tissue, Aβ is also produced in skin, muscles and intestines, but its known toxicity is limited to the brain tissue only (Joachim et al., 1989; Citron et al., 1994).

Like many other proteins in nature, Aβ also exists as several proteoforms. Proteoforms are defined as protein products of the same gene that differ with respect to cleavage and other post-translational modifications. For several years, the definition of Aβ covered only two major proteoforms, $A\beta_{40}$ and $A\beta_{42}$. They correspond to cleavage of C99 at either residue 711 or 713 by γ-secretase and have been targeted vigorously to understand their relative aggregation propensities and neurotoxicity.

However, with the advancement in protein extraction and top-down mass spectrometric approaches, many shorter and post-translationally modified proteoforms have been detected in Aβ-associated neurodegenerative pathologies (Wildburger et al., 2017). In addition to γ-secretase, other enzymes including α-secretase, β-secretase, IDE, ECE and Nep can cleave Aβ at multiple sites (Eckman and Eckman, 2005). Additionally, several residues within this peptide can act as hotspots for post-translational modifications, thereby aiding the diversity of its proteoforms (Kummer and Heneka, 2014). The generation of fibrils by various components of the Aβ-ome and their pathological relevance are an active target of research in the present decade.

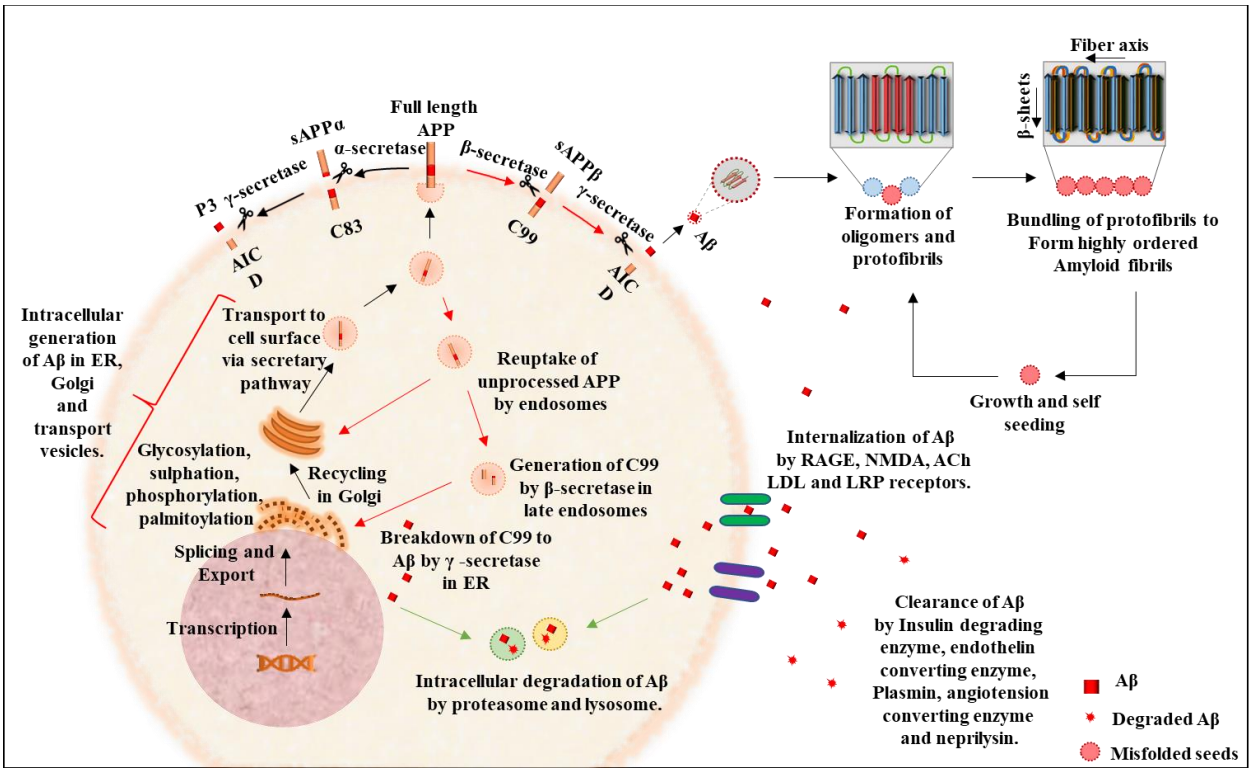

Figure 1: Processing of APP and generation of Aβ. The figure presents a summary of APP processing via non-amyloidogenic (black arrows) and amyloidogenic (red arrows) pathways within the plasma membrane and the subsequent fibrillization of generated Aβ. Aβ is also generated in ER, Golgi bodies and transport vesicles following the reuptake of APP (red arrows). Under physiological conditions, most Aβ is degraded in proteasome and lysosome intracellularly (green arrows) and by various proteases on the cell surface before being removed via CSF and lymph.

1.1.2 Aβ amyloid formation

The amyloid fibrils are a product of a cascade of events initiated at the formation of altered monomeric species due to mutations, aberrant cleavage or environmental factors that lead to cellular stress. In the case of Aβ, its increased production due to mutations in APP, dysfunctional Aβ-

processing enzymes or inefficient clearance contributes towards this cascade. Aβ is an intrinsically disordered peptide and under physiological conditions, α-helical domains dominate its secondary structure. However, under circumstances that are still not understood, deprotonation of resident amino acids collapses the native structure by breaking the backbone of the helix and prompting interactions between side chains (Ito et al., 2011). The peptide then refolds into a compact β-sheet rich secondary structure that is stabilized by the presence of electrostatic interactions.

The conversion of native helical structure to a thermodynamically favorable β-sheet-rich conformation is also known as 'monomer activation'. These misfolded units can self-replicate by interacting with physiological Aβ peptides and altering their conformation. The combination of these altered structures, or primary nucleation, leads to the formation of an aggregate that can seed the formation of amyloid fibrils (Gillam and MacPhee, 2013). These seeds undergo a repetitive cycle that involves the assembly of multiple toxic oligomeric species leading to the formation of various multimers, protofibrils (2.5 to 3 nm in diameter), and fibrils (a combination of two strands with a diameter of 6 to 10 nm; Khurana et al., 2003). The primary event of nucleation and fibril formation is relatively slow and is referred to as the lag phase of growth. The intertwining of protofibrils and fibrils leads to the formation of mature fibrils that are 60-120 nm in diameter (Figure 2; Serpell, 2000). X-ray diffraction and nuclear magnetic resonance analysis showed spacing of approximately 10 Å between the layers of beta-sheets and approximately 4.7 Å between multiple β-strands depicting a uniform and stable assembly (Gillam and MacPhee, 2013). The addition of monomers to fibrils changes their conformation so that it matches with the residues present in the aggregates leading to the growth of amyloid fibrils, a step referred to as 'secondary nucleation' (Scheidt et al., 2019). At this point, the growth of amyloid fibrils reaches an exponential phase causing rapid accumulation of aggregates.

In contrast to its native counterpart, this β-sheet structure is highly hydrophobic. Consequently, the functions of various domains within this structure also change. The residues 1-13 constitute the metal-binding domain, residues 15 and 21 have the aggregation core while residues 25-35 are required for exerting neurotoxic effects thereby constituting the functional domains. The C-terminal tail is critical for the conversion of native α-helical structure to amyloids (Chen et al., 2017). The smaller oligomeric species can propagate to various parts of the brain via exosome-mediated

neuronal transfer and spread the disease pathology from the primary site of amyloid formation, usually the posterior cortex, to other regions of the brain (Palmqvist et al., 2017; Sinha et al., 2018).

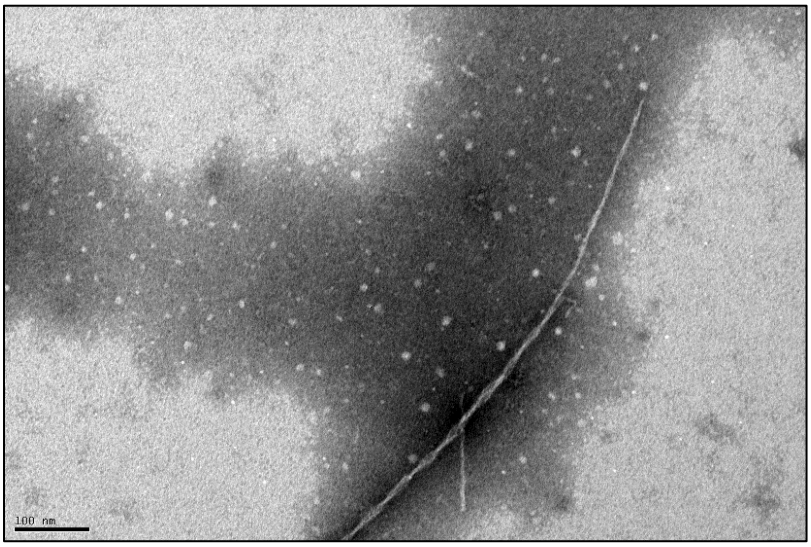

Figure 2: Structure of fibrils generated via *in vitro* aggregation of synthetic $A\beta_{40}$. Protofibrils twist around each other to form thicker ribbon-like fibrils, as observed by negative stain electron microscopy following *in vivo* fibrillization of $A\beta_{40}$ (Zafer et al., submitted). Scale bar represents 100 nm.

Aβ amyloid formation is a dynamic process and there is a room for heterogeneity at various steps. Different proteoforms of Aβ vary with respect to their aggregation propensity and kinetics. Heterogeneity has also been reported in the exact three-dimensional conformation adopted by Aβ fibrils depending on aggregating proteoform and surrounding conditions (Sgourakis et al., 2007). Early X-ray diffraction experiments showed that $A\beta_{19-28}$, $A\beta_{13-28}$, $A\beta_{12-28}$, $A\beta_{11-28}$, $A\beta_{9-28}$, $A\beta_{1-28}$, $A\beta_{1-38}$, $A\beta_{1-40}$, $A\beta_{6-25}$, $A\beta_{11-25}$ and $A\beta_{34-42}$ form fibrillar assemblies with hydrogen bonding in the direction of fiber axis resulting in highly ordered crystalline lattices. $A\beta_{18-28}$, $A\beta_{17-28}$, and $A\beta_{15-28}$, on the other hand, form plate-like assemblies extending in both directions, while peptides $A\beta_{22-35}$ and $A\beta_{26-33}$ have fibrillar assemblies with no preferential direction presenting circular scattering (Inouye et al., 1993). Moreover, although the β-sheet-rich oligomers and amyloids have been targeted for decades with respect to the prevention of neurotoxicity, a recent study suggests that oligomers with non-traditional secondary structures, like α-sheets, are also prone to amyloid formation and cause neurotoxicity (Shea et al., 2019). The direct consequences of this heterogeneity are still not understood, but it may lead to differences in pathology and the resulting disease phenotypes (Rasmussen et al., 2017).

The survival of amyloids and their ability to escape the cell's quality control checkpoints to propagate uncontrollably can be attributed to their structure that is rich in cross-β sheets and creates an opportunity for the continuous formation of hydrogen bonds, imparting stability to the overall structure (Knowles et al., 2014). These structures have been reported to cause around fifty different human diseases that are known by many names (neurodegenerative proteinopathies, protein conformational diseases, prion diseases, aggregopathies and amyloidosis), all explaining the underlying dogma of aggregating proteins. Although amyloids formed by many different proteins follow the same pathways for propagation and form similar structures, the exact mechanisms of toxicity depend on the amyloidogenic protein involved. Several mechanisms have been proposed for Aβ-induced toxicity, as discussed in the following section.

1.1.3 Aβ-associated neurotoxicity

Proteins can exist in various states within the living systems, however their functionality can only be attributed to their specific three-dimensional structures. They have been known to form highly ordered structures containing defined conformations and domains that interact with cofactors and binding partners to bring about the required function. Any alterations in their conformations can have drastic effects on cells and the amyloid structures serve as a perfect example of this phenomenon. The conversion of Aβ from predominantly α-helical secondary structure to fibrils and amyloids changes its pro-survival roles to severely pathological activities.

Aβ can manipulate several pathways that lead to apoptosis and neuronal loss. Several species formed during the amyloidogenesis of Aβ have been tested for relative toxicities. Ever since the discovery of Aβ, it was believed that Aβ fibrils are major species that inflict toxicity, however, mounting evidence suggests that plaque-associated fibrillar Aβ may have a protective role (Davis-Salinas and Van Nostrand, 1995; Wujek et al., 1996). It sequesters the oligomeric and protofibrillar Aβ, species that are now believed to be toxic, and prevents them from inflicting damage to the cells. Conversely, plaques may also act as the reservoir for a constant supply of Aβ, aiding in its neurotoxic effects (Reiss et al., 2018). Although the relative toxicities of various Aβ species are still controversial, the mechanisms involved in Aβ-associated neurotoxicity are now partly understood (Figure 3). Some of the most common mechanisms of Aβ toxicity are discussed as follows.

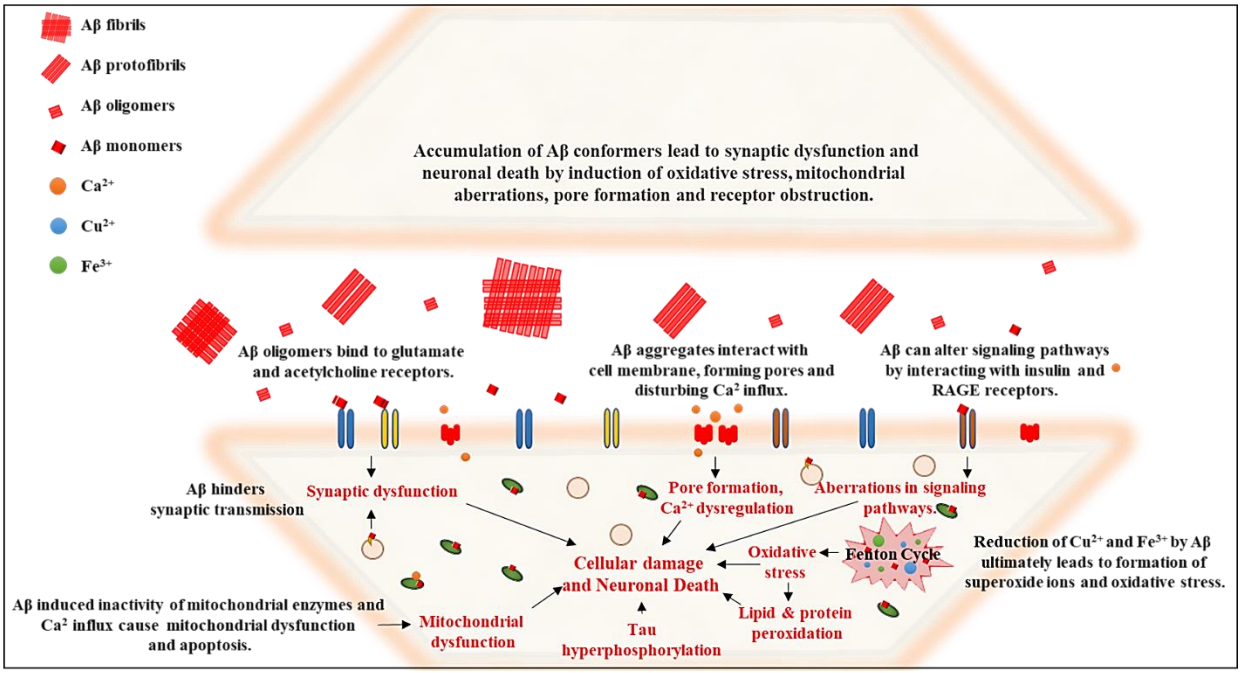

Figure 3: Known neurotoxic effects of various Aβ species. Misfolded Aβ species confer their neurotoxic effects via multiple pathways. Synaptic dysfunction and neuronal death by induction of oxidative stress, mitochondrial aberrations, pore formation and receptor obstruction are some of the most frequently reported mechanisms of Aβ-associated toxicity and have been detailed in this figure.

1.1.3.1 Aberrations in membrane permeability

Aβ can target lipid bilayer by forming channel-like structures that impair the permeability of the plasma membrane (Pollard et al., 1993). Calcium (Ca^{2+}) and potassium (K^{+}) ions can pass through these channels freely (Mattson et al., 1993; Etcheberrigaray et al., 1994). Aberrant ion homeostasis impairs the strictly regulated ion gradient, especially that of Ca^{2+}, within the neurons, triggering pathways that lead to mitochondrial dysfunction, oxidative stress and cell death (Dykens et al., 1994).

1.1.3.2 Oxidative stress

The neuronal tissue houses abundant amounts of copper (Cu), iron (Fe) and zinc (Zn) which function as modulators of protein activity and cell signaling. Under physiological conditions, their concentrations and redox states are tightly regulated (Cheignon et al., 2018). The Aβ peptide, specifically the methionine residue at position 35 within Aβ, possesses the capability to reduce Cu and Fe via Fenton reaction, that react with oxygen in return forming superoxide radicals and hydrogen

peroxide in the process (Yatin et al., 1999; Rival et al., 2009). These radicals oxidize DNA, proteins, lipids and neurotransmitters within the neurons and disrupt various physiological processes (Gabbita et al., 1998; Hardas et al., 2013; Granold et al., 2015).

1.1.3.3 Mitochondrial dysfunction

Mitochondrial dysfunction is abundantly seen in Aβ-associated pathologies. Interaction of Aβ with mitochondria increases the formation of reactive oxidative species (ROS) by Aβ-induced down-regulation of respiratory enzymes and disruption of electron transport chain (Hernandez-Zimbron et al., 2012). Moreover, the mitochondrial membrane potential is disrupted, and mitochondrial fission is promoted in Aβ-treated cells (Han et al., 2017). Together, these effects deprive the neurons of energy, thereby aiding another mechanism of cellular dysfunction and death.

1.1.3.4 Synaptic dysfunction

The neurotoxic effects of Aβ on memory and behavior precede neuronal loss owing to its effects on synapses and neurotransmission. Misfolded Aβ, mainly in oligomeric form, possesses the capability to bind with various synaptic receptors, including glutaminergic (N-methyl-d-aspartate (NMDA), α-amino-3-hydroxyl-5-methyl-4-isoxazole-propionate (AMPA), metabotropic) and cholinergic (both α7 nicotinic and muscarinic receptors) receptors, and functions by either desensitizing or internalizing them. The most profound effects observed as a result of this binding are the inhibition of long-term potentiation, impaired long-term depression, loss of cholinergic transmission, decreased synaptic plasticity and inefficient memory retrieval. Consequently, relative amounts of certain Aβ species correlate with loss of spatial memory in rodent models (Esposito et al., 2013; Rajmohan and Reddy, 2017). The generation of ROS by Aβ and frequent activation of glutaminergic receptors have been proposed to contribute towards calcium dyshomeostasis, leading to excitotoxic damage and neuronal loss (Mattson et al., 1992; Harris et al., 1995). Additionally, Aβ also contributes to synaptic dysfunction by reducing mature dendritic spines and impacting vesicular transport (Ovsepian et al., 2018; Reiss et al., 2018).

1.1.3.5 Modulation of signaling pathways

Synaptic receptors are not the only receptors obstructed by Aβ. Its interplay with receptor for advanced glycation end products (RAGE), cellular prion protein (PrP^{C}) and insulin receptors also has detrimental effects on neuronal function through the modulation of key survival pathways.

Nuclear factor kappa-light-chain-enhancer of activated B cells, tyrosine-protein kinase Fyn, mitogen-activated protein kinase and serine/threonine-protein kinase Akt-1 are aberrantly activated as a result of these interactions and impair processes involved in axonal growth, cell survival, inflammation, and transcription (Zhao et al., 2008; Smith et al., 2017). Hyperphosphorylation of tau and the subsequent formation of neurofibrillary tangles (NFTs) are also products of aberrant activation of previously mentioned kinases or oxidative stress and hold great pathological relevance in several neurodegenerative diseases (Zempel et al., 2010; Lloret et al., 2011).

1.2 Alzheimer's disease and Aβ

AD is the most common form of dementia and affects approximately one tenth of the elderly population above 65 years of age (Gaugler et al., 2019). The formation of Aβ fibrils and their accumulation as senile plaques constitute one of the two major molecular hallmarks of AD, the other one being the presence of intracellular tau tangles. Since the first case study by Alois Alzheimer, evidence that favors the key role of Aβ in AD has grown drastically, however, the exact relationship between Aβ deposits, tau tangles and AD-associated cognitive decline is still not established (Alzheimer, 1907). Over the years several ideas have been presented for the placement of Aβ-induced neurotoxicity and other key features of AD, some of which are stated as follows (Du et al., 2018; Kinney et al., 2018; Pardo, 2019);

1. **Amyloid cascade hypothesis:** This hypothesis is one of the earliest ones explaining the pathophysiology of AD and states that mismetabolism of Aβ and the subsequent fibril formation initiates AD.
2. **Oligomer hypothesis:** Primarily an extension of amyloid cascade hypothesis, this hypothesis states that oligomeric species, instead of fibrils, are the primary culprits behind AD.
3. **Tau hypothesis:** In comparison to its former counterparts, this school of thought focuses on the second molecular hallmark of AD, the tau tangles, and states that tau pathology precedes Aβ deposition and causes AD.
4. **Inflammation hypothesis:** According to this hypothesis, aberrant activation of microglia-associated pathways modulates Aβ and tau pathology and drives AD.
5. **Oxidative stress hypothesis:** This hypothesis acknowledges Aβ-induced mitochondrial dysfunction and oxidative stress as the cause of AD,

6. **Metabolic syndrome hypothesis:** This idea suggests that AD is a product of age-associated aberrations in cerebral glucose metabolism and leads to deposition of Aβ.

Nevertheless, every hypothesis acknowledges the involvement of Aβ in AD, either as a cause or consequence of underlying pathology, due to several known facts. Firstly, mutations in APP and Aβ-processing enzymes, PSEN1 and PSEN2, are major causes of the familial variant of this disease (Goate et al., 1991; Haass, 1996; Plassman and Breitner, 1996). Similarly, genetic interventions to mutate these genes cause AD-like pathology in experimental models (Kitazawa et al., 2012). Moreover, directly injecting brain-derived Aβ in rodents also leads to neurodegeneration (Ruiz-Riquelme et al., 2018). Lastly, clinical studies show that the presence of Aβ plaques in frontoparietal regions of the brain precedes tau pathology and cognitive symptoms of the disease, indicating its pivotal role in disease pathology (Figure 4).

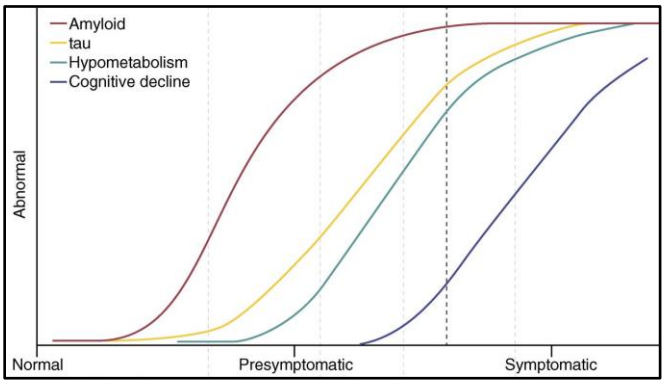

Figure 4: Proposed timeline of AD-associated changes in the brain. Aberrations in CSF Aβ levels and appearance of plaques precede tau pathology, brain atrophy and cognitive symptoms, indicating the pivotal role of Aβ pathology in AD (Stanley et al., 2016).

However, the repeated failures of Aβ-targeting drugs and the presence of Aβ deposits in non-demented individuals question Aβ-related hypotheses of AD and give some evidence in the favor of other hypotheses (Rodrigue et al., 2009; Du et al., 2018). The identification and isolation of clinically relevant Aβ proteoforms and conformers is therefore necessary.

1.2.1 Clinical features of classical AD

Clinically, AD is defined as memory impairment accompanied by changes in executive function, visuospatial capability, speech, behavior and/or movement. Although a definite diagnosis is still not possible before the autopsy, the following criterion is utilized for diagnosis of probable AD (Schmidt et al., 2012; Jack et al., 2018; Baiardi et al., 2019):

1. Decline of three Mini-Mental State Examination (MMSE) points/year
2. Increased tau/phospho-tau (p-tau) and decreased $A\beta_{42}$ levels in CSF
3. Reduced hippocampal volume
4. Hypometabolism in the parietal lobe, temporal lobe and hippocampus
5. Positive amyloid positron-emission tomography

The patients with early AD present problems with recent episodic memory followed by the development of progressive anomia. Aphasia is the next symptom to be reported in most cases along with dysexecutive syndrome. Psychiatric symptoms, including irritability, delusions and hallucinations, are also reported. In the final stages, the patient loses mobility and death occurs due to complications associated with the aforementioned symptoms. The patients survive between 8 to 10 years from the onset of symptoms, as currently there is no cure available for AD (Tang-Wei et al., 2005). The symptoms are managed by acetylcholine esterase inhibitors and memantine (Shao, 2015).

1.2.2 Clinical variants of Alzheimer's disease

AD is a complex disease that features several different clinical variants based on the age of onset, pathological burden, cognitive decline and psychiatric symptoms, some of which are discussed as follows.

1.2.2.1 Familial AD

Although the age of onset in most cases is around 65 years, onset has been observed in a small fraction of patients (1%) as early as 46 years. These cases generally have the familial or autosomal dominant variant of AD (fAD) with mutations in APP, PSEN1, PSEN2 or one of the other 31 risk genes (Moustafa et al., 2017). Heterogeneity within this variant arises from the differential presentation of cognitive symptoms in cases with different mutations (Ryan et al., 2016).

1.2.2.2 Sporadic AD

Early-onset AD (EOAD) has also been observed without genetic causes and constitutes 5% of all AD cases. However, most cases present late-onset AD (LOAD). Both EOAD and LOAD occur due to sporadic causes, but diabetes mellitus, obesity, smoking, lack of activity and ApoE genotype are thought to act as risk factors (Toyota et al., 2007; Awada, 2015; Crous-Bou et al., 2017).

1.2.2.3 Atypical variants of AD

Depending on the affected brain regions, AD can feature an atypical combination of symptoms. Posterior cortical atrophy is frequently associated with AD pathology in visual association areas and presents worse visual deficits. Similarly, primary progressive aphasia features AD pathology in conjunction with language impairment. Aβ deposits and tau pathology are also common in patients of other neurodegenerative diseases like Parkinson's disease (PD), Creutzfeldt–Jakob disease (CJD), Gerstmann-Sträussler Syndrome (GSS), dementia with Lewy bodies (DLB), and frontotemporal dementia (FTD; Mastaglia et al., 1989, Haltia et al., 1991; Amano et al., 1992, Barcikowska et al., 1995, Forman et al., 2006).

1.2.2.4 Rapidly progressive dementia with AD pathology

Rapidly progressive dementias constitute a small subset of dementia patients that are characterized by reports of dementia within 1-2 years (weeks in some cases) of disease onset. The short duration of the disease gives an even shorter window for accurate diagnosis and treatment, presenting a challenge for neurologists and biomedical researchers alike. However, if diagnosed in time, many cases are treatable. The most common causes of rapid progression include vascular anomalies, infections, toxic-metabolic causes, autoimmune diseases, metastasis, iatrogenic causes, neurodegenerative disorders and seizures (Paterson et al., 2012). Although the exact contribution of each of these causes towards the incidence of rapidly progressive dementias is variable in reports from different centers, most cases are attributed to autoimmune diseases and neurodegenerative pathologies. Within the latter untreatable cause, prion diseases, AD and FTD are the most common contributing pathologies. Corticobasal syndrome and DLB also contribute towards rapidly progressive dementias (Poser et al., 1999; Papageorgiou et al., 2009; Neto et al., 2017; Geut et al., 2019).

Owing to its contribution towards the etiology of rapidly progressive dementia, rpAD has now been recognized as an atypical clinical variant of AD. The first paper about rpAD was published in 1989, followed by other reports where AD was misdiagnosed as CJD due to rapid deterioration in memory and shorter survival time (Mann et al., 1989; Poser et al., 1999; Reinwald et al., 2004). Although rpAD researchers and neurologists have not reached a consensus regarding the clinical definition of this disease, many use a decline of at least 6 MMSE points per year and disease duration of less than 3 years (2 years in some centers) as a diagnostic criterion (Figure 5; Abu-Rumeileh et al., 2018; Pillai et al., 2018).

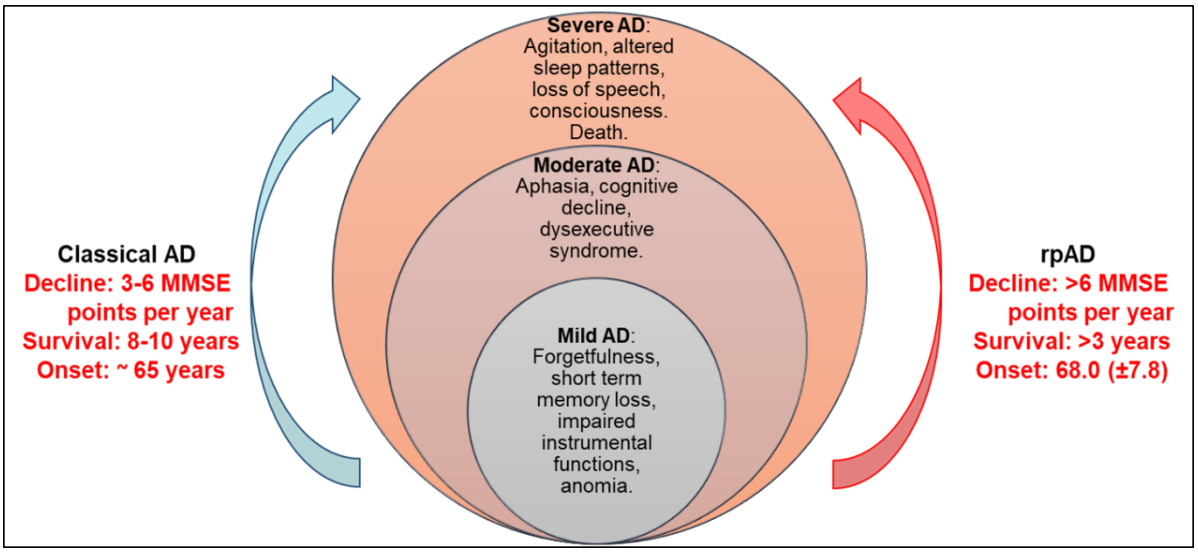

Figure 5: Differences among sAD and rpAD. rpAD follows the same clinical course as classical AD, hereafter referred to as sAD, but the progression is faster and the survival is usually less than three years from the onset of symptoms.

1.2.2.4.1 Clinical and molecular differences in sAD and rpAD

Several differences have been observed in clinical course and biomarker profiles among sAD and rpAD cases. Neurological signs, including executive dysfunction, language impairment and movement disorder, are observed earlier during the disease course in rpAD cases. Moreover, these cases show higher levels of tau and p-tau along with reduced $A\beta_{42}$ in CSF in comparison to sAD, however, the utility of these biomarkers to differentiate sAD from rpAD is still debatable (Llorens et al., 2016). 14-3-3, on the other hand, is only present in rpAD cases and can be used for differential diagnosis (Schmidt et al., 2010; Schmidt et al., 2012, Karch et al., 2016). On an anatomic level, no significant differences are observable in brain atrophy and hippocampal volume. In the context of risk factors, APOE ε4 allelic frequency appears to be lower in rpAD cases in comparison to sAD (Ba et al., 2017; Pillai et al., 2018).

The molecular mechanisms behind rapid progression observed in rpAD are yet to be elucidated. Markers for inflammation (cartilage glycoprotein YKL-40), tissue damage (α-synuclein) and axonal damage (neurofilament light) show no significant differences among sAD and rpAD cases. Moreover, no differences in distribution and structures of plaques and NFTs have been reported (Schmidt et al., 2012). Rapid progression has been attributed to higher levels of PrP^C, a known Aβ receptor, although its levels are also not significantly different among the two variants (Abu-Rumeileh et al., 2018). However, the presence of different structures and interactors of PrP^C have

been validated in rpAD (Zafar et al., 2017). On the proteomic level, plaques in rpAD have several proteins associated with synaptic dysfunction along with fewer active plaque-clearing astrocytes (Drummond et al., 2017).

1.3 Sub-populations of Aβ and clinical variants of AD

Understanding the existence of multiple clinical variants of AD with seemingly similar underlying pathology and key molecular players requires immense research efforts. What causes Aβ and tau to behave differently and initiate pathologies that not only have different clinical features but also alter the rate of progression of the disease? The answer, although still not completely understood, may lie in the strain theory of prion disorders.

Prion is defined as a proteinaceous infectious particle that assembles into fibrillar assemblies. Scrapie isoform of the cellular prion protein (PrP^{Sc}) is one of the thirty pathological amyloidogenic proteins and is best known for its involvement in CJD, GSS and several other debilitating human and animal neurodegenerative diseases. The conversion of PrP^{C} to PrP^{Sc} also follows the same mechanism as Aβ amyloid formation. However, although the underlying mechanism and pathological protein are similar, several variants of prion disease are known to exist (Collinge et al., 2001). This heterogeneity has been attributed to the existence of distinct PrP strains. Strains are defined as conformers of a specific amyloidogenic protein, in this case PrP^{Sc}, that differ with respect to their transmission, brain-lesion profiles, incubation periods and disease phenotypes along with certain biochemical characteristics like post-translational modifications, sensitivity to proteinase K and electrophoretic mobility. The distinct conformational characteristics of each PrP strain are transmitted into the host, where it propagates and causes distinct phenotypes (Morales, 2017). The codon 129 polymorphism gives rise to at least three known strains of PrP in humans (Lewis et al., 2006). The strain theory is also applicable to tau and α-synuclein (Petersen et al., 2019; Jaunmuktane and Brandner, 2019).

In case of Aβ, it has been known for several years that different proteoforms vary in their capability to form amyloids, seeding proficiencies, three-dimensional conformations, transport mechanisms and toxicities (Burdick et al., 1992; Rush et al., 1992; Pike et al.,1995; Martel et al., 1996). Each proteoform can adopt and propagate in multiple conformations (Chakraborty and Das, 2017). These conformers do not only possess distinct biochemical signature but also have different sta-

bilities, distribution and morphology in the brain. They are transmissible among humans and between humans and animals (Rasmussen et al., 2017). These variants fulfill the definition of strains, hence, similar to prion disease, the heterogeneity of clinical phenotypes of AD can be attributed to the presence and distinct involvement of Aβ strains.

1.4 Aims of the study

The current study was designed to apply the strain theory of prions to AD and characterize sAD and rpAD based on differences in Aβ proteoforms and associated conformers. We hypothesized that certain variants of Aβ, their sequences, structures or interactions, may be responsible for the faster progression observed in rpAD. In contrast to studies conducted by other groups, we undertook the challenging task of purifying the extremely hydrophobic and insoluble Aβ peptides generated in the endogenous environment. Brain-derived Aβ peptides were extracted using affinity purification and subsequently subjected to various proteomic methods for their identification and quantification. The fibrils produced by aggregation of these proteoforms were extracted using mild protein purification techniques and amplified via *in vitro* aggregation assays before their biophysical analysis. For a comprehensive characterization of these clinical variants of AD three different aspects of Aβ biology were targeted in this work, and the major aims were as follows:

1. evaluate the alterations in the primary sequence of Aβ proteoforms isolated from sAD and rpAD brains,
2. establish differences in the three-dimensional (3D) architecture of brain-derived Aβ conformers, and
3. define the functional consequences of alterations in Aβ proteoforms and conformers among the targeted clinical variants of AD.

2. Materials and Methods

2.1 Materials

2.1.1 Antibodies

The antibodies used for immunoprecipitation (IP) and immunoblot (IB) analysis in this study are listed in Table 1.

Table 1: List of primary and secondary antibodies utilized in the current study.

Antibody	Origin	Dilution for IB	Dilution for IP	Company/ Catalogue No.
4G8 Aβ	IgG2b Mouse	1:1000	1:100	BioLegend/800701
6E10 Aβ	IgG1 Mouse	1:1000	1:100	BioLegend/803001
ADAM-10	IgG Rabbit	1:1000	-	Abcam/ab124695
BACE-1	IgG Rabbit	1:1000	-	Abcam/ab108349
PSEN-1	IgG2a Mouse	1:200	-	Santa Cruz Biotechnology/ sc365495
PSEN-2	IgG1 Mouse	1:200	-	Santa Cruz Biotechnology/ sc393758
Nicastrin	IgG1 Mouse	1:200	-	Santa Cruz Biotechnology/ sc376513
IDE	IgG1 Mouse	1:200	-	Santa Cruz Biotechnology/ sc393887
Plasminogen	IgG1 Mouse	1:200	-	Santa Cruz Biotechnology/ sc376324
Horseradish peroxidase (HRP)-conjugated anti-mouse	Goat	1:10000	-	JacksonIR Lab/ 115-035-062

HRP conjugated anti-rabbit	Goat	1:10000	-	JacksonIR Lab/ 111-035-144

2.1.2 Chemicals

Unless stated otherwise, the chemicals used for this study were obtained from either Sigma (Deisenhofen, Germany), Merck (Haar, Germany), Serva (Heidelberg, Germany), Roth (Karlsruhe, Germany) or Bio-Rad (Munich, Germany).

2.1.3 Peptides, standards, enzymes and kits

The peptides, standards, enzymes and kits used in the current study are listed in Table 2.

Table 2: List of peptides, standards and kits used in this study.

Product	Company/ Cat. No.	Purpose
$A\beta_{40}$ peptide	Abcam/ ab120479	*In vitro* seeding assays
$A\beta_{42}$ peptide	Abcam/ ab120301	*In vitro* seeding assays
Precision Plus Protein standards	Bio-Rad/ 161-0374	Standard for IB
Peptide calibration standard	Bruker/ 8222570	Calibration of MALDI-ToF MS spectrum
DNase I	Thermo Fisher Scientific/ EN0521	Protein purification
Sequencing grade trypsin	Serva/ 37283	Protein digestion
Protease inhibitor	Roche/ 4693116001	Protein extraction
Phosphatase inhibitor	Roche/ 04906837001	Protein extraction
40% Biolyte 3-10 ampholytes	Bio-Rad/1631112	Isoelectric focusing (IEF)
Dynabeads protein G	Invitrogen/ 10003D	IP
Bradford's reagent	Bio-Rad/ 500-0006	Protein quantification
MemCode reversible protein stain kit	Pierce/ 24580	IB normalization
$A\beta_{1-x}$ ELISA	IBL International/ JP27729	Quantification of Aβ
$A\beta_{x-42}$ ELISA	Biolegend/ 842401	Quantification of Aβ

$A\beta_{1-40}$ ELISA	Biosource/ MBS760432	Quantification of Aβ
MTS assay kit	Abcam/ ab197010	Cell viability assays

2.1.4 SH-SY5Y cells and culture media

SH-SY5Y cells were a kind gift from the Institute of Neuropathology, Saarland University Hospital, Homburg, Germany. Dulbecco's modified Eagle's medium (DMEM; Sigma, Germany) was supplemented with 10% fetal bovine serum (FBS; Sigma, Germany), 1% mixture of penicillin and streptomycin (P/S; MP biomedicals, Germany) and 1% L-glutamate (Gibco, Germany) was used for the maintenance of the culture at 37°C, under 5% CO_2 and 95% humidity. All flasks, plates and other cell culture consumables were obtained from Sarstadt, Germany.

2.1.5 Laboratory instruments and other materials

The laboratory instruments and other materials used for various experiments are enlisted in Table 3.

Table 3: List of laboratory instruments and other materials used for this study

Instrument	Model	Manufacturer
Tissue lyser	85600	Qiagen, Germany.
Tenbroeck tissue grinder	LG-10660-100	Wilmad-LabGlass, USA.
Sonicator	T310/H	Elma, Switzerland.
Spectrophotometers	Ultospec 2100 Pro	Amersham Biosciences, UK.
	NanoDrop™ 1000	Thermo Fisher Scientific, Germany.
	Spectrum 100	Perkin Elmer, USA.
Thermomixer	5436	Eppendorf, Germany.
Centrifuges	5810R	Eppendorf, Germany.
	Optima TL100	Beckmann coulter, Germany.
Speed Vac	SVC 100	Savant, USA.
PROTEAN IEF Cell	1646001	Bio-Rad, Germany
IPG strips (3-10 non-linear)	1632002	Bio-Rad, Germany.
Mini-PROTEAN Tetra cell	10007296D	Bio-Rad, Germany.

Mini Gel Tank	A25977	Invitrogen, USA.
4-20% Bis-Tris gradient gels	NP0330BOX	Invitrogen, USA.
Power supply	Power Pac 300	Bio-Rad, Germany.
Transfer Cell	Trans-blot Turbo 1704150	Bio-Rad, Germany.
	TE 77 PWR	AA Hoefer, USA.
Amersham Hybond P Polyvinylidene fluoride (PVDF) membranes	10600021 (0.2 µm)	Sigma-Aldrich, USA.
	10600023 (0.45 µm)	Sigma-Aldrich, USA.
Amersham Hybond® P nitrocellulose membranes	10600002 (0.45 µm)	Sigma-Aldrich, USA.
ChemiDoc XRS+	170-8265	Bio-Rad, Germany.
Plate Readers	Wallac Victor 1420-002	Wallac, Finland.
	FLUOstar Omega	BMG Labtech, Germany.
Microscopes	Axiovert 25	Carl Zeiss, Germany.
	Zeiss LSM 510 Meta	Carl Zeiss, Germany.
	MFP-3D Infinity	Asylum Research, USA.
Hydraulic Press	15011	Specac, UK.
Biosafety cabinet	Herasafe HS 15	Thermo Fisher Scientific, Germany.
Waterbath	WNB22	Memmert, Germany.
CO_2 Incubator	Hera cell incubator 50049916	Heraeus, UK.
Matrix-assisted laser desorption/ionization (MALDI) mass spectrometer	rapifleXTM MALDI Tissuetyper	Bruker Daltonics, USA.
C18 columns precolumns	20 mm x 0.15 mm ID	Thermo Fisher Scientific, Germany.
PicoFrit revesed phase C18 columns	PF360-75-15-N-5	New Objective, USA.
Nanoflow chromatography system	Easy nLC-1000	Thermo Fisher Scientific, Germany.

Quadrupole-Orbitrap Mass Spectrometer	Q Exactive Hybrid Quadrupole-Orbitrap mass spectrometry system	Thermo Fisher Scientific, Germany.

2.1.6 Software

The following software (Table 4) were employed for visualization and analysis of data in the current study.

Table 4: List of software used in the current study.

Software	Application	Version	Developer
Image Lab	IB analysis	6.0.1	Bio-Rad, Germany.
Delta2D Decodon	Two-dimensional polyacrylamide gel electrophoresis (2D-PAGE) analysis	4.8	Decodon GmbH, Germany.
Igor Pro	Atomic force microscopy (AFM)	6.37	WaveMetrics, USA.
Gwyddion	AFM analysis	2.53	Czech Metrology Institute, Czech Republic.
Zeiss LSM	Confocal microscopy	4.2.0.121	Microimaging GmBH, Germany.
ImageJ	Confocal microscopy	1.52	National Institute of Health, USA
Spectrum	FTIR spectroscopy	6.10	Perkin Elmer, USA.
FlexImaging	MALDI	4.1	Bruker Daltonics, USA.
FlexAnalysis	MALDI analysis	3.4	Bruker Daltonics, USA.
Excalibur	ESI-MS/MS	3.1.6.1	Thermo Fisher Scientific, Germany.
Raw2MSM	ESI-MS/MS	1.17	University of Southern Denmark, Denmark.

Mascot	ESI-MS/MS	2.5.1	Matrix science, UK.
Scaffold	ESI-MS/MS	4.8.9	Proteome Software Inc., USA.
PRISM	Statistical analysis	6.0	GraphPad Software, USA.
RStudio	Statistical analysis	1.1.383	RStudio, Inc., USA.

2.1.7 Stock solutions

Lysis Buffers:

Urea-Thiourea Lysis buffer: 7 M Urea, 2 M thiourea, 4% 3-[(3-cholamidopropyl)-dimethylammonio]-1-propane sulfonate (CHAPS), 2% ampholytes, 1% dithiothreitol (DTT), phosphatase and protease inhibitors in dH_2O.

Tris-Triton Lysis Buffer: 50 mM Tris-HCl pH 8.0, 0.5% CHAPS, 1 mM ethylenediaminetetraacetic acid (EDTA), 1 mM DTT, 1% Triton-X100, phosphatase and protease inhibitors in dH_2O.

Solutions for one-dimensional polyacrylamide gel electrophoresis (1D-PAGE):

Laemmli buffer (4x): 0.25 M Tris-Cl, 8% sodium dodecyl sulphate (SDS), 40% glycerol, 20% β-mercaptoethanol and 0.008% bromophenol blue in dH_2O (pH 6.8).

Stacking Gel buffer: 0.5 M Tris-base and 0.4% SDS in dH_2O (pH 6.8).

Resolving Gel buffer: 1.5 M Tris-base and 0.4% SDS in dH_2O (pH 8.8).

Electrophoresis buffer: 192 mM Glycine, 0.1% SDS and 25 mM Tris-HCl in dH_2O (pH 8.3).

Solutions for IEF:

Elution Buffer for IP/ Rehydration buffer: 8.3 M Urea, 0.5% CHAPS, 20 mM DTT and 0.5% (v/v) ampholytes in ddH_2O.

Equilibration buffer I: 6 M Urea, 2% SDS, 30% glycerin, 0.375 M Tris-base (pH 8.8), 2% (w/v) DTT in ddH_2O.

Equilibration buffer II: 6 M Urea, 2% SDS, 30% glycerin, 0.375 M Tris-base (pH 8.8), 2.5% (w/v) IAA and bromophenol blue in traces in ddH_2O.

Solutions for native polyacrylamide gel electrophoresis (native PAGE):

Sample buffer (2x): 62.5 mM Tris-Cl, 25% glycerol and 0.01% bromophenol blue in dH_2O (pH 6.8).

Stacking Gel buffer: 2.5 M Tris-base in dH_2O (pH 6.8).

Resolving Gel buffer: 1.5 M Tris-base in dH_2O (pH 8.8).

Electrophoresis buffer: 192 mM Glycine and 25 mM Tris-HCl in dH_2O (pH 8.3).

Solutions for Western blot:

Tris-Glycine Transfer buffer: 48 mM Tris-base, 39 mM glycine, 1.0 mM SDS and 20% methanol in dH_2O (pH 8.3).

Tris-Glycine Transfer buffer for Aβ: 25 mM Tris-base, 190 mM glycine and 20% methanol in dH_2O (pH 8.3).

Phosphate-buffered saline with Tween-20 (PBS-T): 9.55 g/L PBS and 0.0005% tween-20 in ddH_2O.

Blocking Buffer: 5% Milk powder in PBS-T.

Enhanced chemiluminescence (ECL) solution: 0.15 M Tris-HCl (pH 8.5), 1.25 mmol luminol, 0.55 mmol coumaric acid and 0.0003% hydrogen peroxide in dH_2O.

Reblotting Buffer: 0.2 M Glycine, 3.5 mM SDS, 1% Tween-20 (pH 2.2) in dH_2O.

Solutions for Coomassie Staining:

Fixative solution: 50% Methanol in 12% acetic acid in ddH_2O.

Coomassie G-250 solution: 0.25% Coomassie G-250 in the fixative solution.

Destaining solution: 10% Acetic acid, 10% methanol in ddH_2O.

Solutions for Silver Staining:

Fixative solution: 50% Methanol, 12% acetic acid in ddH_2O.

Sensitization solution: 0.8 mM Sodium thiosulphate in ddH_2O.

Staining solution: 0.2% Silver nitrate and 0.026% formaldehyde in ddH_2O.

Developing Solution: 6% Sodium carbonate, 0.0185% formaldehyde and 16 µM sodium thio-sulphate in ddH_2O.

Solutions for MALDI-Time of flight mass spectrometry (MALDI-ToF MS):

Elution buffer for IP: 10% Formic acid (FA) in ultrapure ddH_2O.

Sinapinic Acid (SA) matrix: 10 mg/ml of SA in 50% acetonitrile, 50% proteomics grade water and 0.1% trifluoroacetic acid (TFA).

α-Cyano-4-hydroxycinnamic acid (HCCA) matrix: 10 mg/ml of HCCA in 70% acetonitrile, 30% proteomics grade water and 0.2% TFA.

Dihydroxybenzoic acid (DHB) matrix: 15 mg/ml of DHB in 90% acetonitrile, 10% proteomics grade water and 0.1% TFA.

Solutions for Protein Digestion:

Trypsin solution: 12.5 ng/µl Trypsin in 50 mM ammonium bicarbonate.

Solutions for fibril purification:

Solution A: 10 mM Tris-HCl (pH 7.4), 0.25 M sucrose, 3 mM EDTA, one protease Inhibitor tablet per 50 ml and 0.1% sodium azide.

Solution B: 10 mM Tris-HCl (pH 7.4), 1.9 M sucrose, 3 mM EDTA, one protease inhibitor tablet per 50 ml and 0.1% sodium azide.

Solution C: 50 mM Tris buffer (pH 8.0)

Solution D: 50 mM Tris buffer (pH 8.0) and 2 mM calcium chloride.

Solution E: 50 mM Tris buffer (pH 8.0), 1.3 M sucrose and 1% SDS.

Real-time quaking-induced conversion (RT-QuIC) seeding Buffer: 7.5 mM Sodium phosphate dibasic and 2.5 mM sodium phosphate monobasic (pH 7.4).

2.2 Methods

2.2.1 Ethics statement

All sAD, rpAD and control brain samples were obtained from the Institute of Neuropathology brain bank, Barcelona, Spain (HUB-ICO-IDIBELL Biobank), according to Spanish legislation (Ley de la Investigación Biomédica 2013 and Real DecretoBiobancos, 2014) following informed consent of participants or their legal next of kin and the approval of the local ethics committee. Sporadic CJD samples were provided by the Department of Neuropathology, University Medical Center, Hamburg, Germany. CSF samples, sAD, rpAD and controls were provided by the Department of Neurology, University Medical Center, Göttingen, following informed consent of the patients or their guardians. The study was approved by the local ethics committee in Göttingen (No. 24/8/12).

2.2.2 Collection of brain samples

Frontal cortex samples were obtained from 15 sAD (mean age of 76.8 ± 2.5 years), 8 rpAD (79.8 ± 2.72 years), 8 non-demented control (71.9 ± 2.84 years) and 4 sporadic Creutzfeldt–Jakob disease (sCJD) brains (74.0 ± 4.0 years). Tissue sections (1 cm thick) from one hemisphere were snap-frozen for molecular analysis and stored in -80°C until use. The second hemisphere was used for neuropathological assessment to validate the clinical diagnosis. All sAD cases met the Consortium to Establish a Registry for Alzheimer's Disease (CERAD) criteria for the diagnosis of the disease. The rpAD samples were selected according to the current definitions of rpAD (Schmidt et al., 2010). Samples with comorbid pathologies that may contribute towards rapid decline and those with a family history of AD were excluded from the rpAD cohort. The non-demented controls were chosen such that they had no underlying pathologies that may contribute towards neurodegeneration. For all sAD, rpAD and control cases, Aβ pathology was scored based on the CERAD scoring system, while the Braak and Braak staging system was used to score NFTs (Boluda et al., 2014; Braak and Braak, 1991). sCJD cases were diagnosed and selected according to current criteria (Zerr et al., 2009). The sample selection was aimed to ensure that no significant differences in postmortem delay were evident among various experimental groups (Figure 32). The clinical data for all the brain samples utilized in this study are summarized in Appendix A.

CSF samples were also selected based on the aforementioned criteria. All samples were collected through a lumbar puncture, centrifuged at 2000 times gravity (x g) for 10 minutes (min) at 4°C and stored at -80°C until further analysis.

2.2.3 Protein extraction

For IP, brain tissue (10% w/v) was homogenized in Tris-Triton lysis buffer. Tissue sections in lysis buffer were placed in the tissue lyzer for 15 min at 50 Hertz (Hz) to ensure complete lysis. The homogenate was incubated at 4°C overnight. The Tris-soluble fraction was isolated by centrifuging the samples at 14,000 revolutions per minute (rpm) for 45 min at 4°C. The resultant pellet was resuspended in 70% FA, supplemented with protease inhibitor, by sonication on ice for 10 min to prepare a 10% w/v homogenate again. The supernatant collected from subsequent centrifugation (14000 rpm, 45 min, 4°C) was saved as FA-soluble fraction.

For 1D-PAGE experiments, brain tissue (10% w/v) was homogenized in Urea-Thiourea lysis buffer using a tissue lyzer, followed by overnight incubation at 4°C. The samples were centrifuged (14000 rpm, 45 min, 4°C), and the supernatant was saved at -80°C until use.

2.2.4 Protein quantification

Proteins extracted in Tris-Triton and Urea-Thiourea lysis buffers were quantified using Bradford's assay (Bradford et al., 1976). Briefly, bovine serum albumin was serially diluted (0.0 µg/ml to 1000 µg/ml, 20 µl per tube) mixed with 980 µl of Bradford's reagent to make a final volume of 1000 µl. Similarly, Bradford's reagent was added to 20 µl of the diluted sample (sample and ddH_2O in a ratio of 1:20). The mixtures were incubated at room temperature for 10 min. The absorbance at 595 nm was recorded for each standard and sample in duplicates using the Ultospec 2100 spectrophotometer. The quantity of protein in samples was estimated using a standard curve of bovine serum albumin dilutions. In the case of FA-soluble fractions, proteins were quantified by measuring absorbance at 280 nm by Nanodrop spectrophotometer.

2.2.5 Immunoprecipitation

IP of Aβ was performed by slight modifications in the protocol established by Portelius et al., (2015). Dynabeads (1.5 mg/0.5 mg of protein sample) were given two washes with 0.3% CHAPS and incubated with 4 µl each of two Aβ antibodies, 4G8 and 6E10, for 30 min at 4°C. Tris-soluble

fraction, 500 µg, was added directly to the coated beads, while the FA-soluble fraction was neutralized with 5 M sodium hydroxide in 1 M Tris before addition. The mixture was incubated overnight at 4°C. Subsequently, the beads were washed with 0.3% CHAPS to remove non-specific proteins bound to the beads. The samples were then eluted in either rehydration buffer for 2D-PAGE or 10% FA for top-down mass spectrometry by rotating the beads for 10 min at room temperature. The eluates for top-down mass spectrometry were dried in a Speed Vac (30 min). The eluates were stored at -20°C until further processing.

2.2.6 SDS-PAGE and IB analysis

2D-PAGE for brain-derived and synthetic Aβ was performed with minor modifications in the protocol optimized previously (Maler et al., 2007). Briefly, IP eluates were diluted with rehydration buffer, and isoelectric focusing was performed with pH 3-10, 7 cm, non-linear immobilized pH gradient (IPG) strips using previously described program [30 min/300 V, 30 min/800 V, 1 h/2000 V gradient and 2000 V (Σ15000 volt hours)]. The synthetic peptides, 10 ng of $A\beta_{40}$ and $A\beta_{42}$ were resuspended in rehydration buffer and loaded onto IPG strips and subjected to the same protocol. The strips were equilibrated in equilibration buffer I and II for 8 min each. The second-dimension separation was conducted using 4-12% gradient Bis-Tris gels, according to the manufacturer's protocol using ready-made 2-(N-morpholino)ethanesulfonic acid (MES) running buffer (Thermo Fisher Scientific, Germany). Proteins were transferred onto 0.20 µm PVDF membranes under semi-dry conditions with Tris-glycine transfer buffer without SDS (1 mA/cm^2, 45 min). The membranes were boiled in PBS for 3 min (antigen retrieval for Aβ antibodies only) and were blocked with 5% milk in PBS-T for 1 hour (hr) and incubated with 6E10 antibody (1:1000) overnight at 4°C. They were rinsed with PBS-T (four washes) followed by incubation with HRP-conjugated secondary anti-mouse antibody (1:10000) for 1 hr at room temperature. The unbound antibody was removed by washing the blots with PBS-T again. They were then incubated in ECL solution for 1 min. The chemiluminescence signal was detected using an ECL solution and ChemiDoc Imaging System. The images were analyzed using Delta 2D software.

The semi-quantitative analysis of various Aβ-cleaving enzymes was performed using 1D-PAGE (Laemmli et al., 1970). Tris-glycine resolving (8%) and stacking (6%) gels were prepared using the recipes stated in Table 5. The gels were polymerized at room temperature for 20 min each and stored at 4 °C until use. Protein samples (50 µg) were diluted with 4x Laemmli buffer and boiled

at 95°C for 5 min before being loaded on the gels along with the protein standard (5 µl). The gels were run at 100 V at room temperature.

Table 5: Recipe for gels used for 1D SDS-PAGE.

	Resolving gel (8%)	Stacking Gel (6%)
ddH_2O (ml)	4.2	1.3
Buffer (ml)	2.08 (Resolving gel buffer)	0.525 (Stacking gel buffer)
40% Acrylamide (ml; Roti-phorese Gel 40, Carl Roth)	1.6	0.42
10% Ammonium persulfate (µl)	80.0	22.5
Tetramethylethylenediamine (µl; TEMED)	8.0	2.5

Proteins were then transferred onto 0.45 µm PVDF membranes under semidry conditions using Tris-glycine transfer buffer (14 V, 60 min). Immunoblotting was performed as described above for 2D-PAGE. For reblotting, the membranes were incubated in the reblotting buffer for 20 min, followed by four washes with PBS-T (5 min each) before being blocked and incubated with primary antibody again. All blots were stained with MemCode reversible protein stain according to the manufacturer's instructions and normalized through total protein normalization. The images were analyzed using Image Lab software. The presented data were obtained from a minimum of three independent experiments for each antibody.

For dot-blot assays, 2 µl sample was directly pipetted on the nitrocellulose membrane. The membranes were dried for 25 min before being blocked and incubated in the primary antibody. Washing and imaging were performed as described above for 2D-PAGE.

2.2.7 Mass spectrometry

2.2.7.1 Top-down MALDI-TOF mass spectrometry

Fresh dilutions of matrices (SA, HCCA and DHB) were prepared for each analysis. IP eluates, eluted in 10% FA and dried as described in section 2.2.5, were resuspended in 0.1% TFA and mixed with the matrix in a ratio of 1:1. In total, 1.5 µl of this mixture was deposited immediately

on the MALDI plate and incubated for 20 min at room temperature to ensure complete cocrystallization. The resuspended samples that were not deposited immediately on the MALDI plate were stored at -20°C until use and sonicated on ice for 10 min to break any oligomers immediately before analysis.

Spectra were calibrated using peptide standard II before each run and peaks were acquired using repiflex MALDI Tissuetyper in a m/z range of 1000 to 6000 using positive linear mode. Five measurements were taken for each sample and the average spectrum was generated. Peaks were analyzed in FlexAnalysis. The background was subtracted and peaks were smoothed according to in-built algorithms. Aβ proteoforms were manually annotated based on m/z values. Proteoforms with a deviation of more than 5 Da from theoretical mass were excluded from the analysis. The analysis was replicated thrice and only the peptides that were detected in at least two out of three independent replicates were included in the report.

2.2.7.2 Liquid chromatography/electrospray ionization tandem mass spectrometry (LC-ESI MS/MS)

Samples were diluted in Laemmli buffer, boiled for 5 min and allowed to run on 4-12% Bis-Tris gradient gels to a length of 1 cm using the manufacturer's protocol. The gels were washed with ddH_2O twice (5 min each) and were incubated in Coomassie G-250 for 45 min. They were rinsed with ddH_2O (twice, 5 min each) again and incubated in the destaining solution overnight. The bands were excised and washed with ddH_2O followed by reduction with 10 mM DTT, alkylation with 55 mM IAA and digestion with trypsin overnight at 37°C. Peptides were extracted by adding 5% FA and 100% acetonitrile. The supernatant was collected, dried and stored at -20°C until analysis.

The peptide mixtures were concentrated on a reversed-phase C18 precolumn and separated on a reversed-phase C18 nanoflow chromatography column (self-packed with Reprosil-Pur C18 AQ 3 µm material) using a linear gradient (5-35% acetonitrile vs. 0.1% FA; 15 min) at a flow rate of 300 nL/min in an Easy nLC-1000 nanoflow chromatography system. The Q Exactive hybrid quadrupole/orbitrap MS system (paired with Excalibur software) was used to analyze the eluates using the Top10 method in the data-dependent acquisition mode. Tandem mass spectra were obtained using Raw2MSM software. MS/MS spectra were analyzed using Mascot instructed for searching Swissprot Homo sapiens reference proteome (revision 10.2018) with a mass tolerance of 10 ppm

for precursors and 0.05 Da for fragments. Methionine oxidation was regarded as a variable post-translational modification, whereas cysteine modification was set as a fixed modification. MS/MS-based identification was validated using Scaffold software. A confidence threshold greater than 95.0% was used for accepting peptide identifications, while a confidence threshold of 99.0%, paired with a minimum of two identified peptides, was employed as a prerequisite for accepting protein identification.

2.2.8 Enzyme-linked immunosorbent assay (ELISA)

N-terminally and C-terminally truncated proteoforms of Aβ were quantified using $Aβ_{x-42}$ (Biolegend, Germany), $Aβ_{1-x}$ (IBL International, Germany) and $Aβ_{1-40}$ (Biosource, USA) ELISA kits. Tris-soluble and FA-soluble fractions were prepared and quantified as per to the manufacturer's instructions. Briefly, samples were homogenized in Tris-Triton buffer (20% w/v) and proteins were extracted by spinning the samples at 350,000 x g (20 minutes, 4°C). The supernatant was collected, and the pellet was resuspended in 70% FA (10% w/v). The FA-soluble fraction was extracted by centrifuging the samples at 350,000 x g again. The fractions were quantified by measuring their absorbance at 280 nm by Nanodrop spectrophotometer. The samples were either analyzed immediately after extraction or stored at -20°C until use. In case of brain extracts, 100 µg of protein sample were diluted and loaded in each well, while all CSF samples were diluted in a ratio of 1:4 with the sample diluent provided with the kit for analysis. ELISA was performed as instructed by the manufacturer. All samples were quantified in duplicates and the average readings were analyzed.

2.2.9 *In vitro* seeding assay

2.2.9.1 Fibril purification

Amyloid fibrils were extracted using minor modifications in the protocol optimized by Lu et al. (2013). Briefly, 85 mg of brain tissue were homogenized in 1.7 ml of buffer A using the Tenbroeck tissue grinder and incubated overnight at 4°C. Sucrose was added to the homogenate to raise the concentration of sucrose to 1.2 M and the mixture was centrifuged at for 30 min 250,000 x g at 4°C. The pellet was resuspended in 12 volumes of buffer B and centrifuged for 30 min at 125,000 x g at 4°C. The top-most solid layer was collected and mixed with 200 µl of buffer C followed by centrifugation at 8,000 x g for 15 min to remove sucrose. The pellet was dissolved in Buffer D and incubated with DNase I (0.01 mg/ml) at room temperature for 2 hr. The mixture was centrifuged

at 8,000 x g for 15 min again and the pellet was resuspended in Buffer E followed by another centrifugation for 45 min at 200,000 x g at 4°C. The pellet was washed with ultrapure H_2O and saved at -20°C. Aβ fibrils (10% w/v), corresponding to Tris-soluble fraction, were extracted in PBS supplemented with protease and phosphatase inhibitors as described in section 2.2.3.

2.2.9.2 RT-QuIC

Purified fibrils were resuspended in 15 µl of RT-QuIC seeding buffer and quantified by Nanodrop spectrophotometer. Half of the brain extract (7.5 µl; 2-3 µg/µl) was further diluted with the seeding buffer to a final volume of 88 µl and sonicated on ice for 10 min. Alternatively, Aβ extracted in PBS (15 µl) was used directly. Synthetic peptides were dissolved in hexafluoroisopropanol, aliquoted, dried and stored at -20°C until use. $A\beta_{40}$ and $A\beta_{42}$ were diluted in DMSO (50 µM) and sonicated for 30 min immediately prior to the reaction and added to diluted brain extract along with 2 µl of Thioflavin-T in PBS (Th-T; 1 mM) solution. The final reaction volume of each mixture was 100 µl. Multiple technical replicates from each sample were incubated simultaneously in FLUOstar Omega plate reader for 46 hr at an intermittent shaking mode (600 rpm for 1 min after every 29 min) at 37°C. Fluorescent measurements were recorded every 30 min (excitation 450 nm, emission 480 nm) and used for analysis.

2.2.10 Native PAGE

Native gels (8%) were prepared according to the recipes listed in Table 6. The RT-QuIC product (8 µl) was added to an equal volume of 2x sample buffer, thoroughly mixed and loaded directly into the wells along with the protein standard (1 µl). The gel was run at 150 V on ice until the tracking dye reached the bottom of the gel.

Table 6: Recipe for resolving and stacking gels used for Native PAGE.

	Resolving gel (8%)	Stacking Gel (6%)
ddH_2O (ml)	4.0	2.6
Buffer (ml)	2.5 (Resolving gel buffer)	1.0 (Stacking gel buffer)
40% Acrylamide (ml)	1.0	0.4
10% Ammonium persulfate (µl)	50.0	20.0
TEMED (µl)	5.0	5.0

The proteins were visualized using silver staining. The gels were stored in fixative solution overnight. Subsequently, they were washed with 50% and 30% ethanol solution (20 min each), incubated in sensitization solution (1 min) followed by silver nitrate solution (20 min). The bands were visualized by shifting the gel to the developing solution for 5 min. The gel was washed to remove any remnant solutions and scanned immediately.

2.2.11 Confocal laser scanning microscopy

Th-T dye (1 mM) was added to RT-QuIC products in a ratio of 1:10. The resulting mixture (1 µl) was added to glass slides and directly imaged at 488 nm using Zeiss LSM 510 Meta Confocal laser scanning microscope.

2.2.12 Atomic force microscopy

RT-QuIC products (5 µl) were added to freshly stripped micas and incubated for 20 min at room temperature. The coated micas were washed thrice with ultrapure H_2O (10 µl) to remove salts and other impurities, and excess H_2O was removed with a gentle nitrogen stream. The samples were imaged in intermittent contact mode (tapping mode) using the MFP-3D Infinity microscope and Olympus microcantilevers (OMCL-AC160TS) at a drive frequency of 260.058 kHz, guided by Igor Pro software. The scan area for each image was 10 μm^2 and the scan rate was 0.5 Hz.

2.2.13 Fourier-transform infrared spectroscopy (FT-IR)

Potassium bromide pellets were prepared in a hydraulic press and coated with RT-QuIC products (20 µl). The samples were scanned in the range of 400-4000 cm^{-1} in a Spectrum 100 spectrophotometer using Spectrum software and the percentage transmittance was recorded. For each sample, spectra recorded for two separate reactions were averaged and used for final analysis.

2.2.14 Toxicity assays

2.2.14.1 Preparation of oligomeric and fibrillar fractions

RT-QuIC products from each target well were diluted with Optimem serum-free medium (Gibco, Germany) to a final concentration of 20 µM and centrifuged at 20,000 x g for 10 min to separate oligomeric and fibrillar fractions. The pellet was resuspended in 25 µl of the medium, while the supernatant was used directly.

2.2.14.2 Cell treatments and MTS assay

SH-SY5Y cells (30,000 cells/well) were platted in a 96 well plate in Optimem supplemented with 1% P/S at 37 °C, 5% CO_2. After 24 hr, the medium was replaced with 100 µl Optimem containing fractionated extract and incubated for another 24 hr. MTS reagent (10 µl) was added to each well and the absorbance at the wavelength of 490 nm was recorded after 3 hr.

2.2.15 Bioinformatic tools and statistical analysis

The data were analyzed and visualized using PRISM and RStudio. P-values were determined using either one-way ANOVA followed by Tuckey's post hoc test or unpaired Student's t-test, and values ≤ 0.05 were considered significant. All data are expressed as mean ± standard error of the mean (SEM), unless stated otherwise. Functional categorization of proteins was performed using UniPortKB database (release 2019_07).

3. Results

3.1 Extraction and identification of Aβ proteoforms

The characterization of Aβ proteoforms is crucial for our understanding of the pathways involved in common neurodegenerative pathologies, especially AD and its clinical subtypes. However, the low concentrations of targeted proteoforms and their resistance to standard biochemical and molecular techniques complicates their analysis. Moreover, a majority of studies have focused on $A\beta_{40}$ and $A\beta_{42}$ only, ignoring the potential role of other proteoforms. This part of the study focused on extraction and identification of brain-derived proteoforms from clinical subtypes of AD. Brain proteome was divided into two pathologically relevant fractions, namely Tris-soluble and FA-soluble fractions. Tris-soluble fractions comprise of smaller, soluble Aβ species that impart toxic effects within the cell body. The FA-soluble fraction, on the other hand, corresponds to insoluble Aβ species deposited as fibrils and plaques that sequester circulating Aβ and may function as a reservoir.

3.1.1 Various Aβ proteoforms are present in sAD and rpAD brains

Aβ-enriched fractions were prepared by IP of proteins extracted from Tris-soluble and FA-soluble fractions using antibodies against two domains of the Aβ peptide to ensure the extraction of all endogenously cleaved proteoforms. The IP protocol was optimized to reduce the loss of proteoforms captured by the beads during the washes (Figure 6). The elution buffers were selected to minimize fibrillization of Aβ and maintain extracted Aβ proteoforms as monomeric species for further analysis by modulating the amount of urea (8.3%) or FA (10%).

2D-PAGE, followed by IB analysis with either 6E10 and 4G8 antibody, was used to validate the presence of various Aβ proteoforms in IP eluates before further analysis. Although an overall signature of total Aβ was visualized by 6E10 and 4G8 antibodies, the expression of specific proteoforms could not be tested due to the lack of proteoform-specific antibodies. Therefore, a virtual 2D map of common Aβ proteoforms, in their monomeric form, presented in Figure 7A, was used to annotate various spots, in addition to the 2D-PAGE analysis conducted for synthetic proteoforms of Aβ (Figure 7B and C).

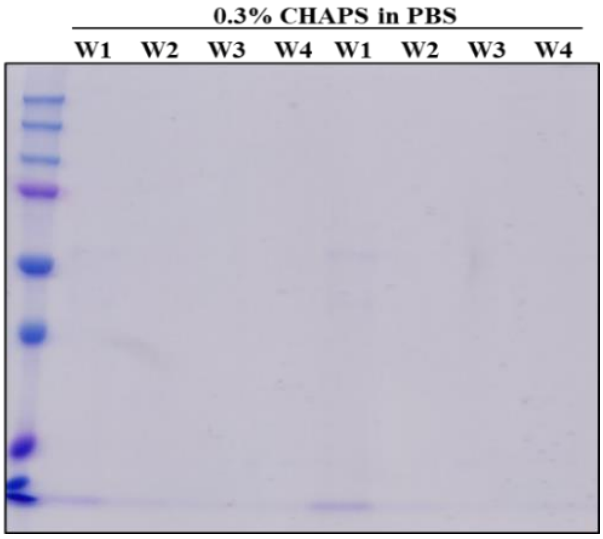

Figure 6: Coomassie-stained gel of IP washes validates the efficiency of IP protocol. IP washes (W1-W4) from two different samples were run on a 12% Tris-Glycine gels and stained to ensure that protein loss was kept to a minimum during IP protocol. Absence of the typical bands of Aβ, usually visualized at 20 kilodaltons (kDa), 24 kDa and 56 kDa in 1D-PAGE, indicated no loss of Aβ proteoforms bound to beads.

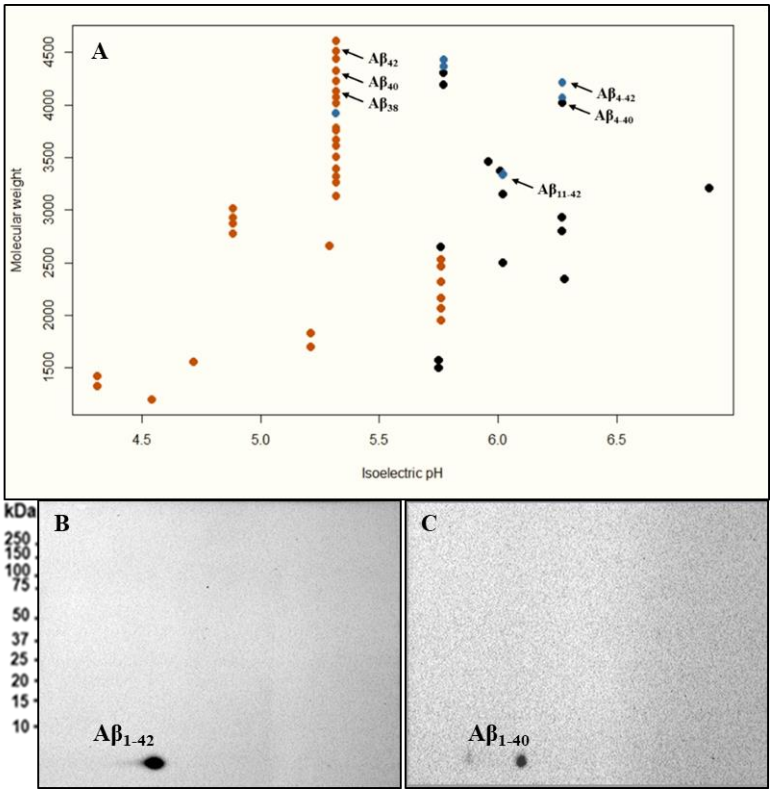

Figure 7: Virtual 2D-PAGE map of common Aβ proteoforms and IB analysis of synthetic peptides. (A) Virtual 2D map of common Aβ proteoforms showing different locations of various C-terminally truncated (orange), N-terminally truncated (blue) and both C and N-terminally truncated (black) proteoforms based on their molecular weight and isoelectric pH (pI). Arrowheads

indicate few proteoforms from our dataset. The immunoblot image for synthetic (B) $A\beta_{42}$ and (C) $A\beta_{40}$ is also presented.

In all tested samples, the molecular weight-based pattern of Aβ monomers and oligomers obtained was in accordance with previous reports for 1D-PAGE and major spots were obtained at 4 kDa, 20 kDa, 24 kDa and 56 kDa, corresponding to monomers, pentamers, hexamers and dodecamers respectively (Figure 8). A similar signature was also obtained by IB using the 4G8 antibody. The pI-based resolution presented the major spots for various N-terminally and C-terminally truncated monomeric Aβ at 4.89, 5.31, 5.76 and 6.27. The presence of spots at pI other than 5.31 validated the presence of proteoforms other than $A\beta_{40}$ and $A\beta_{42}$ in sAD and rpAD brains and confirmed the efficiency of the IP protocol.

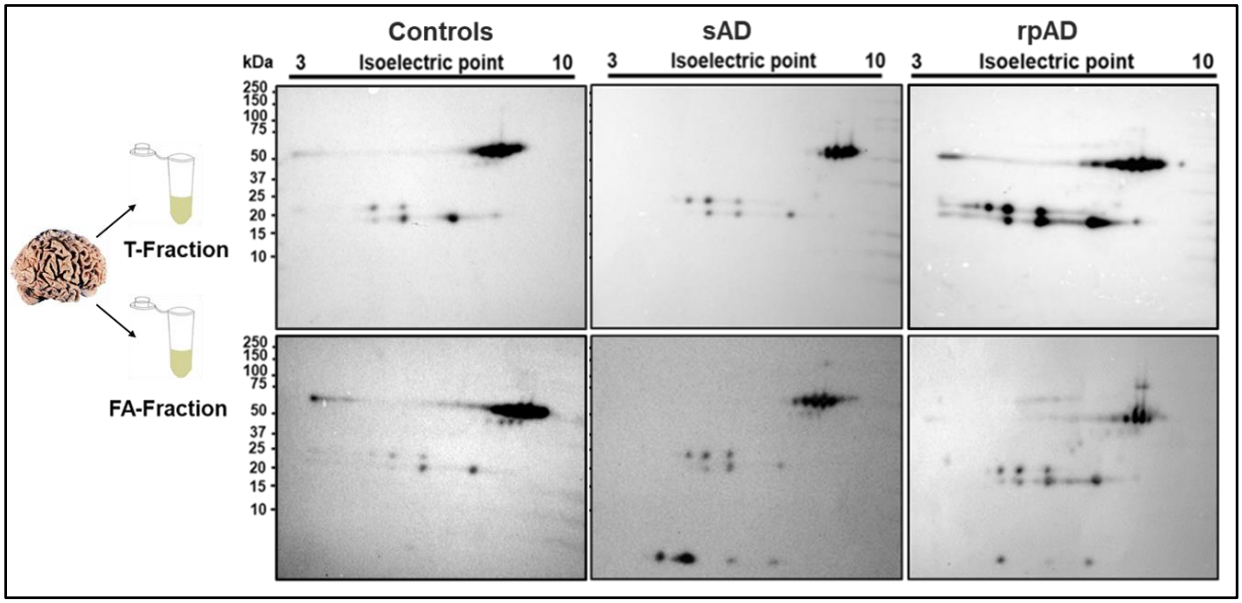

Figure 8: Representative blots for expression of monomeric and oligomeric Aβ proteoforms in sAD, rpAD and control brains. 2D IB, with 6E10 antibody, indicated various N-terminally and C-terminally truncated Aβ proteoforms as monomers, pentamers, hexamers and dodecamers in Tris-soluble and FA-soluble fractions isolated from the brain. Each membrane represents one sample. T-fraction stands for the Tris-soluble fraction.

3.1.2 Aβ-proteoform signature is different in sAD and rpAD

The spots on membranes from all experimental groups were matched using Delta2D software by 100% spot matching approach (Figure 9). Although both Tris-soluble and FA-soluble fractions from sAD and rpAD cases as well as controls were tested, the sensitivity of Western blot allowed the detection of monomeric proteoforms in FA fractions from sAD and rpAD brains only. All tested sAD cases showed spots at pI of 5.31 (corresponding to C-terminally truncated proteoforms,

including $A\beta_{40}$, $A\beta_{42}$, $A\beta_{38}$), 5.76 (presenting shorter C-terminally truncated proteoforms including $A\beta_{20}$, $A\beta_{18}$, $A\beta_{16}$) and 6.27 (showing N-terminally truncated proteoforms including $A\beta_{4\text{-}42}$). An additional spot was detected at pI of 4.89 in one sAD case, that indicates the presence of intermediate C-terminally truncated proteoforms including $A\beta_{26}$. In rpAD cases, on the other hand, the two major spots detected were at pI of 5.31 and 6.27 and only one case showed a faint spot at 5.71.

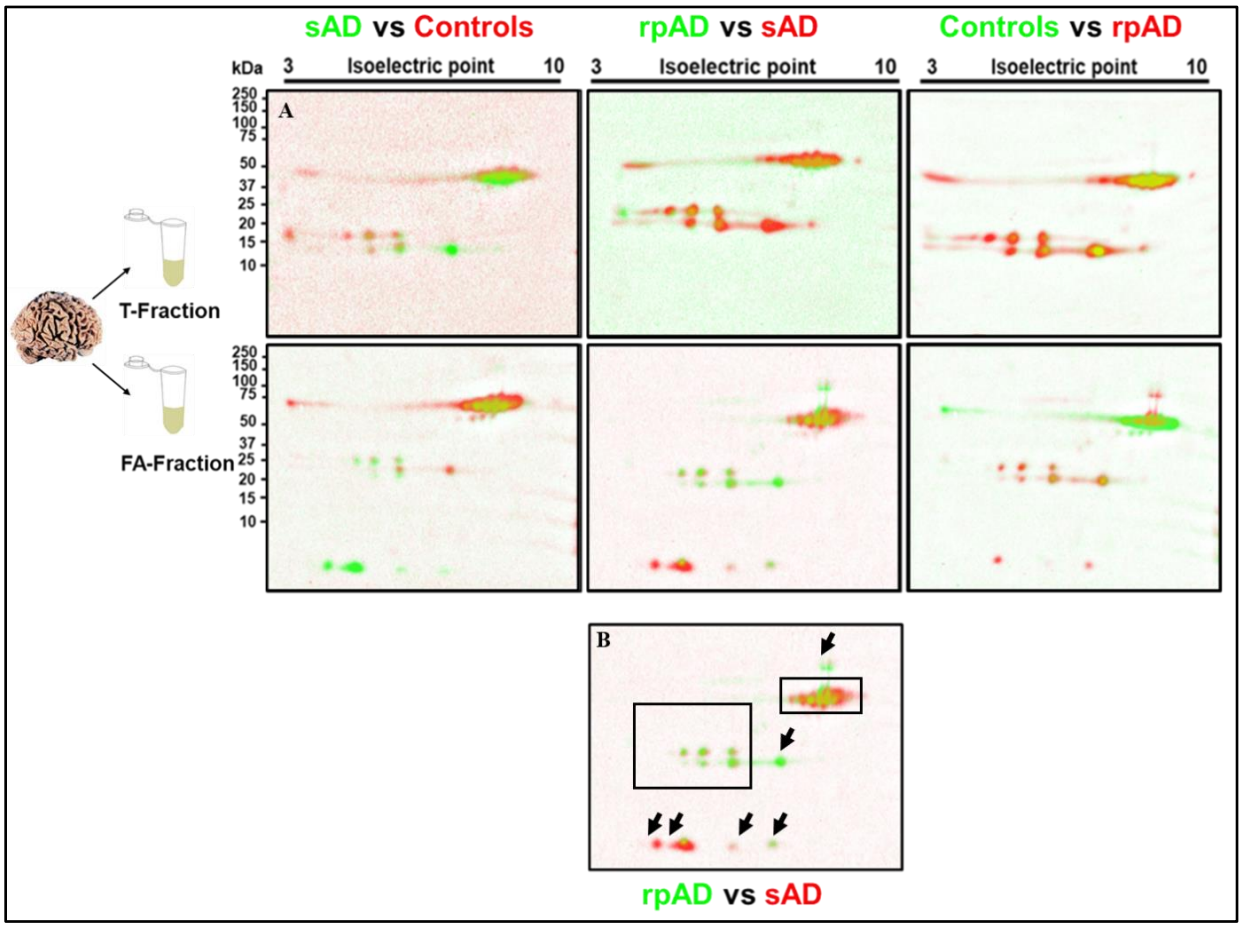

Figure 9: Delta 2D visualized the presence of differentially expressed Aβ proteoforms in sAD, rpAD and control cases. (A) 2D Western blot indicated differential expression of monomeric and oligomeric Aβ proteoforms in sAD, rpAD and control brains. (B) Arrowheads indicate the differentially expressed proteoforms among sAD and rpAD cases. Each membrane represents one sample. A total of five replicates per group were tested for Aβ proteoforms. T-fraction stands for the Tris-soluble fraction.

It is noteworthy that, in all rpAD cases, Aβ was concentrated in 56 kDa and 24 kDa range and fewer spots were present at 4 kDa region, portraying a higher propensity of Aβ from rpAD brains to aggregate in response to SDS in gels (Figure 9). Conversely, sAD cases showed greater variety and expression in 4 kDa region.

3.1.3 $A\beta_{40}$, $A\beta_{42}$, $A\beta_{4\text{-}42}$, $A\beta_{11\text{-}42}$ and their pyroglutamate counterparts are the primary proteoforms in FA-soluble fractions of sAD and rpAD brains

The lack of proteoform-specific antibodies limited the utility of IB analysis for this study therefore, the identification of proteoforms was conducted using various mass spectrometric tools. The first method of choice was LC-ESI MS and spots from Coomassie-stained gels were extracted, digested and subjected to identification via a bottom-up approach. The presence of Aβ was verified in targeted spots, however, tryptic digestion created inference problems by cleaving proteoforms further and masking the endogenous signature (Figure 10A). The top-down approach was then utilized to identify Aβ and dried IP eluates, resuspended in a mixture of FA, isopropanol and ddH_2O (4:4:1), which were directly injected in the column for identification. Peaks for $A\beta_{3\text{-}42}$, $A\beta_{40}$ and $A\beta_{42}$ were identified through this strategy (Figure 10B). Upon replication, this method gave highly non-reproducible findings and the multiply ionized species, characteristic of electrospray ionization method, complicated downstream analysis of identified proteoforms.

Top-down MALDI-ToF MS was next tested for its capability to resolve the signature of endogenous Aβ proteoforms. The dried IP eluates were resuspended in 0.1% TFA and directly spotted on the MALDI plate. Initially, three matrices, namely SA, HCCA, and DHB, known for an efficient ionization of peptides and small proteins were used for ionization. The signal-to-noise ratio (S/N) and the qualities of peaks for all matrices were compared. Using this approach, SA was selected for further analysis based on best resolution, highest S/N ratio, reproducibility and analyzable quality of peaks (Figure 11).

As predicted by Western blot data from 2D-PAGE, identifiable peaks of monomeric Aβ proteoforms were detected only in FA-soluble fractions from sAD and rpAD brains. $A\beta_{40}$ was detected in FA-soluble fractions of some control cases, however these cases were excluded from the analysis as the quality of peaks was poor, resulting in non-reproducible findings. The Tris-soluble fractions presented a pattern similar to the negative controls, indicating that the amount of Aβ was below the detection limit (Figure 11).

Initial experiments identified 38 differentially cleaved Aβ proteoforms through top-down mass spectrometry. However, only the proteoforms that were detected in at least two out of three inde-

pendent experiments were included in the final dataset (Appendix B). Of the 33 proteoforms selected for analysis in sAD and rpAD brains by MALDI-ToF MS, $A\beta_{40}$, $A\beta_{42}$, $A\beta_{4\text{-}42}$, $A\beta_{11\text{-}42}$, pyroglutamate $A\beta_{3\text{-}42}$ ($A\beta_{p3\text{-}42}$) and pyroglutamate $A\beta_{11\text{-}42}$ ($A\beta_{p11\text{-}42}$) were common to both sAD and rpAD cases. $A\beta_{42}$ and $A\beta_{4\text{-}42}$ were most abundant proteoforms in all cases studied. $A\beta_{1\text{-}12}$, $A\beta_{2\text{-}14}$, $A\beta_{3\text{-}14}$, $A\beta_{15\text{-}38}$ and $A\beta_{4\text{-}40}$ were found to be more common in sAD cases, whereas $A\beta_{5\text{-}27}$ and $A\beta_{9\text{-}40}$ were more common in rpAD cases. A heatmap depicting the relative amounts of various proteoforms extracted from individual cases is presented in Figure 12. Experimentally induced modifications were avoided by omitting tryptic digestion, however a 16 Da modification was observed for some proteoforms due to FA treatment.

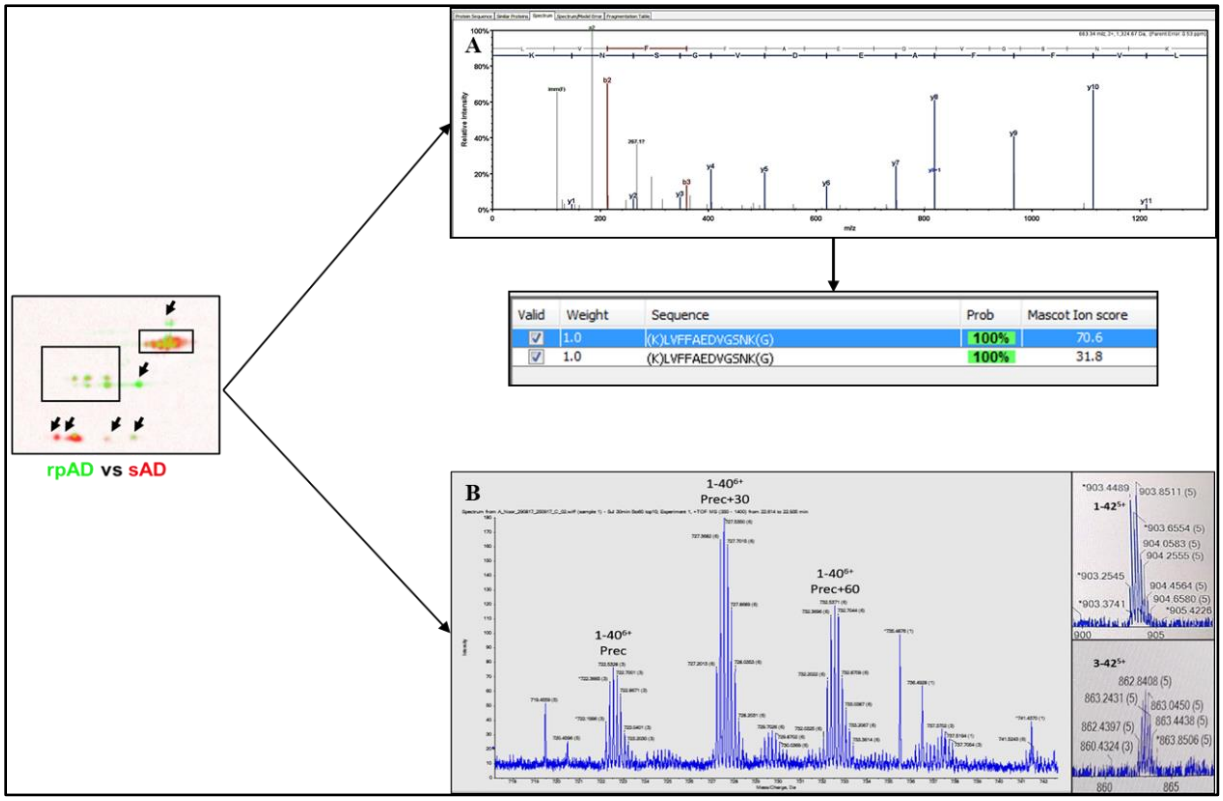

Figure 10: Strategy for identification of Aβ proteoforms through LC-ESI MS. Proteoform signature of Aβ was identified by subjecting either stained gel spots or IP eluates to LC-ESI-MS. (A) The gel-based, bottom-up approach validated the presence of Aβ presented as the extracted ion chromatogram and sequence identified with 100% probability. (B) Peaks for multiply charged ions of $A\beta_{3\text{-}42}$, $A\beta_{40}$ and $A\beta_{42}$ observed through top-down LC-ESI MS.

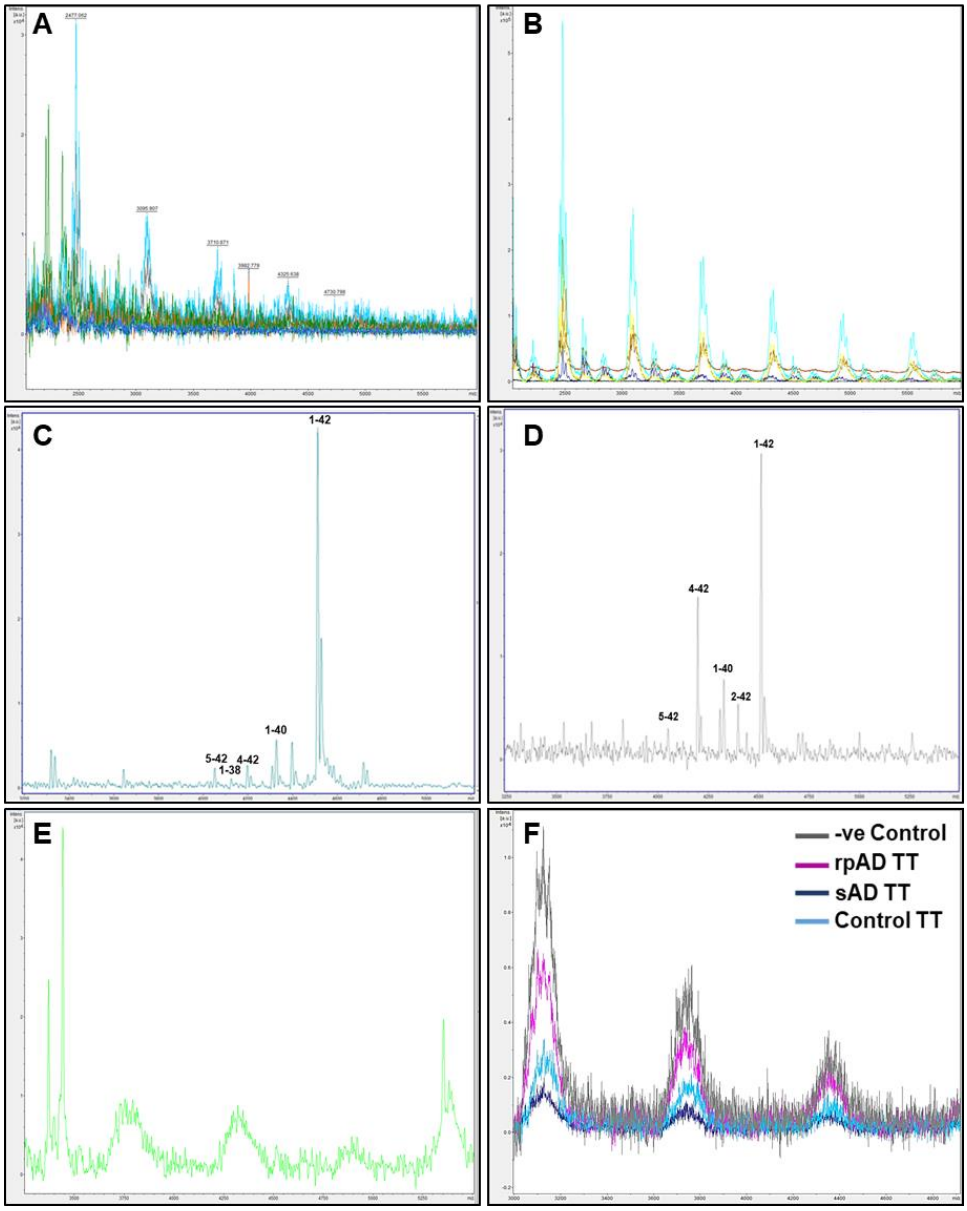

Figure 11: Representative spectra obtained from various fractions isolated from sAD, rpAD and control brains in various matrices. Spectra obtained from various samples in (A) HCCA and (B) DHB overlapped with the spectrum of negative controls and gave very low S/N ratio. On the other hand, samples ionized with SA, especially (C) sAD and (D) rpAD were resolved with high S/N ratio, thus SA was selected for further analysis. Peaks for singly charged $A\beta_{1\text{-}38}$, $A\beta_{2\text{-}42}$, $A\beta_{4\text{-}42}$, $A\beta_{5\text{-}42}$, $A\beta_{40}$ and $A\beta_{42}$ can be observed in both spectra. However, the concentrations of proteoforms in FA-soluble controls (E) and Tris-soluble fractions for all groups (F) were below the detection limits and were excluded from the analysis.

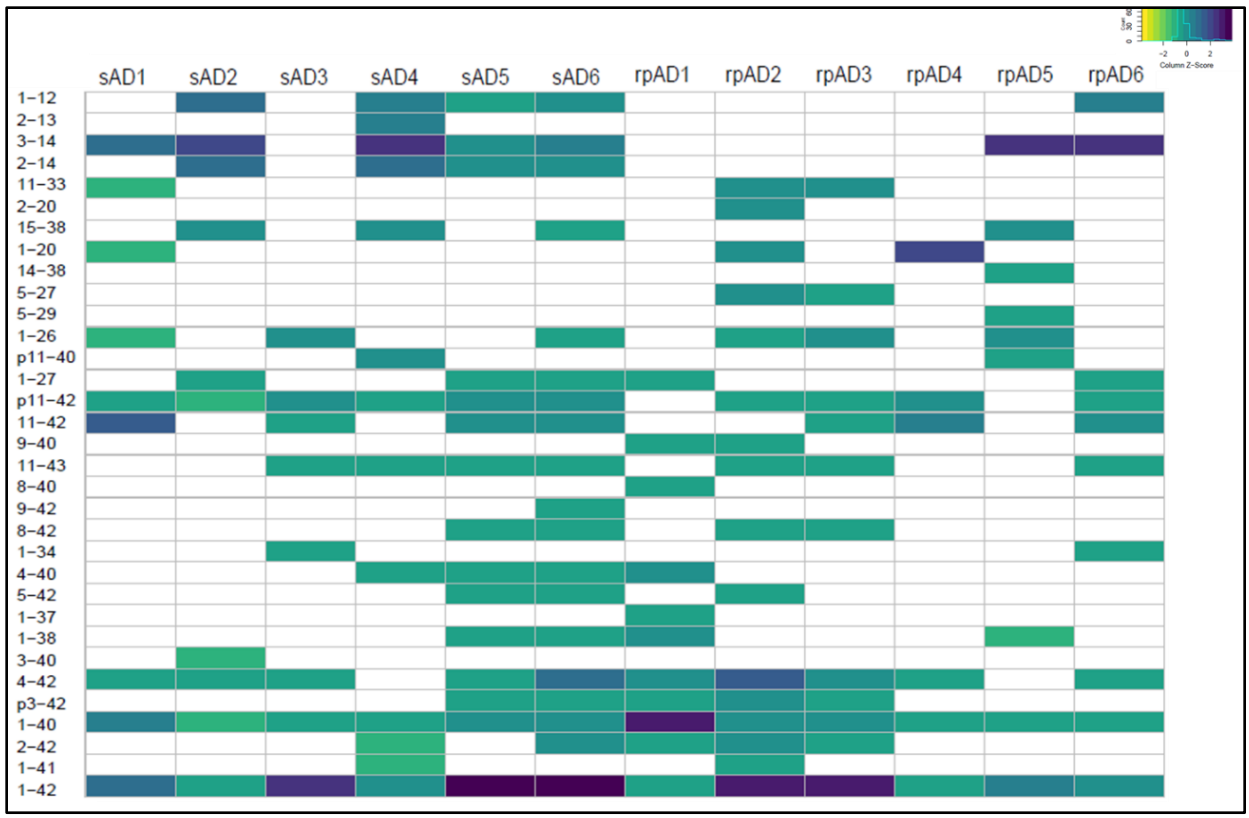

Figure 12: Diversity in proteoforms identified in FA-soluble fraction from sAD and rpAD brains. Top-down MALDI-ToF MS identified 33 different proteoforms of Aβ. Although inter-subject variability is evident in proteoform signature obtained from various cases, $Aβ_{p11-42}$, $Aβ_{11-42}$, $Aβ_{4-42}$, $Aβ_{1-40}$ and $Aβ_{1-42}$ are the most dominant proteoforms. The heatmap depicts the relative intensities of all identified proteoforms, calculated using the average area under the curve (AUC) from five measurements taken for each sample. The intensities were normalized for each sample and the respective Z-scores of proteoforms were used for this plot. pAβ represents pyroglutamate Aβ proteoforms.

3.1.4 No differences are evident in the quantity of APP and Aβ proteoforms in sAD and rpAD

The relative expression of APP affects the downstream generation of Aβ proteoforms. The amount of APP was thus quantified in controls, as well as in sAD and rpAD cases by performing densitometric analysis of 100 kDa band visualized in IB analysis with 6E10 antibody in the Tris-soluble fraction of brain proteins. However, no differences were evident among the three groups. The amount of $Aβ_{Total}$ was also tested in these samples and the 4 kDa band for monomeric Aβ was only visualized in FA-soluble fractions of sAD and rpAD cases, as predicted by 2D-IB and MALDI-ToF MS. Although rpAD appeared to have higher expression of $Aβ_{Total}$, the differences among the two clinical variants were not statistically significant (Figure 13).

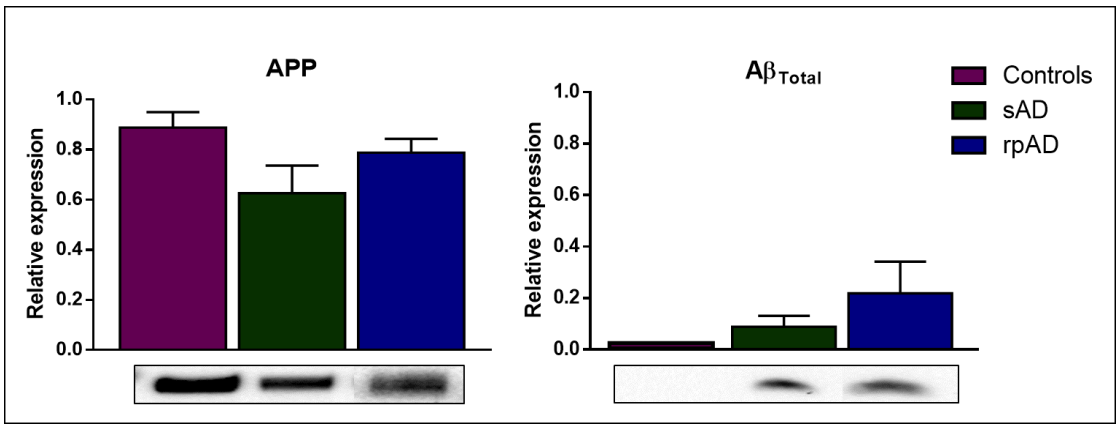

Figure 13: Relative expression of APP and $A\beta_{Total}$ in sAD and rpAD cases. The expression of APP and $A\beta_{Total}$ was quantified using IB analysis with 6E10 antibody (n = 5). Tris-soluble fractions were loaded directly, whereas the FA-soluble fractions were dried, resuspended in Laemmli buffer and sonicated for 10 min before being loaded. APP was only present in Tris-soluble fractions and $A\beta_{Total}$ was present in FA-soluble fraction only. No significant differences were visualized in either IB when tested with one-way ANOVA. All blots were subjected to total protein normalization, and data from three independent experiments were used for densitometric analysis. Error bars represent SEM.

Western blot analysis did not detect Aβ in control cases and the proteoform-specific signature also could not be tested due to the lack of specific antibodies. Therefore, ELISA was performed to test the relative quantities of C-terminally truncated Aβ proteoforms in controls, sAD and rpAD brains. Their quantity was significantly higher in FA-soluble fraction of sAD and rpAD cases in comparison to controls. However, no such trend was evident in the Tris-soluble fraction (Figure 14A). Similarly, results from ELISA measurements for N-terminally truncated proteoforms also showed the highest amounts in the FA-soluble fraction of sAD, followed by rpAD and controls, however, the differences were not significant. Likewise, there were no significant differences among the Tris-fractions (Figure 14B).

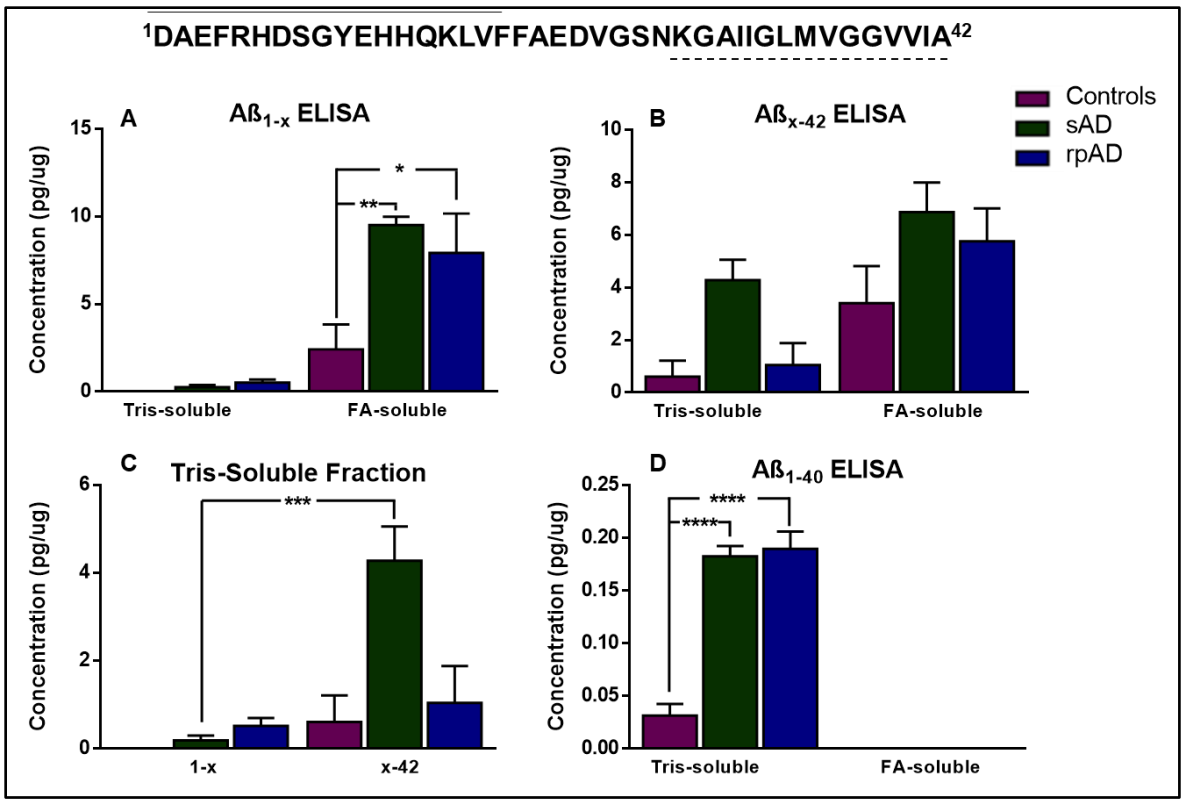

Figure 14: Relative expression of N-terminally and C-terminally truncated proteoforms of Aβ in brain samples. The graph presents the quantities (pg/µg of total brain protein) of various (A) C-terminally and (B) N-terminally truncated proteoforms isolated from Tris-soluble and FA-soluble fractions from controls, sAD and rpAD cases (n = 4-6). (C) Comparison of various truncations within the Tris-soluble fractions. (D) The relative quantity of $A\beta_{1\text{-}40}$ in various experimental groups. All samples were measured as duplicates and the average concentrations were used for analysis. One-way ANOVA, followed by Tukey's multiple comparisons test, was used for statistical analysis. Error bars represent SEM. (*=p≤0.05; **= p≤0.01; ***= p≤0.001)

In Tris-soluble fractions, ELISA results showed a lower amount of C-terminally truncated proteoforms in comparison to N-terminal truncations in all control, sAD and rpAD cases. This trend was especially evident in sAD cases, where the amount of N-terminally truncated Aβ was significantly higher than its C-terminal counterparts, possibly because shorter proteoforms are less prone to aggregation and are frequently formed during the clearance of highly aggregated, larger proteoforms (Figure 14C). The FA-soluble fractions showed no significant differences among N-terminally and C-terminally truncated pools. Additionally, $A\beta_{40}$ was only present in detectable amounts in Tris-soluble fraction and its quantity was significantly higher in sAD and rpAD cases in comparison to controls (Figure 14D).

CSF from sAD, rpAD and control cases was also tested for N-terminal and C-terminal truncations. Although the amount of C-terminally truncated proteoforms was significantly higher ($p \leq 0.0001$) in all three study groups than their N-terminally truncated counterparts, no significant trend was evident within groups for either ELISA test (Figure 15).

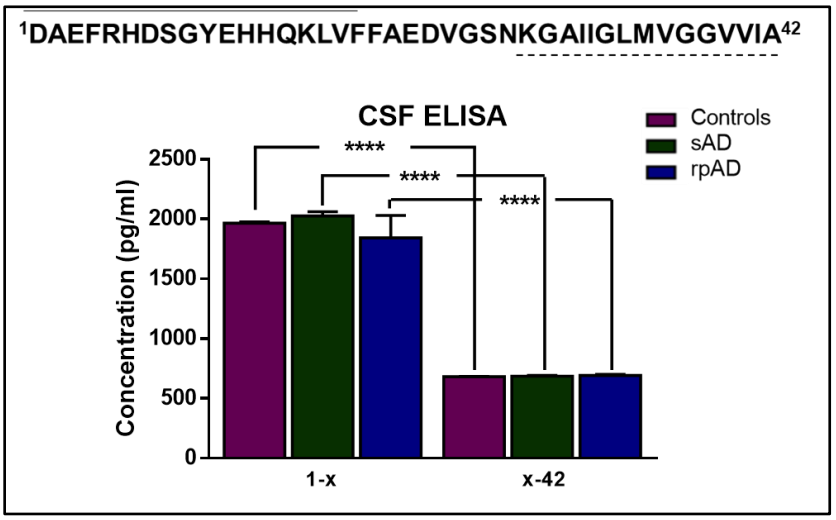

Figure 15: Relative expression of N-terminally and C-terminally truncated proteoforms of Aβ in CSF samples. No significant differences were observed among experimental groups for either ELISA test, but the amount of C-terminally truncated proteoforms was significantly higher than N-terminally truncated proteoforms in all three study groups (n = 6). All samples were measured as duplicates and the average concentrations were used for analysis. One-way ANOVA, followed by Tukey's multiple comparisons test, was used for statistical analysis. Error bars represent SEM. (****= $p \leq 0.001$).

3.1.5 The expression of β-secretase, relative to α-secretase, is significantly higher in rpAD

The slight differences in the signature of proteoforms among sAD and rpAD cases called for the quantification of Aβ-cleaving enzymes. Western blot analysis was performed for enzymes that take part in the generation and clearance of Aβ, including α-secretase (ADAM-10), β-secretase (BACE-1), γ-secretase (PSEN-1, PSEN-2 and Nicastrin), plasmin and IDE. Owing to the alteration in the expression of enzymes in various stages of the disease, sAD cases were divided into two groups corresponding to Braak stages I-III (early sAD) and Braak stages IV-VI (late sAD). However, no significant differences were observed in their expression levels among controls, sAD and rpAD cases for the tested proteases (Figure 16).

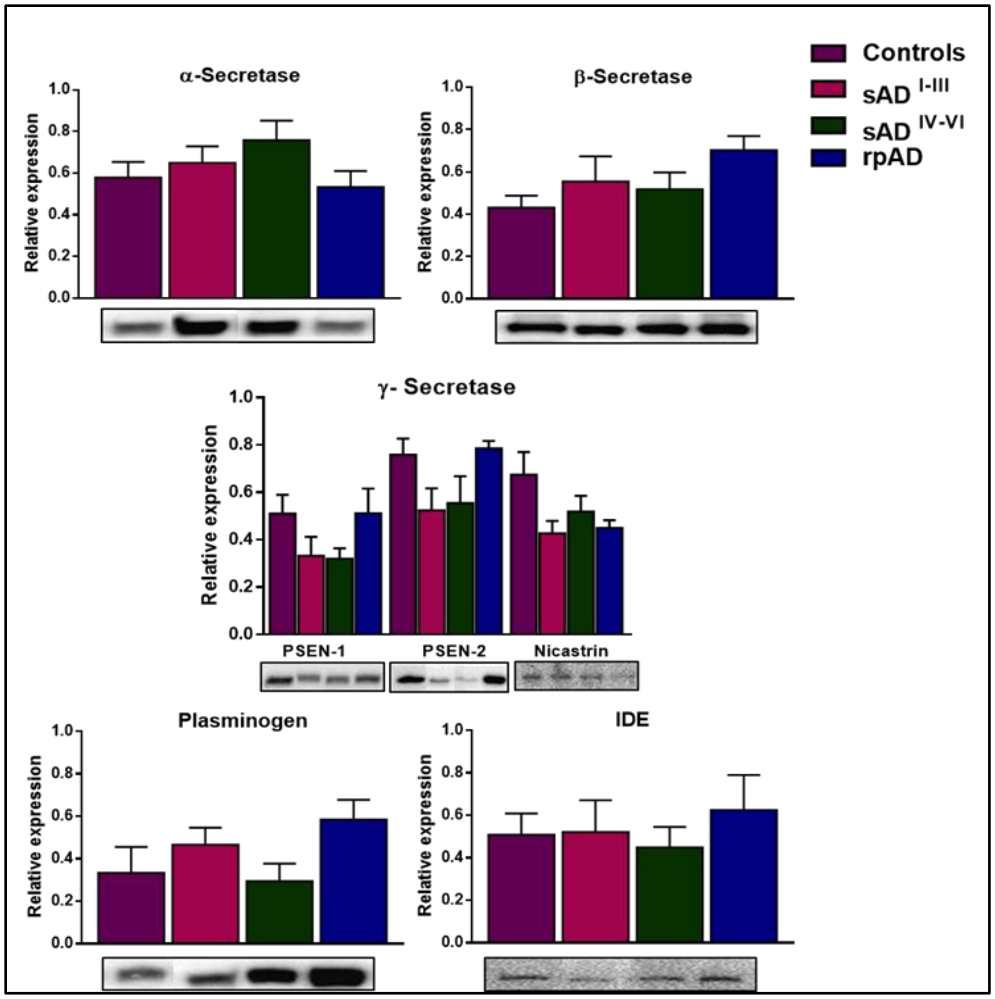

Figure 16: Western blot analysis for the relative expression of major Aβ-cleaving enzymes. The relative expression of α-secretase, β-secretase, γ-secretase, plasmin and IDE in non-demented controls, early sAD (Braak stages I-III), late sAD (Braak stages IV-VI) and rpAD cases demonstrated no significant differences (n = 6). All blots were subjected to total protein normalization. Densitometric analysis was conducted using data from three independent experiments. One-way ANOVA, followed by Tukey's multiple comparisons test, was used for statistical analysis. Error bars represent SEM.

Interestingly, the expression of BACE1, our targeted β-secretase, relative to ADAM-10, was significantly higher in rpAD in comparison to other groups, indicating increased cleavage of Aβ through the amyloidogenic pathway in these cases (Figure 17).

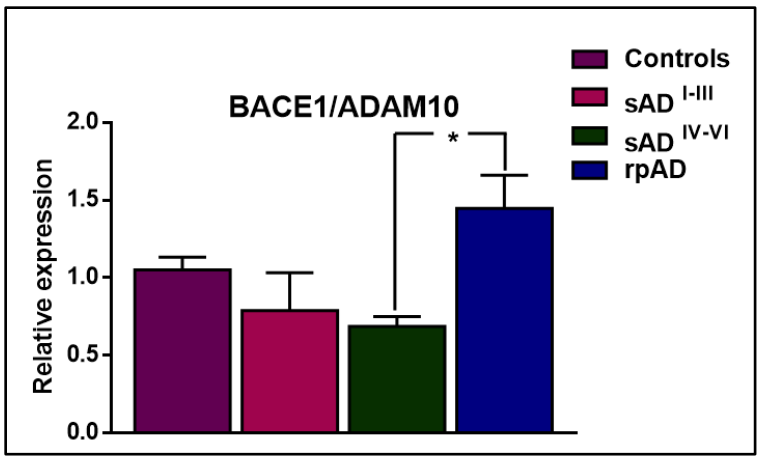

Figure 17: Ratio of BACE-1/ADAM-10 in typical and rapidly progressive AD. The graph depicts the expression of BACE-1 in relation to ADAM-10 in non-demented controls, early sAD (Braak stages I-III), late sAD (Braak stages IV-VI), and rpAD cases (n = 6). One-way ANOVA, followed by Tukey's multiple comparisons test, was used for statistical analysis. Error bars represent SEM. (* = $p \leq 0.05$).

3.2 Structural heterogeneity in fibrils extracted from sAD and rpAD brains

Structural alterations in fibrillar aggregates formed by Aβ proteoforms are another source of variability in the Aβ-induced toxic effects and are frequently used as an explanation of heterogeneity in the clinical presentation of AD cases. Slight alterations in structure translate to modified biochemical properties, incubation periods, propagation and toxicities. As our IB and ELISA experiments detected no significant differences in the quantities of Aβ proteoforms in section 3.1.4, it was proposed that the differences in the clinical presentation may lie in the attributes of fibrils rather than their quantities. Hence, this part of the project focused on establishing if fibrils extracted from sAD and rpAD cases have differences in aggregation kinetics, secondary structure and 3D morphologies.

The study of structural differences within endogenously generated fibrils requires mild purification protocols where tissue homogenization methodology and extraction agents do not damage and alter the specific 3D morphology of fibrils. Consequently, the total amount of extracted fibrils is reduced, and large amounts of brain tissue are required for biophysical studies. To overcome these challenges, Aβ fibrils were extracted by slight alterations in previously optimized protocols featuring homogenization of brain tissue by mild methodology using differential ultracentrifugation (Lu et al., 2013). The presence of fibrils in the extracted fractions was confirmed by Th-T staining (Figure 18). They were sonicated to increase the number of seeding units and amplified using RT-

QuIC reactions. RT-QuIC ensures that the structural characteristics of fibrils are copied onto substrate proteoforms added in the reaction. The total amount of brain tissue utilized was thus reduced and analyzable quantities of fibrils were obtained. As reported in section 3.1.3 of this study, $A\beta_{40}$ and $A\beta_{42}$ are some of the most common proteoforms reported in aggregates in both sAD and rpAD patients. Therefore, synthetic $A\beta_{40}$ and $A\beta_{42}$ were used as a substrate for RT-QuIC reactions.

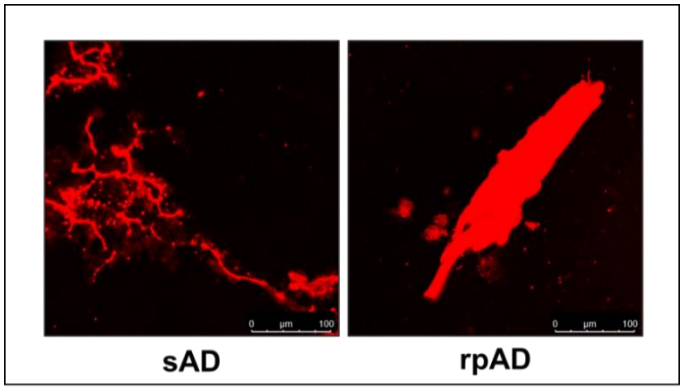

Figure 18: Thioflavin-T-stained images of Aβ fibrils extracted from sAD and rpAD brains. Fibrils purified via ultracentrifugation were mixed with Th-T (10:1) and imaged using confocal microscopy to validate the efficiency of our purification protocol. The image shows fibrils visualized in sAD and rpAD samples. The number of fibrils in control samples was too low, therefore, an image for that experimental group is not included. Scale bar represents 100 µm.

3.2.1 Brain-derived Aβ fibrils from sAD and rpAD cases feature different aggregation kinetics

Fibrils extracted from all experimental groups were amplified and their subsequent RT-QuIC profiles were utilized to establish differences in their aggregation kinetics. Unlike other amyloidogenic proteins, where the aggregating seed is only present in cases with the disease, fibrillar Aβ is also present in healthy controls, and the substrate itself (especially longer proteoforms including $A\beta_{40}$ and $A\beta_{42}$) has a high propensity to self-aggregate. Hence, the efforts to optimize the protocol were initially targeted to ensure that samples without any seed (substrate-only controls) undergo minimal aggregation. The signal obtained for unseeded reaction was negligible in comparison to their seeded counterparts. The samples without any substrates (seed-only controls) were also not positive for RT-QuIC (Figure 19). A similar trend was also observed in non-demented controls, where the signal showed no increase throughout the reaction, showing that Aβ proteoforms in these cases were probably not enough to seed the conversion under our reaction conditions (Figure 19B). Only reactions seeded with the extract from sAD and rpAD brain showed an increase in Th-T

signal in this experiment. Interestingly, the conversion of monomeric substrate to its fibrillar, β-sheet-rich counterpart was faster in sAD cases in comparison to rpAD, as indicated by kinetic curves in Figure 19C. However, seeds corresponding to Tris-soluble fraction showed no such trend (Figure 19D).

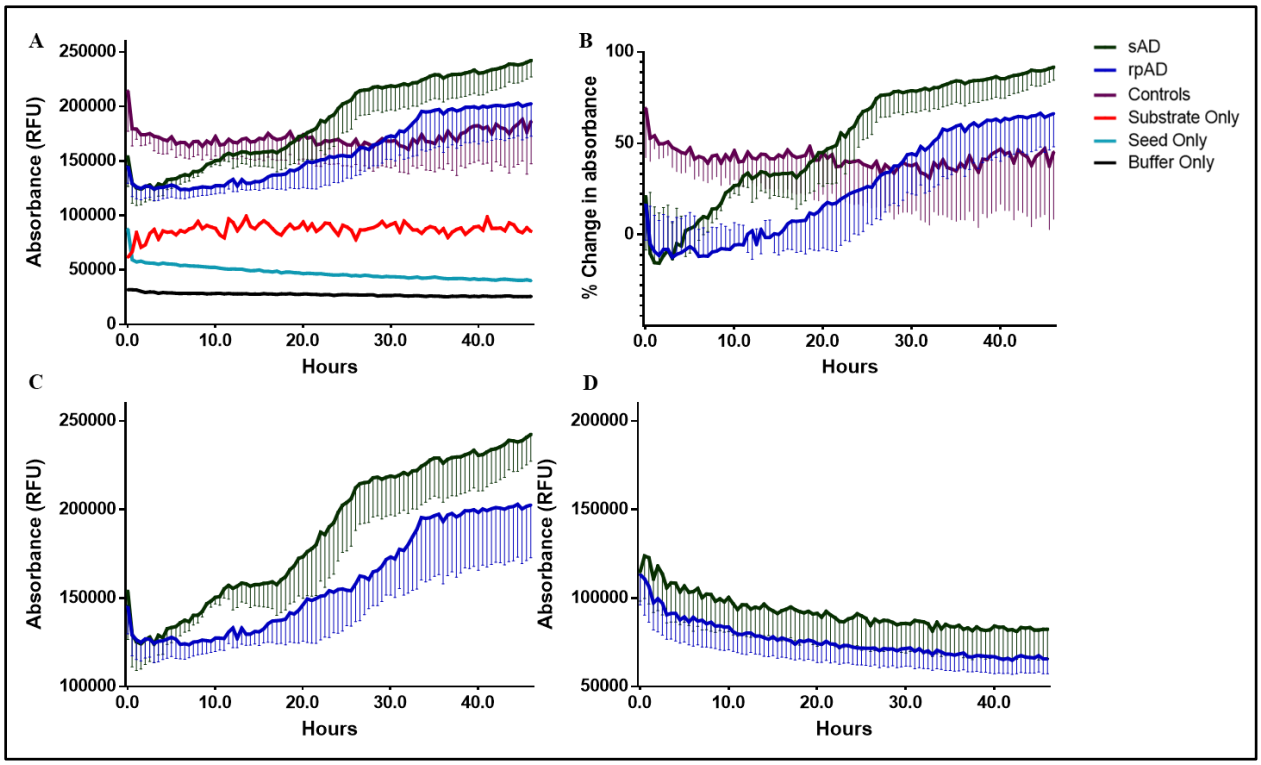

Figure 19: Kinetic curves obtained for Aβ RT-QuIC reactions seeded with the fibrillar extract from sAD, rpAD, and controls. (A) The graph was plotted using an average of four measurements recorded for each of three biological replicates in every experimental group in two independent experiments. One reading was recorded every 30 min for 46 hr. No seeding was observed in seed-only and substrate-only controls. (B) Non-demented controls depicted higher absorbance in comparison seed-only and substrate-only controls, however, no increase was recorded in the signal throughout the experiments, indicating that no seeding occurred in this group. (C) Only the rpAD and sAD showed an increase in Th-T signal and seeding occurred faster in sAD cases. (D) Seeds extracted in PBS (corresponding to Tris-soluble fraction) failed to undergo aggregation under these reaction conditions. Error bars represent SEM.

The trend observed in RT-QuIC profiles was further verified by running the products on native-PAGE (Figure 20). Two major bands (around 28 kDa and 250 kDa) were detected by silver staining. Their intensity was higher in rpAD and sAD cases (250 kDa band had higher intensity than 28 kDa band) in comparison to other groups, suggesting more efficient conversion of substrate into aggregates. Faint bands were present in non-demented and seed-only controls, however, the absence of an increase in Th-T signals in these cases depicts that these might be the components

of the reaction mixture in their original confirmation or that the control cases might be aggregating very slowly. Importantly, no higher-order aggregates (250 kDa and higher) were detectable in substrate-only controls, demonstrating that conversion was only positive in the presence of seed.

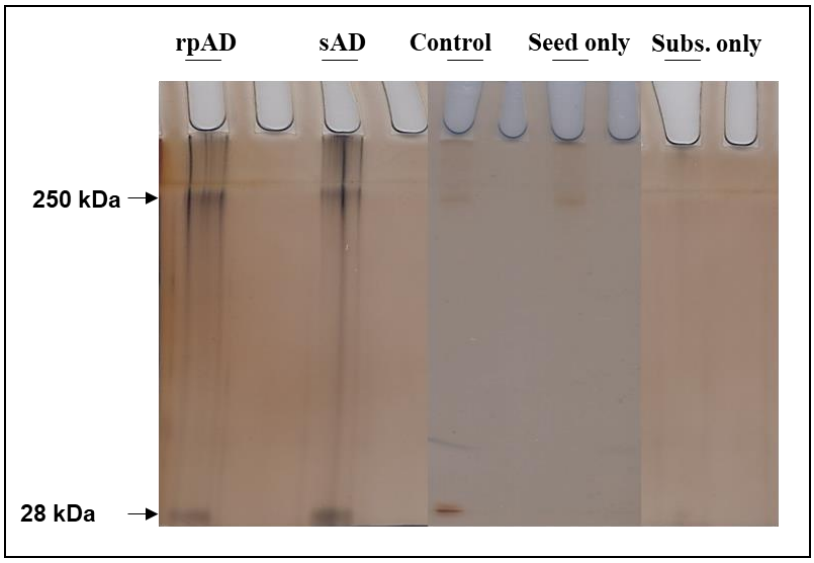

Figure 20: Native gels for verification of Aβ aggregation in RT-QuIC reaction. RT-QuIC products were resolved on native gels and the bands were visualized using silver staining. The intensity of higher-order aggregates (> 250 kDa) was higher in sAD and rpAD cases than non-demented controls, while they were completely absent in substrate-only controls ruling out the self-aggregation of the substrate.

Although the ELISA and IB results in section 3.1.4 showed that the amount of various Aβ proteoforms was not significantly different in sAD and rpAD cases, additional dot-blot assays were employed to characterize the RT-QuIC reaction mixtures and ensure that the differences in aggregation kinetics are attributed to the biochemical nature of the seeds, not their quantity. No significant differences were observed in both the concentration of Aβ in the reaction mixture and Th-T absorbance of purified fibrils before RT-QuIC analysis, thereby confirming the existence of different Aβ strains in brain extract obtained from sAD and rpAD (Figure 21).

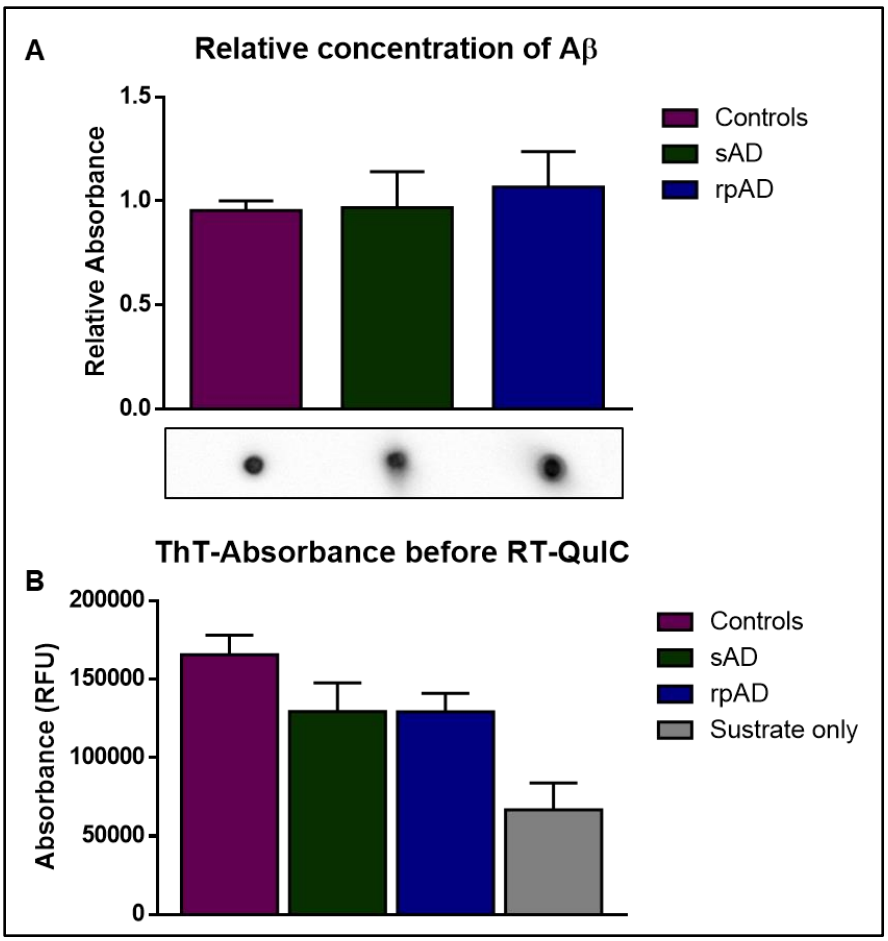

Figure 21: Characterization of RT-QuIC reaction mixtures. (A) The total amount of Aβ in RT-QuIC reaction mixtures was assessed via dot-blot assays with 6E10 antibody. No significant differences were evident in the relative absorbance. Data from three independent experiments were used for analysis. (B) Th-T absorbance, another parameter to analyze the total amount of amyloids in the mixture, also demonstrated no significant differences in fibrillar Aβ among sAD and rpAD cases. One-way ANOVA, followed by Tukey's multiple comparisons test, was used for statistical analysis. Error bars represent SEM.

3.2.2 Aβ aggregates from clinical subtypes of AD vary in size and morphology

Differences in Aβ aggregates seeded using extracts from sAD, rpAD and control brains were visualized using confocal and atomic force microscopy. The RT-QuIC reactions seeded with rpAD brain extracts yielded significantly larger aggregates in comparison to aggregates generated by sAD and non-demented controls, despite their slower rates of aggregation observed in section 3.2.1. sAD cases produced smaller but more frequent aggregates, but their size was not signifi-

cantly different from controls (Figure 22). Smaller aggregates were also present in seed and substrate-only, however, the fact that that no increase in Th-T signal was observed during their generation indicated that these structures did not change during the reaction. Moreover, their frequency was too low for analysis, so these samples were not included in the graph.

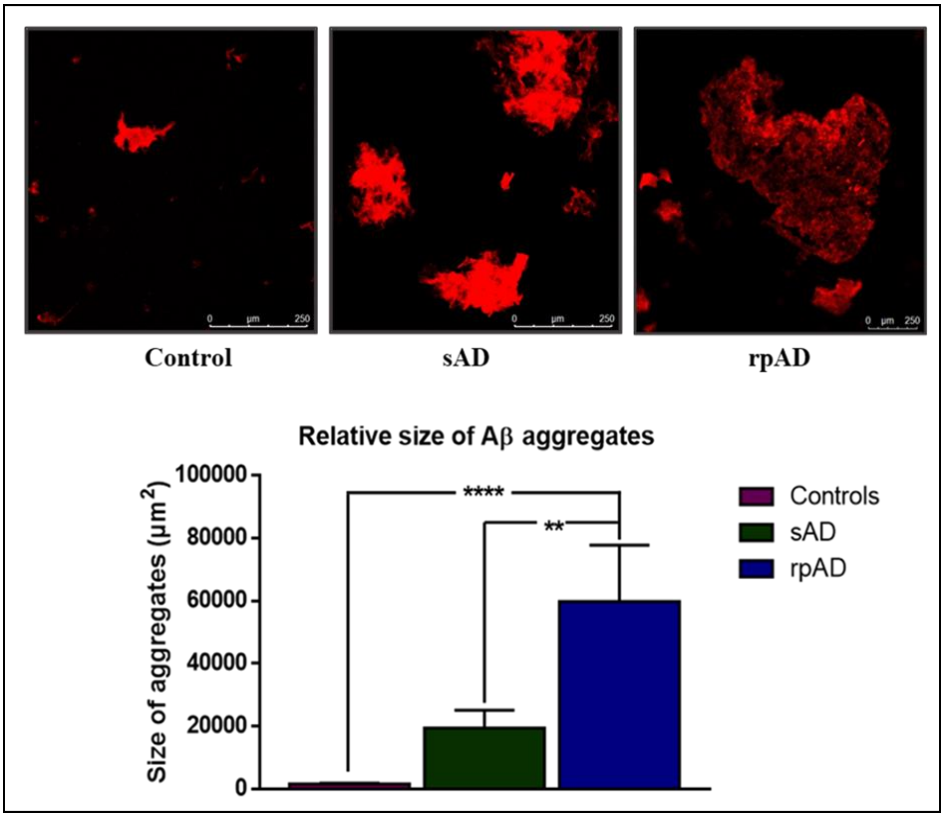

Figure 22: Differences in sizes of aggregates from sAD and rpAD visualized by Th-T staining and confocal microscopy. RT-QuIC products from each well were mixed with Th-T (1:10), deposited on glass slides and imaged immediately using 488 nm filter. The size of the aggregates was calculated by measuring the average size of 40-50 structures per experimental group. The aggregates from rpAD were significantly larger than those observed for controls and sAD. One-way ANOVA, followed by Tukey's multiple comparisons test, was used for statistical analysis. Scale bar represents 250 µm and error bars present SEM (**= $p \leq 0.01$; ****= $p \leq 0.0001$).

Although confocal microscopy was useful to calculate the average size of aggregates, its resolution was not sufficient to visualize alterations in the 3D structure of individual fibrils. Therefore, atomic force microscopy was performed on RT-QuIC products. As expected, a similar trend was observed for the three experimental groups. rpAD samples featured large amorphous structures, whereas sAD cases presented smaller aggregates with well-defined fibrils. The amorphous structures observed for rpAD may be products of highly hydrophobic fibrils that have higher propensity to bind with each other and generate a plaque-like morphology. The control samples just presented small

globular structures suggesting that these cases did not seed the aggregation of the substrate (Figure 23).

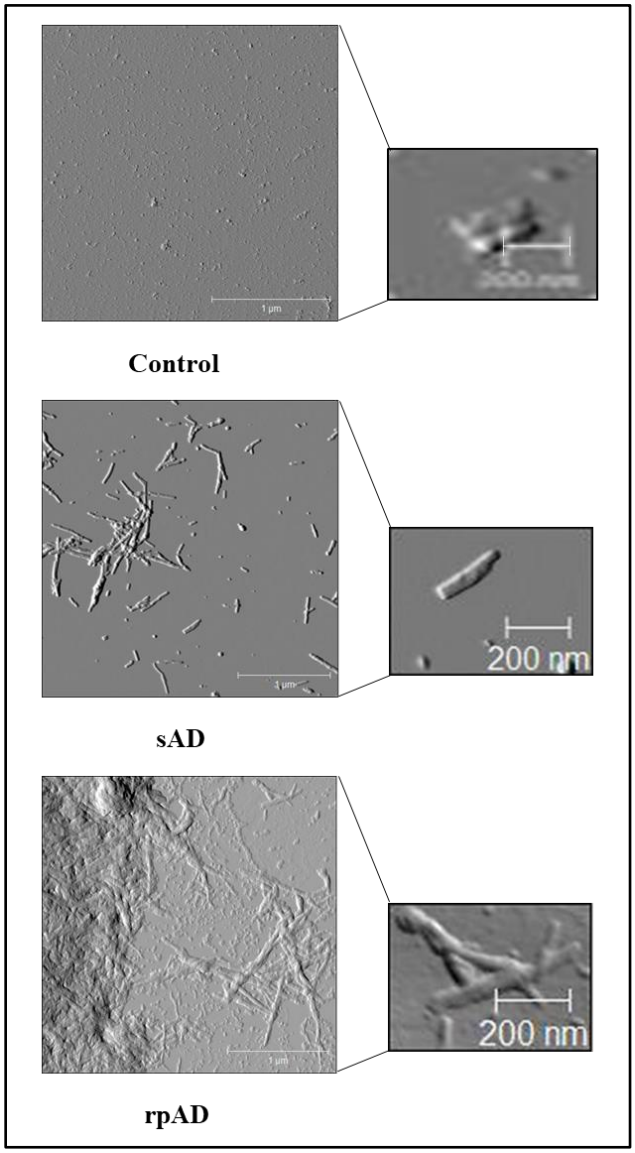

Figure 23: Representative amplitude images obtained for RT-QuIC products via tapping mode atomic force microscopy. Samples were coated on freshly cleaved mica and imaged immediately. Control cases presented globular seeds-only, whereas sAD and rpAD cases showed fibrillar and amorphous aggregates respectively. Zoomed in figures present the detailed structure of fibrils. Scale bar represents 1 µm and 200 nm.

The average thickness of fibrils obtained from sAD and rpAD samples was calculated to further validate the differences in 3D folding of Aβ. The fibrillar structures observed in sAD seeded reactions had significantly lesser thickness in comparison to those seeded by rpAD extract. Importantly, only the thickness of distinct fibrils was measured and larger aggregates, where fibrils

were buried inside the structure, were ignored to avoid bias in data (Figure 24A). The maximum height of aggregates observed was also higher for rpAD cases in comparison to sAD cases (Figure 24B and C). Since no distinct fibrils were visible in control cases, their measurements were not included in the data set. The globular aggregates they formed had an average diameter of 200 ± 16.6 nm and might just present seeds that failed to undergo any aggregation.

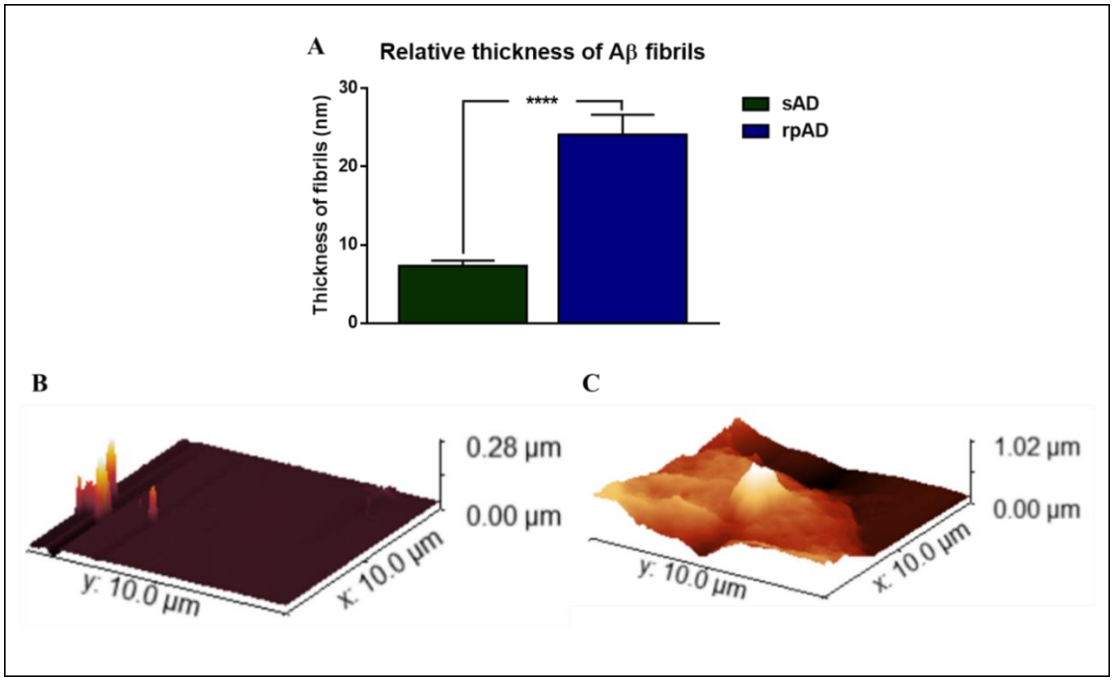

Figure 24: Differences in fibrils and aggregates seeded with sAD and rpAD brain extract. All atomic force microscopy data was levelled by three-point levelling tool and heights of individual fibrils and larger aggregates were measured using 2-3 height retrace images per sample. (A) rpAD cases featured thicker fibrils in comparison to sAD cases. Consequently, the maximum height of aggregates observed for sAD cases (B) was much lower than that observed for rpAD cases (C), as seen in the 3D height profiles. Statistical analysis was performed using unpaired Student's T-test. Error bars represent SEM. (****= $p \leq 0.001$).

3.2.3 FTIR spectroscopy detected no differences within secondary structures in Aβ aggregates

The stability of amyloid fibrils relies on their secondary structures. FTIR spectroscopy was used to study the amide I, II and III bands, located at 1645, 1551 and 1230 cm^{-1} of the infrared spectrum, respectively, and to analyze differences in the secondary structures of fibrils generated by sAD and rpAD samples in RT-QuIC reactions. The amide I band is especially useful in predicting the percentage of α-helices and β-sheets within amyloid fibrils. However, no differences were detected in the location of peaks for sAD and rpAD fibrils indicating that secondary structures of fibrils

from these experimental groups were highly similar. A greater intensity of peaks for sAD cases within the Amide I region, reflects a higher concentration of ordered fibrils, in comparison to rpAD. Interestingly, control cases also presented a similar spectrum depicting that the secondary structure of misfolded seeds within these samples was also similar to the one translated onto growing fibrils (Figure 25).

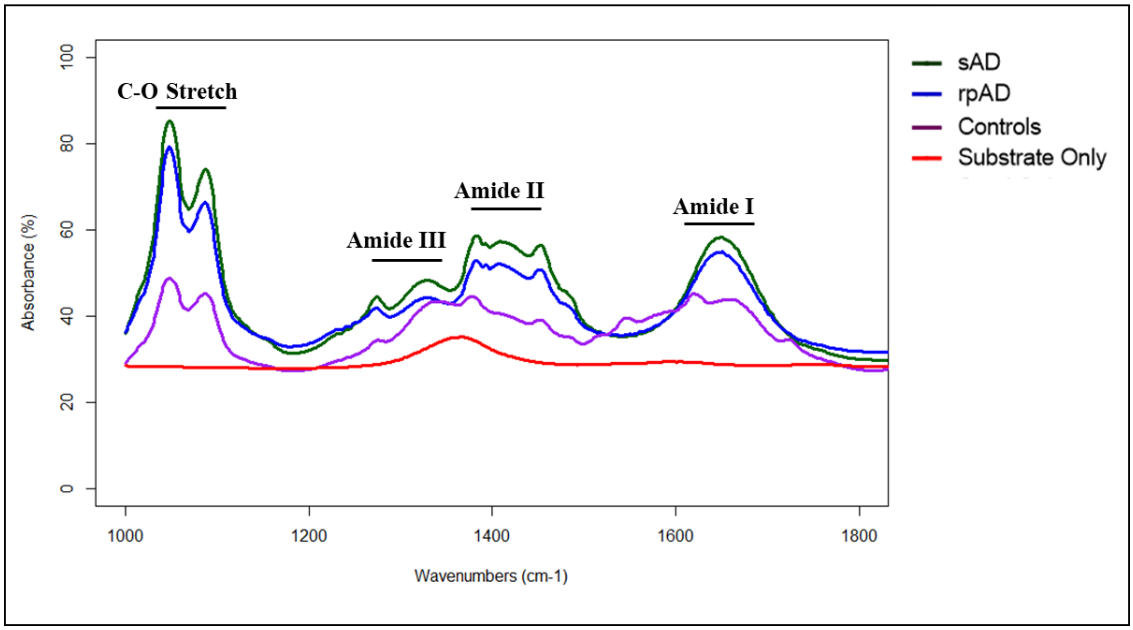

Figure 25: Difference in secondary structures of RT-QuIC products seeded by brain extracts from different experimental groups. FTIR spectroscopy detected no shifts in peaks obtained for different amide bands from sAD and rpAD cases indicating similarities in secondary structures. The peaks from control samples also resided around the same range of wave lengths, while a decrease in their absorbance reflected a lower amount of targeted functional groups. Substrate-only controls were included to show the background absorbance in the absence of any seed in the reaction. The figure presents the average absorbance recorded from products obtained from two independent experiments for each sample.

3.3 sAD- and rpAD-derived Aβ fibrils have similar toxicities

The toxicities of Aβ proteoforms and their respective fibrillar aggregates rely on their ability to interact with various cellular components and organic molecules. Owing to the heterogeneity in the types of structures obtained by RT-QuIC, the samples were centrifuged before their application on the cells. Two fractions, oligomeric and plaque-associated fibrils were obtained and applied to cells separately. It is noteworthy that the plaque-associated fraction showed little to no protein content, suggesting that the sizes of fibrils obtained from each experimental group qualified to be in the oligomeric fraction. No differences were observed in the survival of SH-SY5Y cells treated

with plaque-associated fibrils from control, sAD and rpAD seeded reactions. Fibrils obtained from sAD and rpAD fractions were more toxic to the cells than the control group, however, the differences within these two groups were not significant (Figure 26).

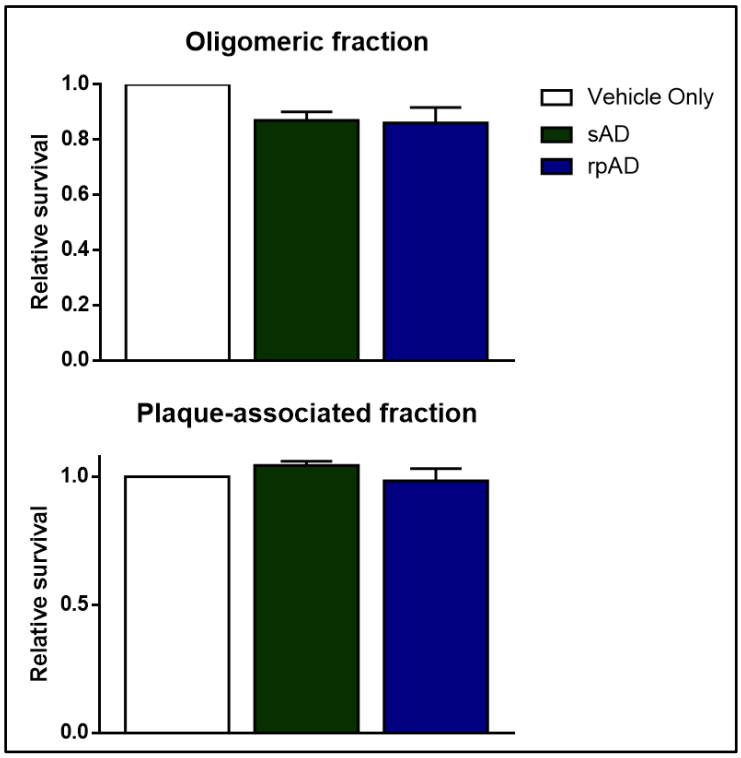

Figure 26: Relative toxicities of sAD- and rpAD-derived fibrils in SH-SY5Y cells. Cells were treated with RT-QuIC products for 24 hr and the toxicity was measured using MTS assay. The survival of samples, relative to vehicle-exposed cells, treated with the oligomeric fraction from sAD and rpAD cases showed higher toxicity compared to cells treated with plaque-associated fractions, however, the differences within these groups were not significant. The plaque associated fractions showed no differences in toxicity. Data from three independent experiments were utilized for this plot. One-way ANOVA, followed by Tukey's multiple comparisons test, was used for statistical analysis.

3.4 sAD and rpAD present a distinct signature of Aβ-interactors and accessory proteins

All protein-forming complexes with Aβ isolated from sAD, rpAD and control brains were identified using co-IP followed by LC-ESI MS/MS. CJD was added as another experimental group to this experimental set-up to test for similarities in Aβ interactors extracted from brains of rpAD and CJD patients. Although Aβ pathology is not the primary driving force behind CJD, Aβ plaques have previously been reported in CJD cases (Rossi et al., 2019). A total of 182 proteins were

detected in this dataset, however, after removing the common contaminants and the proteins that were reported in negative controls, 41 interactors were filtered. Only the proteins that were reported in at least two out of four biological replicates for each experimental group with a spectrum count of more than 2 and a confidence threshold of 99.0% were included in the final dataset. The disease-specific distribution of Aβ interactors is summarized in Figure 27 while the detailed characteristics of identified interactors are presented in Table 7.

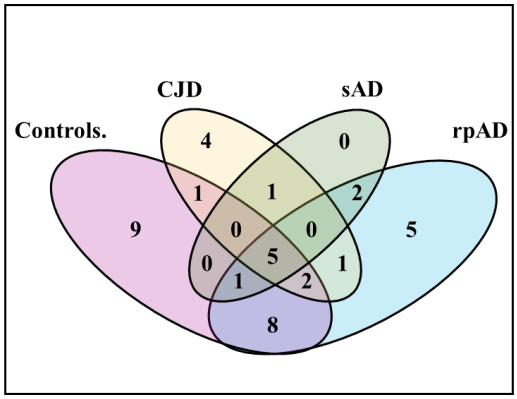

Figure 27: Disease-specific distribution of Aβ interactors isolated from Tris-soluble fractions of brain tissue obtained from controls, sAD, rpAD, and CJD. The signature of Aβ interacting partners was obtained by identifying the proteins purified through co-IP (n = 4). The figure depicts the disease-specific distribution of these interacting partners.

However, several key interactors of the target peptide, like tau and PrP^{C}, were missing in the dataset from the Tris-soluble fractions. In an attempt to get an insight into potential binding partners of remaining Aβ in the FA-soluble fraction, a similar co-IP was performed. However, solubilization and extraction of proteins in FA breaks all the intrinsic interactions and all the interacting partners detected by LC-ESI MS/MS for this fraction are a result of *in vitro* interactions between Aβ and neutralized proteins (proteins undergo partial refolding upon neutralization) formed during overnight incubation. CJD cases were not included in this experiment as they did not present any promising differences in the IP experiment conducted on Tris-soluble fraction. The disease-specific signature of these *in vitro* interactors is shown in Figure 28. Since the interactions were not limited by compartmentalization of proteins, as is the case of *in vivo* interactions, a total of 614 proteins were detected in this dataset, however, after removing the common contaminants and the proteins that were detected in negative controls, 340 interactors were finalized. The specificity, biological functions and localization of these proteins are detailed in Appendix C.

Table 7: Aβ interactors isolated from Tris-soluble fractions of controls, sAD, rpAD and CJD. The list of Aβ-interacting partners obtained through co-IP, along with their localization, function and distribution, is summarized (n = 4). The localization and biological functions of identified Aβ interactors were annotated using the UniProtKB database. 'A' stands or sAD, 'R' for rpAD, 'C' for controls, 'Mit' for mitochondria, 'Nu' for nucleus, 'Cy' for cytoplasm, 'Cysk' for cytoskeleton, 'Mem' for cell membrane and 'ER' for endoplasmic reticulum.

Identified Proteins	UniProt ID	Localization	Functional Category	Specificity
ATP synthase subunit beta	P06576	Mit	Energy metabolism	C, R.
40S/60S ribosomal proteins	P62277	Nu	Translation	C, CJD, R.
Actin-related protein 2, 3	P61160	Nu, Cysk	Cysk organization/Axon growth	C, R.
Adenosylhomocysteinase 2	O43865	ER	Translation	C.
Adenylate kinase isoenzyme	P00568	Cy	Energy metabolism	R.
ADP/ATP translocase 1, 2	P12235	Mit	Energy metabolism	C, R.
AP-2 complex subunit beta	P63010	Mem	Transport, Recycling of synaptic vesicles	CJD.
Band 4.1-like protein 3	Q9Y2J2	Mem, Cysk	Apoptosis, Cysk organization	C.
Citrate synthase	O75390	Mit	Glucose metabolism	C, R, A.
Cleavage and polyadenylation specificity factor	O43809	Nu	mRNA processing	R.
Cysteine-rich protein 2	P52943	Cy	Cell division	C.
Dihydropteridine reductase	P09417	Mit, Cy	Redox homeostasis	R, A.
Dihydropyrimidinase-related protein 2	Q16555	Cy	Axon guidance	R, C.
Fructose-bisphosphate aldolase C	P09972	Cy	Carbohydrate metabolism	All.
GABA receptor-associated protein-like 2	P60520	Golgi	Transport	C, CJD, R.
GTPase KRas	P01116	Cy	Signal transduction	C, R.
GTP-binding nuclear protein Ran	P62826	Nu, Cy	Transport	All.
Immunoglobulin superfamily member 8	Q969P0	Mem	Neurite outgrowth	C.
LanC-like protein 1	O43813	Mem	Signaling	C, CJD, R.
Microtubule-associated protein 1A	P78559	Cysk	Cysk organization, Axonal transport	All.
Peptidyl-prolyl cis-trans isomerase A	P62937	Golgi	Protein refolding	A, R.
Peroxiredoxin-2	P32119	Cy	Redox homeostasis	R.
Phosphoglycerate kinase 1	P00558	Cy	Carbohydrate metabolism	All.
Quinone oxidoreductase	Q08257	Cy	mRNA processing	CJD, R.
Serine/threonine-protein phosphatase PGAM5	Q96HS1	Mit	Necrosis	R.
Synaptotagmin-1	P21579	Mem	Neurotransmission	C, R.
Trifunctional enzyme subunit beta	P55084	Mit, ER	Lipid metabolism	CJD.
Tubulin beta-3 chain	Q13509	Cysk	Axon maintenance	C, R.
Voltage-gated potassium channel subunit beta-2	Q13303	Mem	Neurotransmission	All.

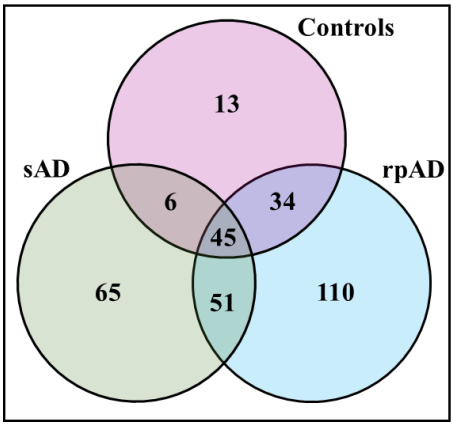

Figure 28: Disease-specific distribution of Aβ interactors isolated from FA-soluble fractions of controls, sAD and rpAD. The signature of Aβ-interacting partners was obtained by identifying the proteins purified through co-IP of pooled samples from each group (n = 3). The figure depicts the disease-specific distribution of these interacting partners.

Additionally, in a separate experiment, the proteins that copurified with Aβ fibrils (seeds for Aβ RT-QuIC) and have the potential to function as accessory proteins for Aβ aggregation were also identified. The replicates from each experimental group were pooled to improve the quantity and detection of proteins through LC-ESI MS/MS. The dataset was then searched for targets that are amyloidogenic, promote amyloidogenesis and prevent fibrillization of amylogenic proteins and the results are presented in Figure 29. The literature supporting the pro- and anti-amyloidogenic capabilities of selected targets is detailed in the discussion. Although the distribution was not very specific, sAD cases showed decreased levels of proteins that prevent fibrillization of Aβ in comparison to rpAD. Moreover, the concentration of amyloidogenic proteins, that may potentiate fibrillization via cross-seeding, was also higher in sAD cases. These differences may underlie distinct aggregation kinetics of sAD and rpAD seeds in RT-QuIC reactions. The dataset was also analyzed for proteins that were reported in the former datasets as Aβ interactors and the results are stated in Appendix C.

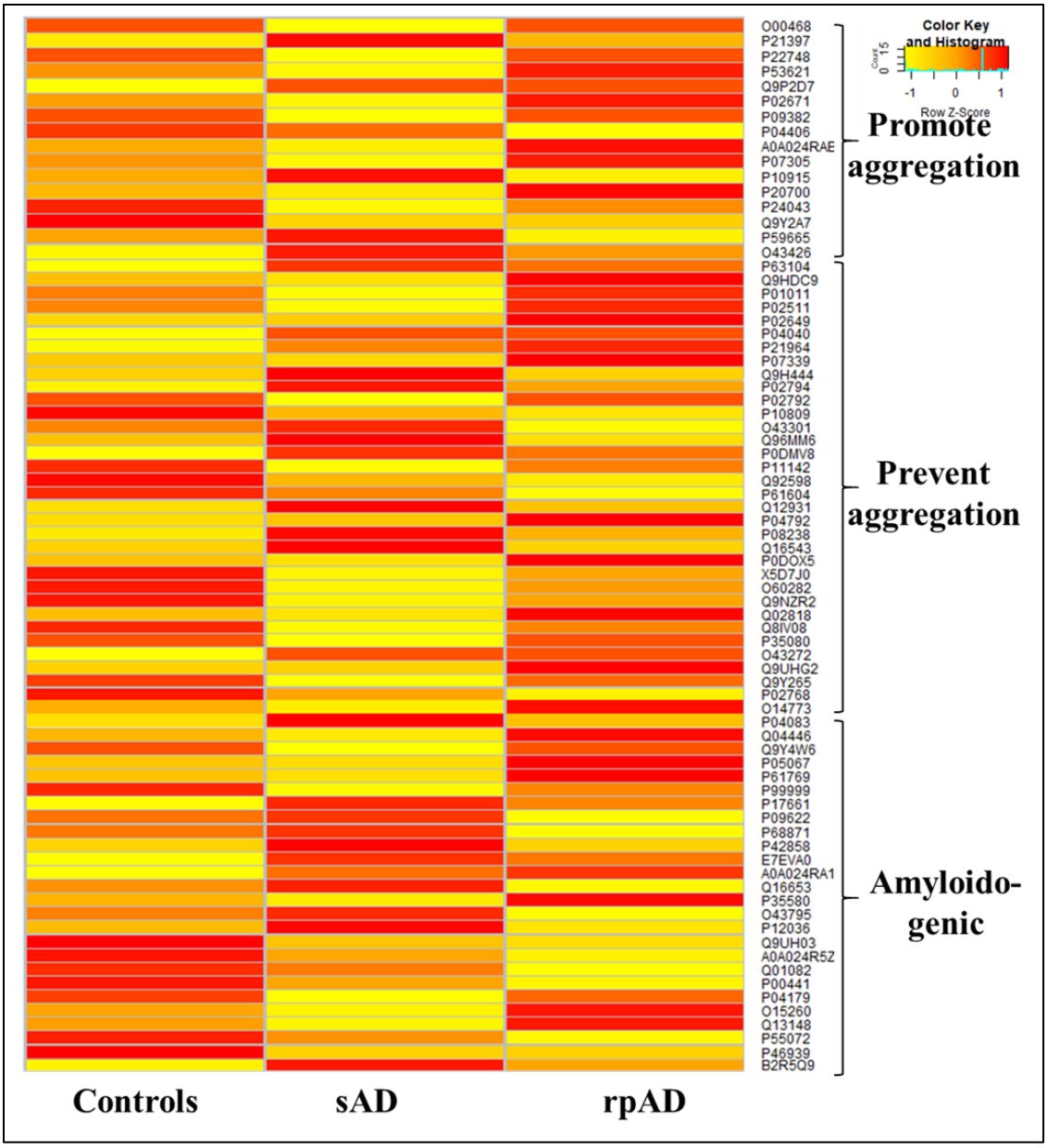

Figure 29: Relative concentration of pro- and anti-fibrillization accessory proteins copurified with fibrils using differential ultracentrifugation. The graph depicts the differences in the spectral counts of pooled samples from sAD, rpAD and controls. sAD cases had lower concentrations of anti-fibrilization proteins in comparison to rpAD cases. The spectral counts were normalized for each protein and the respective Z-scores were used for this plot. Since the dataset was obtained from pooled samples, individual differences were not analyzed statistically.

3.4.1 Comparative analysis of Aβ-modulated pathways in sAD and rpAD

The biological functions of potential Aβ interactors isolated from FA-soluble fraction from various experimental groups were analyzed to detect differentially regulated functional pathways. In rpAD

cases, Aβ-interactors predominantly modulated neurotransmission, neurogenesis (cell cycle/growth/development) and protein folding (chaperones), whereas a majority of Aβ interactors from sAD brains affected the replication, transcription, translation, transport of biomolecules and various metabolic pathways (Figure 30). Owing to the physiological function of Aβ, Aβ-interactors from control brains modulated pathways involved in immune response and maintaining the structural integrity of tissues. The interactors that were common in all groups were mainly chaperones and antimicrobial agents.

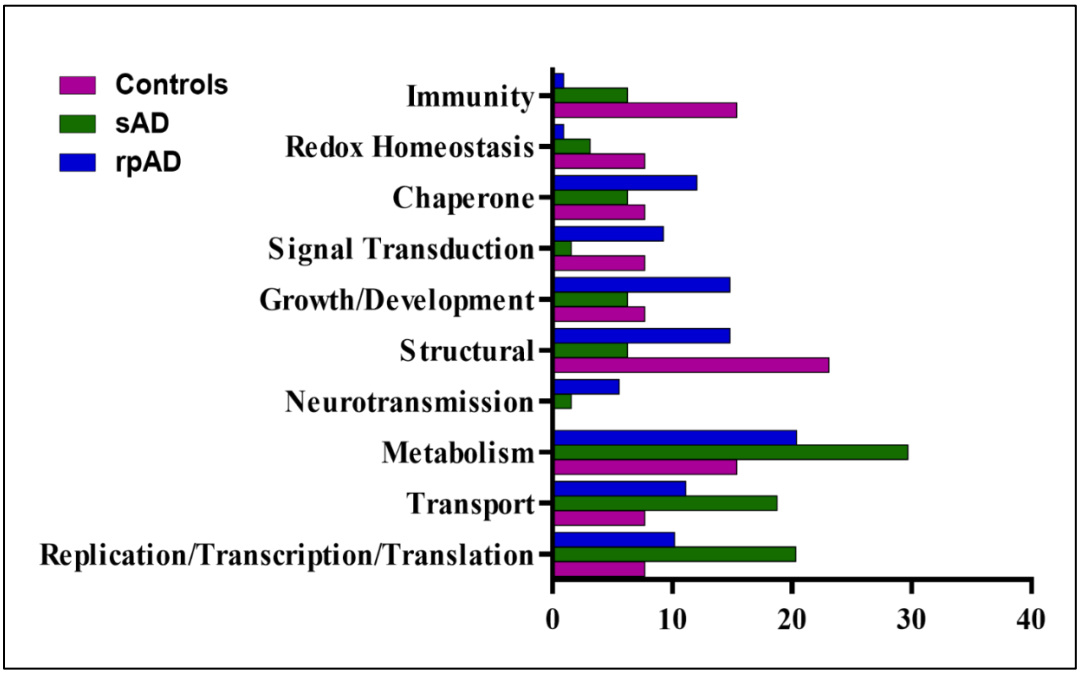

Figure 30: Common functional categories of Aβ-interacting partners extracted from FA-soluble fractions. The graph shows the relative percentage of proteins from all three experimental groups in each functional category. The functions of all proteins in the dataset were annotated using the UniProtKB database.

4. Discussion

An understanding of the discrete pathological mechanisms that lead to the presentation of various clinical subtypes of AD, especially the relatively newly discovered rpAD, are unknown to date. Previous studies have reported that rpAD cases are not significantly different from sAD cases with respect to markers for inflammation and tissue damage or the distribution of plaques and tangles (Schmidt et al., 2012; Abu-Rumeileh et al., 2018). However, proteomic and biophysical studies, especially those targeting the Aβ peptide, presented variations in Aβ as a promising target to understand the molecular differences among these clinical variants of AD (Cohen et al., 2015; Qiang et al., 2017). Expanding on these findings, the present study establishes the presence of previously underrepresented Aβ proteoforms in sAD and rpAD brains, gives an insight into the biosynthesis and relative quantities of these proteoforms and provides evidence for their distinct three-dimensional morphologies, interactions and toxicities.

4.1 The utility of common proteomic techniques for the analysis of Aβ

The evolution of neurodegenerative proteinopathies into the study of specific proteoforms, rather than being limited to one target amyloidogenic protein, has challenged the utility of many previously common proteomic techniques. Furthermore, Aβ itself can readily aggregate, bind to labware and attach to columns used for fractionation, rendering many biochemical techniques useless. Several techniques were therefore tested for the separation and identification of Aβ proteoforms. To resolve minor differences in the sequences of Aβ proteoforms, 1D-PAGE was replaced by the recently revived 2D-PAGE coupled with IB analysis. The first method of choice for their identification was LC-ESI MS/MS (in both bottom-up and top-down mode) owing to its capability to not only identify but also to sequence the isolated proteoforms (Wildburger et al., 2017). However, despite extreme measures to avoid loss of these highly hydrophobic peptides, several proteoforms did not elute from the column and the ones that were detected by analyzer were multiply charged and resulted in bottom-up inference problem or a complicated analysis. The overall results were highly non-reproducible. Hence, the techniques that depended on fractionation or electrospray ionization proved to have limited utility for the current study. MALDI coupled with ToF analyzer was then selected for its capability to generate singly ionized proteoforms, uncomplicated annotation and high sensitivity in case of undigested and low molecular weight proteoforms (Wang et al.,

2018). The results obtained with MALDI-MS fulfilled the requirements of the experiment and were utilized for further analysis.

4.2 Heterogeneity in the signature of Aβ proteoforms from sAD and rpAD samples

2D-PAGE has been used by several groups previously for the characterization of proteoforms of APP and its downstream products (Newton et al., 2006; Bibl et al 2006; Sergeant et al 2003; Maler et al., 2007; Schieb et al., 2011). For an efficient detection of the endogenous signature of Aβ proteoforms from brain tissue, IP was coupled with 2D-PAGE-IB. Aβ was detected as pentamers, hexamers and dodecamers in control, sAD and rpAD cases but monomeric species were detected in FA-soluble fractions of the two latter groups only. As the presence of Aβ pentamers, hexamers and dodecamers is an experimental artifact in SDS-PAGE experiments, the annotation of spots was limited to monomeric species (Watt et al., 2013; Pujol-Pina et al., 2015). Similar to the data reported for sAD cases, major spots were detected at a pI of 5.31 ($Aβ_{40}$ and $Aβ_{42}$), 5.76 (shorter C-terminally truncated Aβ proteoforms) and 6.27 ($Aβ_{4-42}$) in both experimental groups (Sergeant et al., 2003). Although the unavailability of proteoform-specific antibodies limited further analysis of these spots, it is noteworthy that while a greater variety was detected within the monomeric species in sAD cases, the rpAD brains featured more spots as higher-order aggregates, hinting at their differential capability to aggregate in response to SDS in the gels.

In contrast to former 2D-PAGE studies, where peptides were identified using bottom-up proteomics, we utilized top-down MALDI-ToF to avoid alterations due to tryptic digestion. The low molecular weight of Aβ allowed its detection through this technique without any further fractionation thereby avoiding additional purification and washing steps that usually result in the loss of peptides. Previously, MALDI-MS has been reported as a valuable tool for the identification of Aβ signature in the CSF (Gelfanova et al., 2007; Portelius et al., 2010).

In the current dataset, a total of 33 distinct proteoforms were identified and $Aβ_{40}$, $Aβ_{42}$, $Aβ_{4-42}$ as well as $pAβ_{11-42}$ were the most abundant proteoforms in sAD and rpAD cases. Recent studies conducted on sAD brains also reported these targets as the most abundant Aβ proteoforms in the insoluble (FA-soluble) fraction of sAD brains (Portelius et al., 2010; Wildburger et al., 2017). Unexpectedly, apart from one rpAD sample (rpAD1, Figure 12), none of the samples presented subtype-specific differences in the ratios of these major proteoforms. Several shorter proteoforms, on

the other hand, occurred more frequently in either sAD ($A\beta_{1-12}$, $A\beta_{2-14}$, $A\beta_{3-14}$, $A\beta_{15-38}$) or rpAD ($A\beta_{5-27}$ and $A\beta_{9-40}$) but their presence also varied among individual samples in each experimental group. Pyroglutamate proteoforms were frequently detected in the plaque associated proteome of both sAD and rpAD cases. Pyroglutamylation is known to increase the aggregation propensity of various proteoforms and the AD-associated behavioral deficits, hence its presence indicates more toxic counterparts of Aβ proteoforms (Wittnam et al., 2012; Sofola-Adesakin et al., 2016). The exact roles of a majority of these subtype-specific proteoforms are yet to be elucidated.

A comparison of this data set with that reported for brain and CSF cohorts from sAD and its clinical variants by other groups is summarized in Table 8. Other than the aforementioned major proteoforms, the signature appeared to be highly heterogeneous among various studies on brain samples. The CSF signature presented an even greater variation among the two mentioned studies. Although the intersubject variability among studied samples is now generally accepted to play a role in heterogeneity observed for Aβ proteoforms within and between various cohorts, alterations in signatures due to variations in purification and identification methodologies cannot be ignored (Condello et al., 2018).

Table 8: Comparison of the Aβ proteoform signature reported for AD cases in the brain and CSF samples by various groups. Presence of a proteoform is indicated by '+' sign while their absence is shown by '-' sign. The proteoforms detected in all brain studies for sAD cases are indicated in red.

Proteoform	Current study (sAD, rpAD brain)	Gkanatsiou et al., 2019 (sAD, CAA brain)	Wild-burger et al., 2017 (sAD brain)	Portelius et al., 2010 (sAD, fAD brain)	Portelius et al., 2010 (sAD, fAD CSF)	Gelfanova et al., 2007 (sAD CSF)
$A\beta_{1-12}$	+	-	-	-	-	-
$A\beta_{1-13}$	-	-	-	-	+	-
$A\beta_{1-14}$	-	-	-	-	+	-
$A\beta_{1-15}$	-	-	-	-	+	-
$A\beta_{1-16}$	-	-	-	-	+	-
$A\beta_{1-17}$	-	-	-	-	+	-
$A\beta_{1-18}$	-	-	-	-	+	-
$A\beta_{1-19}$	-	-	-	-	+	-
$A\beta_{2-13}$	+	-	-	-	-	-
$A\beta_{3-14}$	+	-	-	-	-	-
$A\beta_{2-14}$	+	-	-	-	-	-
$A\beta_{11-33}$	+	-	-	-	-	-
$A\beta_{11-34}$	-	-	+	-	-	
$A\beta_{2-20}$	+	-	-	-	-	-
$A\beta_{15-38}$	+	-	-	-	-	-

Aβ$_{1-20}$	+	-	+	-	+	-
Aβ$_{14-38}$	+	-	-	-	-	-
Aβ$_{5-27}$	+	-	-	-	-	-
Aβ$_{5-29}$	+	-	-	-	-	-
Aβ$_{1-26}$	+	-	-	-	-	-
pAβ$_{11-40}$	+	-	-	-	-	-
Aβ$_{1-27}$	+	-	-	-	-	-
pAβ$_{11-42}$	+	+	+	+	-	-
Aβ$_{11-42}$	+	+	+	+	-	-
Aβ$_{9-40}$	+	-	-	+	-	-
Aβ$_{11-43}$	+	-	-	-	-	-
Aβ$_{8-40}$	+	-	+	-	-	-
Aβ$_{10-42}$	-	-	-	+	-	-
Aβ$_{9-42}$	+	-	-	+	-	-
Aβ$_{8-42}$	+	+	+	+	-	-
Aβ$_{7-42}$	-	-	-	+	-	-
Aβ$_{1-30}$	-	-	-	-	+	-
Aβ$_{1-33}$	-	-	+	-	+	+
Aβ$_{1-34}$	+	-	+	-	+	+
Aβ$_{4-40}$	+	+	+	+	-	-
Aβ$_{5-40}$	-	-	-	+	-	-
Aβ$_{5-42}$	+	+	+	+	-	-
Aβ$_{1-37}$	+	-	-	+	+	+
Aβ$_{2-38}$	-	-	-	+	-	-
Aβ$_{1-38}$	+	-	-	+	+	+
Aβ$_{1-39}$	-	-	-	+	+	+
Aβ$_{3-40}$	+	-	-	+	-	-
pAβ$_{3-40}$	-	-	-	+	-	-
Aβ$_{4-42}$	+	+	+	+	-	-
Aβ$_{3-42}$	-	-	+	+	-	-
pAβ$_{3-42}$	+	+	+	+	-	-
Aβ$_{1-40}$	+	+	+	+	+	+
Aβ$_{2-42}$	+	+	-	+	-	-
Aβ$_{1-41}$	+	-	-	-	-	-
Aβ$_{1-42}$	+	+	+	+	+	+
Aβ$_{1-43}$	-	-	-	+	-	-

Since the MALDI MS experiments lacked labelled Aβ proteoforms as internal standards, ELISA was used instead of this dataset for quantification. As expected, the amounts of all proteoforms were higher in sAD and rpAD in comparison to controls, however, a significant difference was only evident in the case of C-terminally truncated proteoforms in FA-soluble fraction. No differences could be observed between sAD and rpAD in case of IB for $Aβ_{Total}$ and either ELISA test. Interestingly, the Tris-soluble fraction featured higher N-terminally truncated Aβ proteoforms in comparison to their C-terminally truncated counterparts. A greater variety of N-terminally trun-

cated Aβ proteoforms was also evident in our MALDI MS experiments and a trend has been verified previously in other studies (Sergeant et al., 2003; Miravalle et al., 2005). This trend was significant in our sAD samples but the differences in the other two targeted groups were not significant.

The sequence of proteoforms dictates their folding, aggregation and toxicities. It is now known that the proteoforms with longer C-terminal are more amyloidogenic and feature highly ordered structures with a greater percentage of beta-sheets. Proteoforms lacking an intact C-terminal domain are less prone to aggregation and form disordered aggregates (Vandersteen et al., 2012). The known relevance of extended N-terminal, on the other hand, is limited to pyroglutamylation within this domain and this modification is shown to increase the aggregation propensities by up to 250-fold (Schilling et al., 2006). $A\beta_{5\text{-}42}$, $A\beta_{11\text{-}40}$ and $A\beta_{11\text{-}42}$ are more prone to aggregation than their full-length counterparts and have been reported to cofibrillize with $A\beta_{40}$ and $A\beta_{42}$ (Barritt and Viles, 2015; Barritt et al., 2017; Weiffert et al., 2019).

Most of the studies targeting cellular toxicities have been limited to $A\beta_{40}$ and $A\beta_{42}$ only. However, $A\beta_{3\text{-}42}$, $pA\beta_{3\text{-}42}$, $A\beta_{4\text{-}40}$ and $A\beta_{4\text{-}42}$, have also been postulated to potentiate ion channel formation, to trigger the loss of neurons and to mediate behavioral deficits (Bouter et al., 2013; Gunn et al., 2016; Dunys et al., 2018). Others, as reported for several C terminally truncated Aβ proteoforms, can be intermediates of various Aβ degradation and clearance pathways (Olsson et al., 2014).

Presence of some C-terminally truncated shorter peptides, including $A\beta_{1\text{–}37}$, $A\beta_{1\text{–}38}$ and $A\beta_{1\text{–}39}$, has been shown to prevent the toxic effects of $A\beta_{1\text{-}42}$ although the exact mechanism behind this change is unknown (Moore et al., 2018). Moreover, although the aggregation propensities of $A\beta_{11\text{-}40}$ and $A\beta_{11\text{-}42}$ and their pyroglutamate variants have been reported to be very high, their toxicity in cell culture experiments is lower than other known proteoforms (Sohma et al., 2013).

4.3 The implications of higher BACE1 levels in rpAD

Theoretically, the reduced expression of enzymes involved in the clearance of Aβ and/or upregulation of enzymes that modulate the amyloidogenic pathway should exacerbate AD. However, despite several studies, the expressional profiles of most Aβ-processing enzymes are not fully established. ADAM-10, the major α-secretase, is believed to be reduced in AD (Colciaghi et al., 2002; Sogorb-Esteve et al., 2018). The studies associated with the expression of BACE1 have

many discrepancies in the literature with reference to its generation, expression and activity therefore, no consensus has been reached (Stockley et al., 2007). No significant differences have been found among sAD, fAD and control cases in the expression of PSEN1, a key component of γ-secretase (Hendriks et al., 1997). The expression and activity of IDE also showed no differences among AD and control cases (Wang et al., 2010). The expression of plasmin is downregulated in AD (Ledesma et al., 2000). Individually, none of these enzymes showed significant differences in expression in our cohort. However, it is worth mentioning that in all of the previous studies, and the current study, all samples were tested post-mortem, although Aβ pathology begins very early in the disease course. Thus, the relative levels of enzymes reported might not depict an accurate picture of the changes that lead to differential progression in clinical subtypes of AD.

Nevertheless, a significantly higher ratio of BACE-1, in comparison to ADAM-10, was seen in rpAD in comparison to sAD. Although the activity of these enzymes still needs to be confirmed, this trend indicates higher cleavage of Aβ via the amyloidogenic pathway, consequently leading to the greater formation of amyloidogenic proteoforms. The relatively higher ratio of this β-secretase accompanied with no alterations in Aβ clearance enzymes would lead to a greater plaque burden and possibly exacerbate the disease symptoms.

4.4 Differences in amplification capabilities of sAD and rpAD seeds

With recent advances in *in vitro* seeding assays, especially the RT-QuIC assay, it is now possible to define clinical subtypes of most neurodegenerative proteinopathies with reference to the aggregation kinetics of various strains of the amyloidogenic proteins (Wilham et al., 2010). These alterations in aggregation kinetics can translate to distinct biochemical properties, stabilities, transmission and disease phenotypes (Rasmussen et al., 2017). Although the idea was initially limited to PrP^C, the field has taken many prion-like proteins, including Aβ, under consideration (Di Fede et al., 2018; Candelise et al., 2019; Saijo et al., 2019). Structure-sensitive probes have identified distinct subtypes of AD previously based on alteration in the 3D conformations of resident Aβ (Rasmussen et al., 2017; Condello et al., 2018). Given the lack of expressional differences in major Aβ proteoforms in the MALDI MS dataset, this study also targeted the differences among Aβ strains extracted from sAD and rpAD brains.

Unlike the RT-QuIC assays for PrP^C and α-synuclein, the lack of understanding and availability of efficient and specific Aβ substrates limits the use of generic peptides to monitor aggregation

kinetics. Most of these peptides are prone to self-aggregation and mask differences generated by the brain-derived seeds. However, fibrillization only occurs when a critical threshold of peptide concentration is reached, after which the generation of characteristic fibrils becomes independent of initial concentration and becomes dependent on the biochemical nature of the seeds (Novo et al., 2018; Di Fede et al., 2018). The efforts to optimize the seeding assay employed in the current study were therefore preliminary targeted to adjust the quantity of substrate in a way that self-aggregation is limited to a minimum.

Based on the major proteoforms detected by MALDI MS in the current study, a combination of $A\beta_{40}$ and $A\beta_{42}$ was used as seeds for RT-QuIC reactions in contrast to using a higher concentration of either proteoform in independent assay which leads to self-aggregation. Prior evidence suggests that cross-seeding does not occur among these proteoforms, therefore their use as seeds in a single reaction was not problematic (Xiao et al., 2015). The results confirm that, in the absence of seeds, the substrate does not aggregate and generate a comparable signal or higher-order aggregates. Moreover, despite the fact that Aβ pathology is common in healthy controls as well, the signal suggests the presence of seeds that do not aggregate in the reaction conditions used.

Although the protocol employed here is still in the primary stages of development, subtle differences were observed among targeted clinical variants. sAD cases were observed to aggregate faster with a shorter lag phase and steeper curves in comparison to rpAD cases (Figure 31). These changes in aggregation kinetics reflect directly on the seeding capabilities of seeds extracted from sAD and rpAD. In a similar study with Aβ RT-QuIC, sAD and fAD samples with PSEN mutations showed the faster aggregation and steeper slopes in comparison to fAD cases with APP mutations (Di Fede et al., 2018). It is conceivable that a longer lag phase reflects the presence of Aβ as the more toxic oligomeric species for a longer duration in the brain. As the generation of mature fibrils and plaques is a protective physiological measure to prevent Aβ toxicity, their delayed generation suggests possible pathological implications. Collectively, these changes can lead to more neurodegeneration in rpAD brains in comparison to sAD brains.

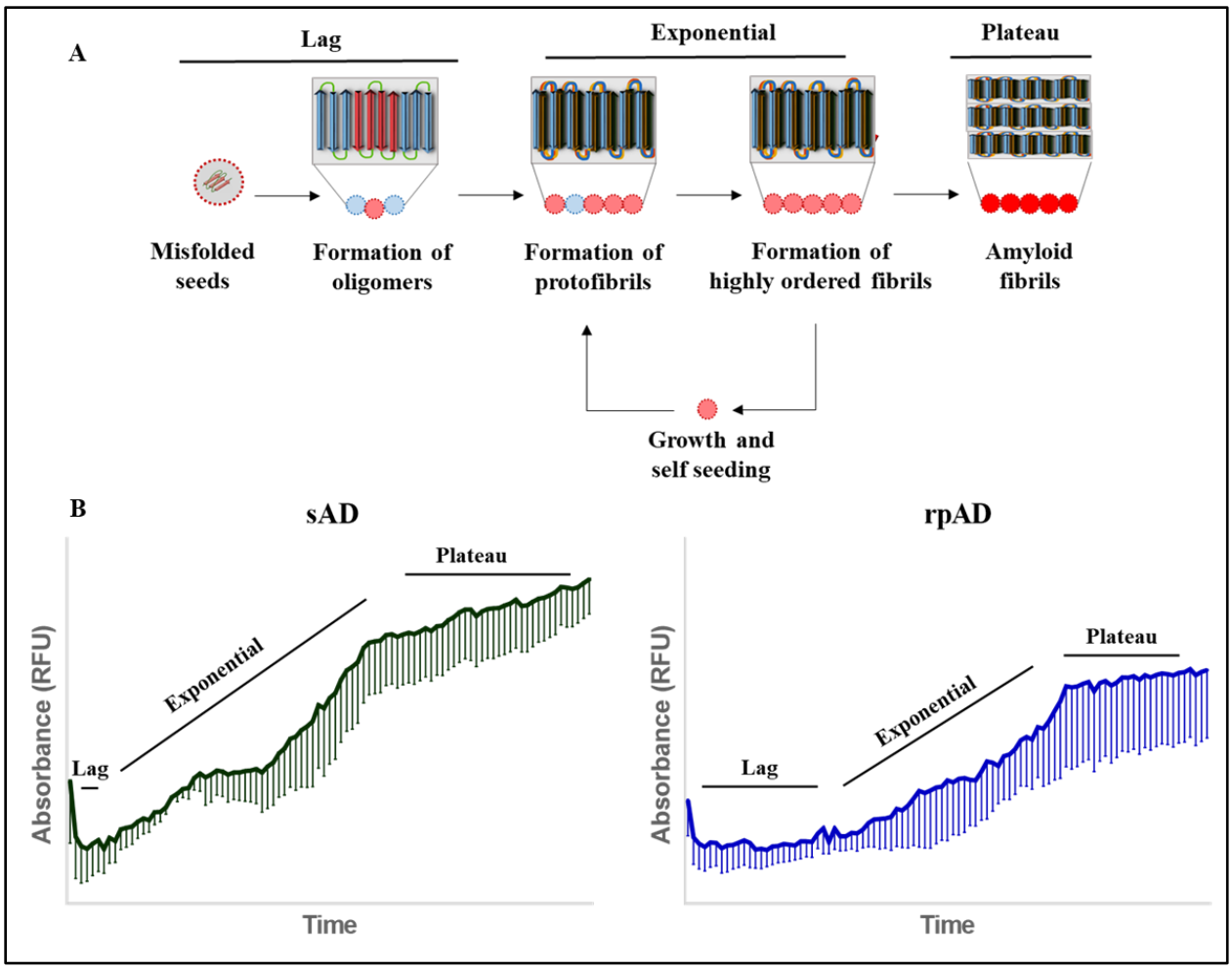

Figure 31: The aggregation kinetics of misfolded Aβ in sAD and rpAD. (A) The seeding of amyloidogenic proteins involves the conversion of monomeric seeds into aggression-prone oligomeric nuclei (lag phase), followed by exponential conversion of oligomers into protofibrils and mature fibrils (exponential phase) until the reaction reaches a plateau due to a lack of monomers or other rate-limiting factors (stationary phase). (B) Kinetic curves for sAD- and rpAD-derived RT-QuIC reactions depict inherent differences in the seeding capabilities of seeds extracted from distinct variants of AD.

4.4.1 The role of accessory proteins in Aβ seeding

Other than the intrinsic differences in the biochemical nature of seeds, amyloidogenesis is also affected by many environmental factors including pH, salt concentration and the presence of specific cofactors (Sikkink and Ramirez-Alvarado, 2008; Pfefferkorn et al., 2010). As the pH and salt concentrations are constant under *in vitro* conditions, the proteins and other biomolecules co-purified with the seeds are a major source of influence on the seeding capabilities of brain-derived fibrils. The impact of these molecular cofactors, including proteoglycans, lipids and polyanions, is becoming increasingly relevant for the propagation of prion and prion-like proteins (Ma, 2012;

Nguyen et al., 2015; Fichou et al., 2018). The current project also targeted these cofactors, specifically those proteinaceous in nature, to further elucidate the reasons underlying the differences in the RT-QuIC profiles between sAD and rpAD brains.

A majority of proteins identified in this dataset were cytoplasmic proteins that have been previously reported to undergo changes in solubility in response to Aβ pathology, leading to their isolation from the insoluble fraction, rather than the soluble fraction of brain proteome (Xu et al., 2013). The analysis was therefore focused on the targets that have been previously associated with assisting or inhibiting the fibril formation of prions or prion-like proteins. Intrinsically disordered proteins, which have the potential to form amyloidogenic or amorphous aggregates, were also added to the list since several of these candidates can cross-seed Aβ and implicate amyloid formation (Furukawa et al., 2009; Keefer et al., 2017; Nizynski et al., 2018; Lim, 2019). The key targets copurified with seeds under the optimized experimental conditions and their potential role in promoting or demoting protein aggregation are listed in Table 9.

The heterogeneity among the clusters of proteins that impact amyloidogenesis directly gives an insight into the environment of fibrils in the brain. The proteins involved in promoting fibril formation were highly enriched in rpAD cases whereas sAD cases presented a higher amount of proteins that can cross-seed Aβ. The anti-amyloidogenic proteins appeared to be equally distributed among the two clinical variants of AD (Figure 29). Collectively, these changes can affect the amyloid formation and contribute towards discrepancies observed in kinetic curves. This list of putative accessory proteins is being validated by seeding Aβ under different concentrations of the accessory proteins, however, those results are beyond the scope of the current study.

Table 9: List of potential accessory proteins purified with Aβ fibrils. The proteins, in addition to Aβ, extracted as fibrillar fraction via differential centrifugation were identified and their potential to interfere with amyloid formation was established through an extensive literature review. The targets that may influence amyloidogenesis either by aiding fibril formation, inhibiting their assembly or cross-seeding Aβ are listed below. Additionally, the proteins in this dataset, that were found to interact with Aβ in the IP experiments conducted in the current study, have been stated as interactors.

Proteins	Accession #	Aβ Interactor	Role	Specificity	Reference
1,4-alpha-glucan-branching enzyme	Q04446	No	Prone to misfolding and aggregation	C, rpAD	Froese et al., 2015
14-3-3 protein	P63104	Yes	Promotes formation of aggresome to avoid amyloid-associated toxicity	All	Shimada et al., 2013
26S proteasome non-ATPase regulatory subunits	Q99460	Yes	Aberrant activity aids the accumulation of misfolded proteins	All	Ciechanover and Kwon, 2015
26S proteasome regulatory subunits	P62333	No	Aberrant activity aids the accumulation of misfolded proteins	All	Ciechanover and Kwon, 2015
40S ribosomal proteins	P46783	Yes	Stimulates aggregation	All	Pathak et al., 2017
60S acidic ribosomal proteins	P05388	Yes	Stimulates aggregation	All	Pathak et al., 2017
Adipocyte plasma membrane-associated protein	Q9HDC9	No	Suppresses Aβ aggregation	All	Mosser et al., 2014
AFG3-like protein 2	Q9Y4W6	No	Intrinsically disordered protein associated with spinocerebellar Ataxia	All	Das and Mukhopadhyay, 2011
Agrin	O00468	No	Accelerates amyloidogenesis	All	Cotman et al., 2000
Alpha-1-antichymotrypsin	P01011	No	Inhibits fibril formation	C, rpAD	Eriksson et al., 1995
Alpha-crystallin B chain	P02511	Yes	Inhibits fibril formation	All	Raman et al., 2005
Amine oxidase	P21397	Yes	Increases the rate of aggregation and size of aggregates indirectly	All	Chen et al., 2006
Annexins	P04083	Yes	Degradation of Aβ and clearance of fibrils	All	Ries et al., 2016
Apolipoprotein E	P02649	Yes	Enhances Aβ deposition into plaques	sAD, rpAD	Endo et al., 2019
Beta-2-microglobulin	P61769	No	Amyloidogenic	All	Drüeke., 2000
Carbonic anhydrase 4	P22748	No	Amyloidogenic	All	Rana et al., 2008
Catalase	P04040	Yes	Suppresses Aβ aggregation	All	Luo et al., 2014
Catechol O-methyltransferase	P21964	No	Suppresses Aβ aggregation	All	Di Giovanni et al., 2010

Cathepsin D	P07339	Yes	Degrades Aβ	All	Sakamoto et al., 2006
CDGSH iron-sulfur domain-containing protein	Q04446	No	Intrinsically disordered protein associated with Wolfram syndrome	All	Das and Mukhopadhyay, 2011
Charged multivesicular body protein 4b	Q9H444	Yes	Clearance of aggregating proteins	sAD	Rusten et al., 2008
Cytochrome c	P99999	No	Prone to amyloid formation	All	Lin et al., 2016
Desmin	P17661	No	Prone to amyloid formation	All	Weihl and Bieschke, 2016
Dihydrolipoyl dehydrogenase,	P09622	Yes	Intrinsically disordered associated with Leigh syndrome	All	Das and Mukhopadhyay., 2011
Dynein heavy chain	Q9P2D7	No	Involved in trafficking and clearance of aggregates	sAD, rpAD	Rubinsztein et al., 2006
E3 ubiquitin-protein ligase	Q7Z6Z7	No	May contribute to clearance	All	Khandelwal and Moussa, 2010
Ferritin	P02794	No	Disrupts aggregates by scavenging iron.	All	Balejčíková et al., 2019
Fibrinogen	P02671	Yes	Cross-seeding	All	Ahn et al., 2010
Galectin	P09382	Yes	Promotes oligomerization	C, sAD	Tao et al., 2020
Glyceraldehyde-3-phosphate dehydrogenase	P04406	Yes	Increases aggregation by blocking chaperones	All	Muronetz et al., 2017
Heat shock proteins	P10809	Yes	Inhibits early stages of aggregation	All	Webster et al., 2019
Hemoglobin subunit beta	P68871	Yes	Aβ interactor/ forms fibrils	All	Jayawardena et al., 2017
Heparan sulfate proteoglycan 2	A0A024RAB6	No	Promotes fibril formation	All	Liu et al., 2016
Histones	P07305	Yes	Favors the aggregation of Aβ and stabilize aggregates	All	Duce et al., 2006; Liu et al., 2016
Huntingtin	P42858	No	Amyloidogenic	sAD	Huang et al., 1998
Hyaluronan and proteoglycan link protein	P10915	Yes	Enhances aggregation	All	Wang et al., 2019
Immunoglobulin gamma-1	P0DOX5	Yes	Anti-amyloidogenic	All	Valls-Comamala et al., 2017
Kinesin family member 1A	X5D7J0	No	Inhibits aggregation	All	Zheng et al., 2016
Kinesin heavy chain isoform	O60282	No	Inhibits aggregation	All	Zheng et al., 2016
Lamin	P20700	Yes	Cross-seeding	All	Groh et al., 2017
Laminin subunits	P24043	No	Inhibits Aβ fibrillation	All	Bronfman et al., 1998
Low-density lipoprotein receptor-related protein 1B	Q9NZR2	No	Reduces Aβ generation	C, rpAD	Cam et al., 2004

Major prion protein	B2R5Q9	Yes	Stabilizes oligomers; cross-seeding	All	Honda 2018; Younan et al., 2018
Microtubule-associated protein	E7EVA0	No	Amyloidogenic	All	Nizynski et al., 2017
Microtubule-associated protein (Tau)	A0A024RA19	Yes	Amyloidogenic	All	Nizynski et al., 2017
Myelin-oligodendrocyte glycoprotein	Q16653	No	Amyloidogenic	All	Araman et al., 2018
Myosin	P35580	Yes	Amyloidogenic	All	Komatsu et al., 2006
Neurofilament	P12036	No	Prone to aggregation	All	Lin and Schlaepfer., 2006
Neuronal-specific septin-3	Q9UH03	Yes	Amyloidogenic	All	Ortore et al., 2015
Neutrophil defensin 1	P59665	Yes	Induces amyloid formation	C, sAD	Horn et al., 2012
Nucleobindin-1	Q02818	No	Inhibits fibril formation	C, rpAD	Bonito-Oliva et al., 2017
Profilin-2	P35080	Yes	Binds to oligomers and prevents fibril formation	All	Posey et al., 2018
ProSAAS	Q9UHG2	Yes	Blocks aggregation and toxicity	All	Jarvela et al., 2016
Pyruvate kinase	A0A024R5Z9	No	Amyloidogenic	All	Grignaschi et al., 2018
RuvB-like 1 /2	Q9Y265	Yes	Disaggregate amyloid fibrils	All	Zaarur et al., 2015
Serum albumin	P02768	No	Prevents Aβ aggregation	C, sAD	Finn et al., 2012
Spectrin	Q01082	No	Amyloidogenic	sAD, rpAD	Morel et al., 2006
Superoxide dismutase [Cu-Zn]	P00441	Yes	Amyloidogenic	C, AD	Khan et al., 2017
Superoxide dismutase [Mn]	P04179	No	Amyloidogenic	All	Khan et al., 2017
Surfeit locus protein 4	O15260	No	Intrinsically disordered protein associated with Leigh syndrome	All	Das and Mukhopadhyay, 2011
Synaptojanin-1	O43426	No	Involved in Aβ Clearance	sAD, rpAD	Zhu et al., 2013
TAR DNA-binding protein 43 TDP43	Q13148	No	Amyloidogenic, cross-seed Aβ	All	Fang et al., 2014
Transitional endoplasmic reticulum ATPase VCP	P55072	Yes	Intrinsically disordered protein associated with FTD	C, sAD	Das and Mukhopadhyay, 2011
Tripeptidyl-peptidase 1	O14773	Yes	Destabilizes fibrillar Aβ	All	Solé-Domènech et al., 2018
Utrophin	P46939	No	Amyloidogenic	C	Singh et al., 2012

4.5 Structure-function relationship of brain-derived fibrils

The technical difficulties in extracting and amplifying brain-derived Aβ fibrils have limited most of the studies to synthetic proteoforms. Among the few nuclear magnetic resonance (NMR) studies and imaging experiments conducted on brain-derived fibrils, polymorphisms among generated structures have been the most prominent observation (Lu et al., 2013; Qiang et al., 2017; Condello et al., 2018). Interestingly, the existence of a greater heterogeneity, especially for $A\beta_{40}$ fibrils, has been associated with the rapid progression observed in some AD cases (Qiang et al., 2017). In the current study, the structure of fibrils generated via RT-QuIC assays was visualized using confocal and atomic force microscopy. Surprisingly, although the aggregation of rpAD fibrils appeared to be slower than sAD fibrils, they featured the presence of larger and more polymorphous (both fibrillar and amorphous) aggregates in comparison to sAD cases. In contrast, sAD-derived reactions had regular well-defined fibrils.

Previous studies have also attributed these differences to alterations in inherent charges of the substrate, hydrophobicity and the capability of proteins to generate secondary structures required for nucleation (Zapadka et al., 2017). Since similar substrate was used for all reactions, the alterations in inherent charges may not have played a major role. To access the alterations in secondary structure, FTIR spectroscopy was performed on the brain-derived fibrils. However, no shifts in peaks were observable for either clinical subtype in these experiments indicating similar proportions of β-sheets, α-helices and other secondary structures. It can, therefore, be postulated that the larger structures observed for rpAD may be products of highly hydrophobic fibrils that have higher propensity to bind with each other and generate a plaque-like morphology. As secondary nucleation is dependent on the availability of fibril surface and rpAD-derived fibrils are buried within larger structures, these results also explain why rpAD cases reached the stationary phase at a lower absorbance in comparison to sAD cases.

The structure of aggregates is closely associated with their mechanisms of toxicity (De et al., 2019). Neuronal cells were treated with brain-derived fibrils and the relative toxicities of sAD and rpAD fibrils were accessed but no significant differences were evident among the two clinical variants. However, it is noteworthy that the experiment was conducted using the end products of RT-QuIC reactions, a time point where toxic species have already converted into the less toxic

fibrillar aggregates. *In vivo* mechanisms of Aβ toxicity were also assessed to address the alterations within the sAD and rpAD brains which will be discussed in the following section.

4.5.1 Aβ-induced aberrations in cellular pathways

Protein-protein interactions play a keen role in physiological and pathological functioning of neurons. The interactions of Aβ with various biomolecules can provide useful insights into the pathobiology of clinical variants of AD. Experiments conducted using co-IP identified proteins involved in growth, neurotransmission, metabolism and transport that aid Aβ by propagating its toxicity to various organelles within the neurons and other brain cells. Both Tris-soluble and FA-soluble pools of Aβ were targeted and contrast was observed in the functional pathways modulated in sAD and rpAD brains. However, the targets identified in FA-soluble fraction can only be interpreted as putative interactors, rather than presenting physiological interactions, due to the effect of FA treatment on protein chemistry.

A majority of Aβ interactors from sAD brains affected the cellular machinery involved in replication, transcription, translation and various metabolic pathways. Previous studies have reported the inhibition of protein synthesis as the major pathway affected by aberrant interactions of Aβ in relation to sAD (Virok et al., 2011). Ribosomal proteins, specifically ribosomal proteins L23A, L31, S13 and S17 have been found to be upregulated in sAD in comparison to rpAD (Garcia-Esparcia et al., 2017). In rpAD cases, Aβ interactors primarily modulated neurotransmission, neurogenesis and protein folding, and the dataset confirmed that Aβ species in these cases may impart toxicity through the modulation of pathways different from sAD cases. Drummond et al., (2017) also reported the enrichment of proteins involved in synaptic dysfunction in plaques from rpAD cases. Owing to the physiological function of Aβ, Aβ interactors from control brains modulated pathways involved in immune response and maintaining the structural integrity of tissues. The key interactors and their implications on the pathobiology of AD have been detailed below.

4.5.1.1 Immune response

One of the few physiological roles of the Aβ peptide reported to date is its capability to act as an antimicrobial agent against viruses and bacteria (Brothers et al., 2018). The generation of Aβ oligomers and fibrils increases in the incident of an infection and is reported as one of the earliest responses of the innate immune system. Aβ fibrils interact with membranes of pathogens to create a physical barrier between host and pathogen and eventually trap them in a matrix generated via

elongating fibrils (Gosztyla et al., 2018; Moir et al., 2018). The current study shows that, in comparison to rpAD (1%), a greater percentage of Aβ interactors in controls (15.3%) and sAD (6.25%) cases were involved in the modulation of the immune response in the FA-soluble fraction of brain proteins. These interactors (arginase, BPI fold-containing family A, eukaryotic initiation factor 4A-I, and ubiquitin carboxyl-terminal hydrolase) are shown to be involved in innate immunity and play a role in facilitating host-virus interactions. These targets can provide an insight into the pathways regulated by Aβ to facilitate its role as an antimicrobial agent under physiological conditions. No immunity-related interactors were detected in Tris-soluble fraction, possibly due to a greater involvement of Aβ fibrils, but not monomers and oligomers, in the immune response.

4.5.1.2 Signal transduction

AD pathology is a product of aberrations in several key pathways, including Wnt/β-catenin, Notch, mitogen-activated protein kinase (MAPK), rapamycin (mTOR) and calcium signaling pathway (Mizuno et al., 2012). Together, these alterations are responsible for the reorganization of the cytoskeleton, neuronal dysfunction, cell cycle abnormalities, Aβ production, mismetabolism and dysregulated recycling of biomolecules (Woo et al., 2009; Hermes et al., 2010; Oddo, 2012; Palomer et al., 2019). Previous studies have reported a direct interaction of Aβ with RAGE, PrP^{C} and insulin receptors and aberrant modulation of their downstream pathways (Zhao et al., 2008; Smith et al., 2017). A direct relationship between Aβ administration and mTOR signaling has also been reported (Oddo, 2012). This evidence highlights the direct involvement of Aβ in disrupting survival pathways. However, no previous studies have targeted the individual culprits responsible for inducing Aβ-directed alterations in these pathways.

Interestingly, serine/threonine-protein phosphatase PGAM5, a key regulator of programmed cell death caused by tumor necrosis factor (TNF-α), oxidative stress and calcium-induced excitotoxicity, was seen to interact with Aβ in Tris-soluble fraction of rpAD brains (Wang et al., 2012). The GTPase KRas, a component of the MAPK pathway, showed a similar specificity. Moreover, peroxiredoxin, involved in the activation of the MAPK pathway, was also observed to interact with Aβ in rpAD, but not sAD, brains. Previous studies have also verified a direct impact of oligomeric Aβ on the MAPK pathway (Young et al., 2009). LanC-like protein 1, involved in the epidermal growth factor receptor pathway, was reported to interact with Aβ in all experimental groups, except for the sAD cases.

A similar pattern was observed in Aβ interactors isolated from FA-soluble fraction as well, with a greater percentage of identified proteins involved in signal transduction in rpAD cases as compared to sAD. Several of these targets, including APC membrane recruitment protein 2, dimethylarginine dimethylaminohydrolase, Na/H exchange regulatory cofactor NHE-RF1, Protein NDRG1 and leucine-rich repeat flightless-interacting protein 2 are involved in Wnt/β-catenin pathway and hint at serious aberrations within pathway in rpAD brains (Liu et al., 2005; Tanneberger et al., 2011; Ardura and Friedman, 2011; Liu et al., 2012; Ye et al., 2017).

4.5.1.3 Structural roles

Cytoskeletal proteins play a key role in the maintenance of neuronal cell bodies. They are also responsible for axon guidance, the formation of dendritic spines and synaptic terminals. Therefore, dysregulation of the cytoskeleton can have a direct impact on neurotransmission and neuronal survival. The role of various cytoskeletal proteins in the pathophysiology of AD has been vigorously targeted over the past few decades and several promising targets, including amyloidogenic tau protein, have emerged (Bamburg and Bloom, 2009). Furthermore, Aβ itself is directly involved in dysregulating the polymerization and post-translational modifications of various cytoskeletal proteins, directly impacting the trafficking of vesicles and organelles along the synaptic cytoskeleton (Henriques et al., 2010).

Cytoskeletal interactors of Aβ associated with the Tris-soluble fraction of brain proteins included actin-related protein 2, Band 4.1-like protein 3, dihydropyrimidinase-related protein 2 and microtubule-associated protein 1A. All of these proteins are involved in the organization of cytoskeleton, however, most of them, except for microtubule-associated protein 1A, were detected in rpAD and control brains only. Similarly, the FA-soluble fraction also identified a greater percentage of rpAD-associated Aβ interactors (14.8%), in contrast to sAD (6.25%), to be involved in cytoskeletal organization and other structural functions. This observation further highlights the involvement of different pathways in the two distinct clinical variants of AD.

4.5.1.4 Neurotransmission

Cognitive dysfunction and memory loss are key clinical symptoms of AD and several other forms of dementia. Aβ contributes towards this pathological phenomenon by hindering the release of neurotransmitters at the synaptic terminals and depleting synaptic vesicles (Parodi et al., 2010;

Russell et al., 2012). Aberrantly modified tangles contribute to synaptic toxicity by inhibiting axonal transport, deregulating synaptic receptors and impairing dendritic spines (Tracy and Gan, 2018). Together, these alterations affect synaptic plasticity resulting in worsening of memory deficits observed in patients.

In the current dataset, Aβ was observed to interact with voltage-gated potassium channels in all experimental groups. However, its higher expression in sAD and rpAD can result in a higher dose-dependent impairment of potassium channels and trigger a greater disturbance in neurotransmission. Aberrant expression of voltage-gated potassium channels and subsequent dysregulation of action potential have previously been associated with neurodegeneration (Angulo et al., 2004; Shirwany et al., 2007). Additionally, synaptotagmin-1 was detected in rpAD cases but not in sAD cases. Synaptotagmin-1 is involved in the release of neurotransmitters through its interactions with the SNARE complex and phospholipid membranes and has been previously reported to be increased in AD-associated pathologies (Südhof et al., 2012; Öhrfelt et al., 2016). Furthermore, it has also been reported to implicate the generation of Aβ through its interaction with PSEN 1 (Zoltowska et al., 2017). The functional categorization of interactors in FA-soluble fraction also revealed a greater number within rpAD (5.5%), in comparison to sAD (1.5%) and control brains (0%), to be involved in neurotransmission.

4.5.1.5 Metabolism and cell cycle

Insulin resistance, misprocessing of glucose, dysregulation of lipids, aberrant levels of cholesterol and reduced energy metabolism have been frequently associated with AD pathology, leading to its interpretation as a metabolic disorder. Together these alterations are believed to accelerate the accumulation of misfolded proteins (Grimm et al., 2007; Demetrius and Driver, 2013; Di Domenico et al., 2017). Several proteins involved in energy and glucose metabolism were also fished out as interactors in Tris-soluble fraction. Adenylate kinase, ATP synthase and ADP/ATP translocase, crucial elements for the generation and availability of ATP, were found to interact with Aβ in rpAD but not in sAD. Glycolytic enzymes, including citrate synthase, fructose-bisphosphate aldolase C and phosphoglycerate kinase, were commonly detected in both subtypes of AD. In the FA-soluble fraction, sAD cases showed a greater percentage (30%) of interactors to be involved in the processing of biomolecules and the generation of energy contrast to rpAD (20%) and control cases (15%).

Several proteins involved in cell cycle and neurogenesis were also found among the interactors. Neurons, unlike most of the other cell types, do not undergo mitosis in adults. Atypical initiation of cell cycle normally results in apoptosis, leading to a loss of neuronal tissue. Evidence in favor of Aβ-induced aberrant re-entry of neurons into the cell cycle and an associated increase in apoptosis has been presented in the past (Moh et al., 2011). An Aβ-induced decrease in adult neurogenesis and neuronal maturation is also being argued as some of the earliest changes in AD (Mu and Gage, 2011; Scopa et al., 2019). In the FA-soluble fraction, 14% of the interactors in rpAD were found to be involved in cell cycle-related mechanisms in comparison to 6.2% and 7.3% in sAD and control cases, respectively. No interactors from this functional category were found in Tris-soluble fraction.

4.5.1.6 Transcriptional and translational machinery

Alterations in ribosomes and protein synthesis have been frequently reported in AD over the last two decades (Ding et al., 2005). Interestingly, differential downregulation of ribosomal proteins has also been associated with rpAD (Garcia-Esparcia et al., 2017). In line with these findings, the current dataset also confirmed the involvement of many interactors, directly or indirectly, in the maturation of mRNA and translation of proteins, in the FA-soluble fraction of sAD (20%), rpAD (10%) and controls (7%). However, in Tris-soluble fractions, the 40S and 60S ribosomal proteins were seen in all subentities except sAD.

4.5.1.7 Redox pathways

Oxidases and reductases constitute important components of the pathways involved in sustaining functions of cells (Dykens, 2007). Several of these enzymes, including flavin reductase, NAD(P) transhydrogenase and dihydropteridine reductase, were seen to interact with Aβ in both Tris- and FA-soluble fractions and highlight a probable effect of Aβ on the metabolism of ATP and other critical biomolecules. Aβ was also seen to interact with peroxiredoxin, a known antioxidant, in the FA-soluble fraction of all experimental groups. Peroxiredoxins have been previously implicated to reduce Aβ-induced oxidative stress and neurotoxicity (Kim et al., 2016; Park et al., 2017).

4.5.1.8 Chaperone activity

A majority of chaperones, including heat shock protein 70, endoplasmic reticulum chaperone BiP and α-crystallin, were detected in all experimental groups in the FA-soluble fraction and constituted the largest functional category of overlapping proteins in various groups. Heat shock proteins and other chaperones are known to play a role in protein folding and clearance of misfolded proteins and undergo expressional anomalies in AD pathology (Yoo et al., 2001; Wilhelmus et al., 2007). Surprisingly, in FA-soluble samples, a greater number of interactors in rpAD cases than in sAD cases were chaperones highlighting probable differences in the folding and clearance of misfolded Aβ in the two variants. In the Tris-soluble fraction, peptidyl-prolyl cis-trans isomerase A, another chaperone, was present in sAD and rpAD cases only.

4.6 Limitations and considerations

Despite cautiously controlled conditions and optimized protocols, a few limitations have to be considered. Although MALDI-MS protocol employed in the current study has been a valuable tool for the analysis of Aβ in the past, our primary method of choice was a sequencing-based mass spectrometric technique. Sequencing provides a better insight into minor proteoform-specific changes, including posttranslational modifications, that are overlooked while manually annotating peaks. However, the hydrophobic nature of the target peptide rendered our LC-coupled MS/MS peptide sequencers useless and the annotation had to be conducted manually based on m/z ratios.

Moreover, the genotyping of rpAD samples has been limited to APOε to date. The data for mutations in Aβ-cleaving enzymes and other proteins that might influence APP processing and amyloidogenesis is the key to explaining differences in the signature and aggregation propensities of sAD and rpAD cases. Although the current project used the proteomic platform extensively, the speculations are only partially useful without understanding the genomic background.

Lastly, the non-demented control samples employed in the current study were chosen age-matched with the diseased cases. However, non-demented individuals also exhibit Aβ pathology. The presence of Aβ, even at lower levels, in the absence of clinical symptoms can complicate several findings especially the study of Aβ-cleaving enzymes and Aβ interactors. An analysis of cases without Aβ pathology can further justify the relative quantities of enzymes and provide a better insight into disease-specific interactors.

5. Summary and conclusion

The molecular mechanisms involved in atypical rapid progression of Alzheimer's disease (AD), as seen in rpAD, are not known. Subtle changes in Aβ-ome have been frequently associated with distinct phenotypic presentations of AD cases. The current project was aimed to define these clinical variants based on alterations in the sequence, processing, folding and toxicity of distinct Aβ peptides and their associated proteoforms. An array of proteomic techniques was used in combination with various biophysical methods to characterize brain-derived Aβ from sAD and rpAD brains. Additionally, a comprehensive analysis of toxic mechanisms mediated by Aβ in sAD and rpAD was also conducted.

Hybrid-IP, followed by 2D gel electrophoresis and top-down MALDI MS, was employed to isolate Aβ from FA-soluble fractions of sAD, rpAD and non-demented control brains to establish a signature of brain-derived proteoforms and 33 Aβ proteoforms were identified. $A\beta_{40}$, $A\beta_{42}$, $A\beta_{4\text{-}42}$, $A\beta_{11\text{-}42}$ and pyroglutamate $A\beta_{11\text{-}42}$ were common in all sAD and rpAD cases, however, several shorter N-terminally and C-terminally truncated proteoforms showed disease-specific involvement. Since the majority of prior studies have focused exclusively on $A\beta_{40}$ and $A\beta_{42}$, the exact function of these shorter peptides, presenting a disease-specific signature, remains unknown to date. Non-demented controls did not produce analyzable peaks due to the lower quantity of Aβ. It is noteworthy that sAD showed a greater variety among monomeric species of proteoforms, whereas the rpAD cases featured more proteoforms as multimers, hinting at their different capabilities to aggregate in response to SDS in 2D GE.

The semi-quantitative analysis of enzymes involved in the generation of Aβ yielded no differences, however, the ratio of BACE-1/ADAM-10 was significantly higher in rpAD samples than in sAD samples, indicating higher cleavage of Aβ via the amyloidogenic pathway. The overall amounts of APP, $A\beta_{Total}$ and its differentially cleaved proteoforms were not significantly different among the sAD and rpAD cases, although both subtypes had amounts that were significantly higher than non-demented controls. In the case of Tris-soluble fraction, ELISA results showed a lower amount of C-terminally truncated proteoforms in comparison to N-terminal truncations in all control, sAD and rpAD cases. This trend was especially evident in sAD cases where the amount of N-terminally truncated Aβ was significantly higher than its C-terminal counterparts, possibly because shorter

proteoforms are less prone to aggregation and are frequently formed during the clearance of highly aggregated, larger proteoforms. However, FA-soluble fraction showed no significant differences among N-terminally and C-terminally truncated pools.

The lack of a well-defined signature of Aβ proteoforms between sAD and rpAD brains, unaltered states of the major proteoforms and non-significant differences in their expression prompted the study of aggregation kinetics and structural variations of sAD- and rpAD-derived fibrils. 'Strain theory' of prion diseases was therefore utilized and Aβ fibrils, purified in their native state via ultracentrifugation, were amplified through RT-QuIC assay. The products were thoroughly assessed for structural variations that might be responsible for differences in the progression of the targeted clinical subtypes. Although FTIR showed that the secondary structure of Aβ amyloids from both subtypes of AD was highly similar, the conversion of monomeric species to β-sheet rich fibrils was faster in sAD cases in comparison to rpAD and the latter presented significantly larger aggregates highlighting the presence of more hydrophobic Aβ seeds in this group. Additionally, the accessory proteins that may contribute towards variation in aggregation kinetics of brain-derived seeds were also identified.

In the light of these findings, it can be postulated that although the fibrils generated by rpAD brains are more hydrophobic and capable of generating larger amorphous aggregates, their conversion from seeds to fibrils appears to be slower. During this process, Aβ may exist as more toxic oligomeric species for a longer duration and impart greater toxicity on surrounding neurons. The clinical phenotype resulting from these changes may, therefore, present a faster rate of progression even though the overall profiles of total Aβ in CSF and brain appear highly similar. Collectively, this evidence supports that differences in aggregation propensities and hydrophobicity may underlie the atypical progression of AD.

To further the understanding of Aβ-associated alterations in sAD and rpAD brains, a functional analysis was also included in this study. An extended treatment of neuronal cells with fibrils generated via RT-QuIC assay resulted in no significant differences in the survival and confirmed that Aβ from sAD and rpAD was equally toxic in its final fibrillar confirmation. The study on human samples conducted using co-IP, on the other hand, identified putative interactors involved in growth, neurotransmission, metabolism and transport and provided useful insights into different functional pathways modulated by Tris-soluble and FA-soluble pools of Aβ. In rpAD cases, Aβ

interactors majorly modulated neurotransmission, neurogenesis and protein folding, whereas a majority of Aβ interactors from sAD brains affected the replication, transcription, translation, transport of biomolecules and various metabolic pathways. Owing to the physiological function of Aβ, Aβ interactors from control brains modulated pathways involved in immune response and maintaining the structural integrity of tissues.

The hypotheses proposing Aβ as the driving force behind AD are a controversial component of AD research in the current era pertaining to the failure of Aβ-targeting therapies. This study sheds light on the possible limitations in Aβ research that have been tilting the odds against these hypotheses. Studies focused on understanding this peptide on a proteomic level do not explain differences in the clinical presentation of AD subtypes nor do they deliver promising results in drug trials. No differences were detected in the expression, quantity and processing of major enzymes in the current study either. As has been the case with a majority of studies in the last decade, these findings can prompt the researchers to turn their attention towards more promising candidates. However, examining Aβ under the lens of strain-based differences cannot only validate the involvement of Aβ in the pathophysiology of AD but also contribute towards our understanding of distinct clinical presentations of this debilitating disorder.

6. Appendix A

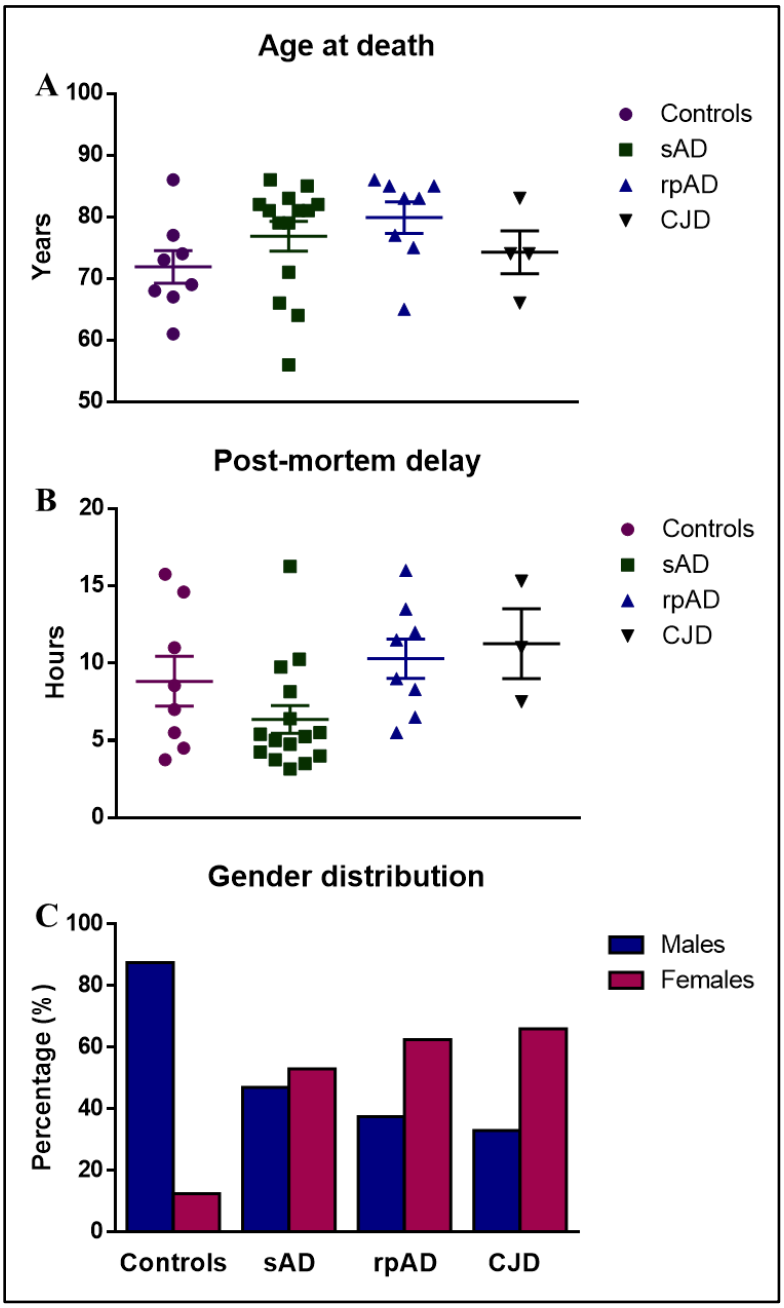

Figure 32: Comparison of ages at death, post-mortem delay and gender distribution of non-demented control, sAD, rpAD and CJD samples used in the current study. No significant differences were observed in the (A) ages at death and (B) post-mortem delays in autopsy among the samples in the four experimental groups. The relative percentage of females was higher in sAD, rpAD and CJD cohorts in comparison to non-demented controls. One-way ANOVA was used for statistical analysis. Error bars present SEM.

Table 10: Clinical data of brain samples utilized in the current study.

No.	Patient ID	Gender	Age	Braak Stages or Subtype
1.	Control 1	Male	86	II/A
2.	Control 2	Male	69	II/A
3.	Control 3	Male	68	I/0
4.	Control 4	Male	77	I/A
5.	Control 5	Male	67	I/0
6.	Control 6	Female	73	I/0
7.	Control 7	Male	61	I/0
8.	Control 8	Male	74	II/A
9.	sAD 1	Female	56	V/C
10.	sAD 2	Female	85	V/C
11.	sAD 3	Female	81	V/C
12.	sAD 4	Female	81	IV/C
13.	sAD 5	Female	82	V/B
14.	sAD 6	Male	81	IV/B
15.	sAD 7	Male	82	V/C
16.	sAD 8	Male	66	V/C
17.	sAD 10	Female	79	I/A
18.	sAD 11	Female	79	I/A
19.	sAD 12	Female	86	II/A
20.	sAD 13	Male	83	III/0
21.	sAD 14	Female	71	III/0
22.	sAD 15	Male	64	II/A
23.	rpAD 1	Male	83	VI/C
24.	rpAD 2	Female	77	IV
25.	rpAD 3	Female	85	V
26.	rpAD 4	Female	85	IV
27.	rpAD 5	Male	83	VI/C
28.	rpAD 6	Male	65	-
29.	rpAD 7	Female	86	-
30.	rpAD 8	Female	75	III
31.	sCJD 1	Female	74	VV2
32.	sCJD 2	Male	66	MM/MV1
33.	sCJD 3	Female	74	MM/MV1
34.	sCJD 4	-	83	MM/MV2

Appendix B

Table 11: Observed masses (Da) for Aβ proteoforms identified by MALDI-ToF MS. pAβ represents pyroglutamate Aβ proteoforms.

	Proteoform	Observed Mass (Da)	Theoretical Mass (Da)
1.	$A\beta_{1-12}$	1426.5	1424
2.	$A\beta_{2-13}$	1448.6	1446
3.	$A\beta_{3-14}$	1515.6	1512
4.	$A\beta_{2-14}$	1587.1	1583
5.	$A\beta_{11-33}$	2115.9	2111
6.	$A\beta_{2-20}$	2349.2	2346
7.	$A\beta_{15-38}$	2448.7	2452
8.	$A\beta_{1-20}$	2463.0	2461
9.	$A\beta_{14-38}$	2584.7	2588
10.	$A\beta_{5-27}$	2671.7	2672
11.	$A\beta_{5-29}$	2852.3	2857
12.	$A\beta_{1-26}$	3017.3	3021
13.	$pA\beta_{11-40}$	3116.7	3115
14.	$A\beta_{1-27}$	3134.5	3134
15.	$pA\beta_{11-42}$	3317.6	3318
16.	$A\beta_{11-42}$	3333.6	3335
17.	$A\beta_{9-40}$	3375.7	3372
18.	$A\beta_{11-43}$	3434.2	3437
19.	$A\beta_{8-40}$	3460.2	3459
20.	$A\beta_{9-42}$	3554.2	3557
21.	$A\beta_{8-42}$	3643.0	3643
22.	$A\beta_{1-34}$	3786.7	3787
23.	$A\beta_{4-40}$	4014.4	4014
24.	$A\beta_{5-42}$	4050.9	4051
25.	$A\beta_{1-37}$	4074.9	4074
26.	$A\beta_{1-38}$	4128.3	4132
27.	$A\beta_{3-40}$	4145.9	4144
28.	$A\beta_{4-42}$	4197.5	4198
29.	$pA\beta_{3-42}$	4309.8	4310
30.	$A\beta_{1-40}$	4327.1	4329
31.	$A\beta_{2-42}$	4397.7	4400
32.	$A\beta_{1-41}$	4445.0	4443
33.	$A\beta_{1-42}$	4513.0	4514

Appendix C

Table 12: List of *in vitro* interactors identified in FA-soluble fraction of sAD (abbreviated as A in the table), rpAD (R) and control (C) brain samples. Peptides were identified from 3 pooled biological replicates per experimental group and identifications were accepted, if established at a greater than 95.0% confidence while a minimum of two confident peptide identifications and a confidence threshold of 99.0% was required for protein identifications. The localization and functional category of identified Aβ interactors was annotated using UniProtKB database. The subset of proteins that co-purified with fibrils in the third MS dataset, have also been indicated. 'Mit' stands for mitochondria, 'Nu' for nucleus, 'Cy' for cytoplasm, 'Cysk' for cytoskeleton, 'Mem' for cell membrane, 'ER' for endoplasmic reticulum, 'Ly' for lysosome and 'Ex' for extracellular. The symbol * indicates the presence of different subunits of the stated protein complex in the fibrillar fraction.

Identified Proteins	UniProt ID	Localization	Functional Category	Specificity	Purified with fibrils
10 kDa heat shock protein	P61604	Mit	Chaperone	R	No
14-3-3 protein	P62258	Nu	Signal Transduction	A, C	Yes
26S proteasome non-ATPase regulatory subunit	O75832	Nu	Chaperone, Apoptosis	A, R	Yes
28S ribosomal protein	P82663	Mit	Translation	R	No
39S ribosomal protein	Q9H0U6	Mit	Translation, Chaperone	A, R	No
4-aminobutyrate aminotransferase	P80404	Mit	Neurotransmission	R	Yes
55 kDa erythrocyte membrane protein	Q00013	Mem	Signal Transduction	A, R	No
60S ribosomal protein	P62913	Nu	Translation	A, R	Yes
Phosphogluconolactonase	O95336	Cy	Glucose Metabolism	R	No
Abl interactor 1	Q8IZP0	Nu, Cy, Cysk	Dendrite growth	R	Yes
Abscission/NoCut checkpoint regulator	Q96K21	Cysk	Cell division	R	No
Acetyl-CoA acetyltransferase	Q9BWD1	Mit, Cy	Fatty acid metabolism	A	No
Aconitate hydratase	Q99798	Mit	Glucose metabolism	A, R	Yes
Actin-like protein 6B	O94805	Nu	Neurogenesis, Transcription	R	Yes*
Activator of 90 kDa heat shock protein ATPase	O95433	ER, Cy	Chaperone, Stress response	R, C	No
Acyl-CoA dehydrogenase family member 9	Q9H845	Mit	Oxidoreductase	A	No
Adaptin ear-binding coat-associated protein 1	Q8NC96	Mem	Transport	R	No
Adenosylhomocysteinase	P23526	Cy	Glucose metabolism	A, C	Yes
Adenylate kinase isoenzyme 1	P00568	Mit	Energy metabolism	R	No
ADP/ATP translocase 1	P12235	Mit	Transport	A, R	Yes
ADP-ribosylation factor 4	P18085	Golgi	Transport	A, R	Yes
Aldehyde dehydrogenase	P05091	Mit	Oxidoreductase	A, R	Yes

Alpha-actinin-2	P35609	Cy	Apoptosis	R, C	Yes
Alpha-crystallin B chain	P02511	Nu	Chaperone	All	No
Alpha-enolase	P06733	Nu, Cy	Glucose metabolism	All	Yes
Amine oxidase	P27338	Mit	Oxidoreductase	A	No
Amphiphysin	P49418	Cysk	Synaptic Transmission	R	Yes
Annexin	P50995	Nu	Cell cycle, Cell division	All	Yes
AP-2 complex subunits	O95782	Mem	Transport	R	Yes
APC membrane recruitment protein	Q8N7J2	Mem	Signal Transduction	R	No
Apolipoprotein D	P05090	Ex	Transport	A	No
Apolipoprotein E	P02649	Ex	Transport	R	Yes
Apoptosis-inducing factor 1	O95831	Nu	Apoptosis	A	No
Arginase-1	P05089	Cy	Immunity	All	No
Aspartate aminotransferase	P00505	Mem	Transport	A, R	No
Aspartate-tRNA ligase	P14868	Cy	Protein biosynthesis	A	Yes
ATP synthase subunit O	P48047	Mit	Transport	R	Yes
ATPase ASNA1	O43681	Nu, ER	Transport	R	No
ATP-binding cassette sub-family B member 8	Q9NUT2	Mit	Transport, ATP Binding	A	No
ATP-dependent RNA helicase	Q7Z478	Cy	Protein metabolism	A, R	Yes
BPI fold-containing family A, B member 1	Q9NP55	Ex	Immunity	C	No
Breast carcinoma-amplified sequence 1	O75363	Mem	Mylination	R	No
Calcium/calmodulin-dependent protein kinase type II subunit α	Q9UQM7	Mem	Kinase, Transferase	R, C	Yes
Calponin-3	Q15417	Cy	Cell-cell adhesion	A	Yes
Calreticulin	P27797	Cy, Mem	Chaperone	A	Yes
cAMP-dependent protein kinase	P10644	Mem	Signal Transduction	R, C	Yes
Carbonyl reductase 1	P16152	Cy	Oxidoreductase	R	Yes
Caspase-14	P31944	Nu	Differentiation	All	No
Catalase	P04040	Peroxisome	Stress response	A	No
Cathepsin D	P07339	Ex, Ly	Protein processing	A, R	No
Caveolae-associated protein 1	Q6NZI2	Nu, Cy	Transcription	A, R	No
CB1 cannabinoid receptor-interacting protein 1	Q96F85	Mem	Signal Transduction	R	No
CD44 antigen	P16070	Mem	Cell adhesion	A	No
CD59 glycoprotein	P13987	Mem	Vesicle transport	A	No
Cell adhesion molecule 4	Q8NFZ8	Mem	Cell adhesion	R	No
Charged multivesicular body protein	Q9HD42	Nu, Cy	Cell cycle, Transport	C	No
Chloride intracellular channel protein 4	Q9Y696	Mem, Mit	Transport	A, R	No
Citrate synthase	O75390	Mit	Glucose Metabolism	All	Yes
Clathrin heavy chain 1	Q00610	Cysk	Mitosis	R, C	Yes

Cofilin-1	P23528	Cy, Mem, Nu	Signal Transduction	All	Yes
Collagen alpha-2(I) chain	P08123	Ex	Collagen fibril organization	C	Yes
Contactin-1	Q12860	Ex	Cell adhesion, cell signalling	R, C	Yes
COP9 signalosome complex subunit 4	Q9BT78	Nu	DNA damage repair	R, C	No
Copine-1	Q99829	Nu, Mem	Transcription	A, R	No
Corneodesmosin	Q15517	Ex	Cell Adhesion	All	No
Coronin	Q9BR76	Cysk	Cytoskeleton organization	R	No
Creatine kinase	P06732	Cy	Kinase, Transferase	All	Yes
CUGBP Elav-like family member 1	Q92879	Nu	mRNA processing	R	Yes
Cystatin-B and C	P04080	Nu	Protease inhibitor	R	Yes
Cysteine and glycine-rich protein 1	P21291	Nu	Platelet aggregation	A, R	No
Cytochrome b-c1 complex	P31930	Mit	Energy Metabolism	All	Yes*
Cytosol aminopeptidase	P28838	Cy	Protein processing	A	Yes
Cytosolic non-specific dipeptidase	Q96KP4	Cy	Protein processing	A, R	Yes
Delta-1-pyrroline-5-carboxylate dehydrogenase	P30038	Mit	Proline metabolism	A	No
Dematin	Q08495	Cy	Actin cytoskeleton organization	R	Yes
Deoxyuridine 5'-triphosphate nucleotidohydrolase	P33316	Mit, Nu	Nucleotide metabolism	A	No
Dihydrolipoyl dehydrogenase	P09622	Mit, Nu	Redox homeostasis	A, R	No
Dihydrolipoyllysine-residue of pyruvate-dehydrogenase complex	P10515	Mit	Carbohydrate metabolism	A	Yes
succinyltransferase component of 2-oxoglutarate dehydrogenase complex	P36957	Mit, Nu	Tricarboxylic acid cycle	All	Yes
Dihydropteridine reductase	P09417	Cy	Protein metabolism	R	No
Dihydropyrimidinase-related protein	Q14195	Cy	Protein processing	R	Yes*
Diphosphoinositol polyphosphate phosphohydrolase 2	Q9NZJ9	Cy	Signal Transduction	R	Yes
DNA-directed RNApolymerases	O15160	Nu	Transcription	R	No
DnaJ family A member 2	O60884	Mem	Chaperone	R	No
DnaJ homolog subfamily B	P25686	Nu, ER	Chaperone	All	Yes
Drebrin	Q16643	Cy	Differentiation, Neurogenesis	R	No
Dynactin subunit	Q13561	Cysk	Cell cycle	All	No
Dynamin-1	Q05193	Cysk	Transport	R, C	Yes
EH domain-containing protein 2	Q9NZN4	Cy	Endocytic recycling	A	Yes*
Electron transfer flavoprotein	P13804	Mit	Transport	A	Yes
Electron transfer flavoprotein-ubiquinone oxidoreductase	Q16134	Mit	Transport	A	Yes

Elongation factor	P29692	Nu	Protein metabolism, transcription	R, C	Yes
Endophilin	Q99962	Cy	Endocytosis	R, C	Yes
ER chaperone BiP	P11021	ER	Chaperone, Hydrolase	All	Yes
ER resident protein 29	P30040	ER	Transport	R	Yes
Endoplasmin	P14625	ER	Chaperone	R	No
Enoyl-CoA hydratase	P30084	Mit	Fatty acid metabolism	R	Yes
Erlin-2	O94905	ER	Lipid metabolism	R, C	Yes
Eukaryotic initiation factor 4A-I	P60842	Cy	Host-virus interaction	C	Yes
Eukaryotic peptide chain release factor subunit 1	P62495	Cy	Protein metabolism	A	No
Eukaryotic translation initiation factor	P47813	Cy	Protein metabolism	All	Yes
F-actin-capping protein subunit	P47756	Cysk	Cytoskeleton organization	R	Yes
Fascin	Q16658	Cysk	Cytoskeleton organization	A, R	Yes
Fibrinogen	P02679	Ex	Hemostasis	R, C	Yes
Filaggrin	P20930	Cysk	Developmental protein	All	Yes
Filamin-C	Q14315	Cysk	Cell junction assembly	R	Yes*
Flavin reductase	P30043	Cy	Oxidoreductase	C	Yes
Fructose-bisphosphate aldolase	P04075	Cy	Carbohydrate metabolism	All	Yes
Fumarate hydratase	P07954	Mit	Carbohydrate metabolism	R	Yes
Galectin	P09382	Ex	Apoptosis	All	Yes
GABA receptor-associated protein	P60520	Golgi	Transport	R	No
Gamma-enolase	P09104	Mem	Carbohydrate metabolism	All	Yes
Gelsolin	P06396	Ex	Cytoskeleton organization	R, C	No
Glucose-6-phosphate isomerase	P06744	Ex	Carbohydrate metabolism	A, R	Yes
Glutamate dehydrogenase	P00367	Mit	Carbohydrate metabolism	All	No
Glutaminase kidney isoform	O94925	Cy, Mit	Glutaminase activity	A, C	Yes
Glutamine amidotransferase-like	P0DPI2	Mit	-	C	No
Glutaredoxin-3	O76003	Cy	Homeostasis	A	No
Glutathione reductase	P00390	Mit	Redox homeostasis	R	No
Glutathione S-transferase	P78417	Cy	Oxidoreductase, Transferase	A, R	Yes
Glyceraldehyde-3-phosphate dehydrogenase	P04406	Cy, Nu	Apoptosis, Translation regulation	All	Yes
Glycogen phosphorylase	P11217	Cy	Carbohydrate metabolism	R	Yes
G-rich sequence factor 1	Q12849	Mit	mRNA processing	R	No
Growth arrest-specific protein 7	O60861	Cysk	Differentiation, Neurogenesis	R	No
Growth factor receptor-bound protein	P62993	Nu, Golgi	Signal transduction	All	No
Guanine deaminase	Q9Y2T3	Cy	Nervous system development	R	No
Guanine nucleotide-binding protein	P62873	Cy, Ly, Mem	Signal Transduction	All	No
Guanylate kinase	Q16774	Cy	Transport	C	No

Haptoglobin	P00738	Ex	Immunity	R	No
Heat shock 70 kDa protein 1A	PDMV8	Nu, Mem	Chaperone, Stress response	All	Yes
Heat shock 71 kDa protein	P11142	Nu, Mem	Chaperone	All	Yes
Heat shock protein beta-1	P04792	Nu	Chaperone, Stress response	All	Yes
Heat shock protein HSP 90	P07900	Nu, Mem	Chaperone	R, C	Yes
Heme-binding protein 1	Q9NRV9	Cy	Signal Transduction	A, C	No
Hemoglobin subunit alpha/ beta	P69905	Cy, Mem	Transport	All	Yes
Heparan sulfate proteoglycan core protein	P98160	Ex	Angiogenesis	A	Yes
Hepatoma-derived growth factor	P51858	Nu	Transcription regulation	A	No
Heterogeneous nuclear ribonucleoprotein	Q99729	Nu	Transcription regulation	All	Yes
Hexokinase-1	P19367	Mit	Carbohydrate metabolism	R	No
Histone deacetylase complex subunit	O00422	Nu	Transcription regulation	R	Yes
Histone H2A, 2B, H4	P20671	Nu	Chromatin organization	All	Yes
Histone-binding protein RBBP4	Q09028	Nu	Transcription regulation	A	Yes
HLA class I antigen	P04439	Mem	Immunity	A	No
Homer protein homolog	Q86YM7	Mem	Transport	R, C	No
Hsc70-interacting protein	P50502	Cy	Chaperone	All	No
Hsp90 co-chaperone Cdc37	Q16543	Nu, Mem	Chaperone	R, C	No
Hyaluronan and proteoglycan link protein 2	Q9GZV7	Ex	Cell adhesion	R	Yes
Hypoxanthine-guanine phosphoribosyl-transferase	P00492	Cy	Purine nucleotide biosynthetic process	R	No
Inosine-5'-monophosphate dehydrogenase 2	P12268	Nu	GMP biosynthesis, Purine bio-synthesis	R	No
Inter-alpha-trypsin inhibitor	P19823	Ex	Protein processing	R	No
Interleukin enhancer-binding factor 2	Q12905	Nu	Transcription regulation	A	Yes
Intracellular hyaluronan-binding protein 4	Q5JVS0	Nu	Transcription regulation	R	No
IQ motif and SEC7 domain-containing pro-tein 1	Q6DN90	Nu	Cytoskeleton organization	R, C	Yes
Isocitrate dehydrogenase	O75874	Cy	Carbohydrate metabolism	A	Yes
Junction plakoglobin	P14923	Cysk	Cell adhesion	All	Yes
Kininogen-1	P01042	Ex	Inflammatory response	A	No
Lamin-B2	Q03252	Nu	Structural molecule activity	R	Yes
Leucine-rich repeat flightless-interacting protein 2	Q9Y608	Nu	Wnt signaling pathway	R	No
Lipoamide acyltransferase component of branched-chain alpha-keto acid dehydro-genase	P11182	Mit	Glyoxylate metabolism	R	No
L-lactate dehydrogenase	P00338	Cy	Carbohydrate metabolism	R	Yes
Lysozyme C	P61626	Ex	Antimicrobial	All	No

Macrophage-capping protein	P40121	Nu	Actin capping, Actin-binding	A, R	No
MAGUK p55 subfamily member 6	Q9NZW5	Mem	-	R	Yes
Major prion protein	P04156	Mem, Golgi	Cell cycle, Growth arrest	All	Yes
Malate dehydrogenase	P40925	Cy	Carbohydrate metabolism	A, R	Yes
Mammaglobin-B	O75556	Ex	Protein processing	C	No
Mammalian ependymin-related protein 1	Q9UM22	Ex	Cell-matrix adhesion	A, R	Yes
MAP6 domain-containing protein 1	Q9H9H5	Cy, Golgi	Cytoskeleton organization	R	No
Methanethiol oxidase	Q13228	Cy, Mem, Nu	Transport	A	No
Methionine aminopeptidase 2	P50579	Cy	Protein processing	R	No
Methylmalonate-semialdehyde dehydrogenase [acylating]	Q02252	Mit	Protein metabolism	A, R	No
Methyltransferase-like 26	Q96S19	-	-	R	No
MICOS complex subunit MIC	Q9NX63	Mit, Nu	Transcription regulation	C	Yes
Microtubule-associated protein 1	P46821	Cy	Cytoskeleton organization	R, C	Yes
Microtubule-associated protein 2	P11137	Cysk	Cytoskeleton organization	R	Yes
Microtubule-associated protein RP/EB family member 2	Q15555	Cysk	Cell cycle, Cell division, Mitosis	R	Yes
Microtubule-associated protein tau	P10636	Cysk, Mem	Synapse organization	A, R	Yes
Mucin-like protein 1	Q96DR8	Ex	Signaling pathway	A	No
Myc box-dependent-interacting protein 1	O00499	Nu, Mem, Cy	Differentiation, Host-virus interaction	R	No
Myelin proteolipid protein	P60201	Mem	Axon development	A	No
Myelin-associated glycoprotein	P20916	Mem	Cell adhesion	A, R	Yes
Myosin light chain 6B	P14649	Cy	Motor protein	A, R	Yes*
Myosin-10	P35580	Cy	Cell adhesion, Cell shape	R, C	Yes
Myosin-binding protein C, cardiac-type	Q14896	Cy	Cell adhesion	R	No
N(G),N(G)-dimethylarginine dimethylaminohydrolase 2	O95865	Cy, Mit	Signal transduction	R	No
$Na^{(+)}/H^{(+)}$ exchange regulatory cofactor NHE-RF1	O14745	Cy	Wnt signaling pathway	R	No
NAD(P) transhydrogenase	Q13423	Mit	Redox homeostasis	A, R	Yes
NAD-dependent protein deacetylase sirtuin-2	Q8IXJ6	Nu, Cysk, Mem	Autophagy, Immunity, Transcription regulation	R	No
NADH dehydrogenase	Q9P0J0	Nu, Mit	Apoptosis, Transport	All	Yes
NADH-ubiquinone oxidoreductase	P28331	Mit	Transport	R	Yes
NADP-dependent malic enzyme	Q16798	Mit	Carbohydrate metabolism	A	Yes
NADPH:adrenodoxin oxidoreductase	P22570	Mit	Lipid metabolism	R	Yes
NCK-interacting protein	Q9NZQ3	Nu	Cytoskeleton organization	R	Yes
Neuroblast differentiation-associated protein AHNAK	Q09666	Nu	Regulation of voltage-gated calcium channel activity	A	Yes

Neuroendocrine convertase 1	P29120	Cy	Release of protein hormones.	R	No
Neurofascin	O94856	Mem	Cell adhesion	C	Yes
Neurogranin	Q92686	Cy	Signal transduction	R	No
Neuronal-specific septin-3	Q9UH03	Cy	Cell cycle, Cell division	R, C	Yes
Neutrophil defensin 3	P59666	Ex	Antimicrobial, Fungicide	A	Yes*
Nicotinamide phosphoribosyltransferase	P43490	Nu, Ex	Biological rhythms, Pyridine nucleotide biosynthesis	A	Yes
Non-POU domain-containing octamer-binding protein	Q15233	Nu	Immunity, Transcription regulation	A, R	Yes
Nuclear distribution protein nudE homolog 1	Q9NXR1	Cysk	Cell cycle, Neurogenesis	R	No
Nuclear migration protein nudC	Q9Y266	Cy, Nu	Cell cycle	All	Yes
Nucleophosmin	P06748	Nu, Cy	Chaperone	A	Yes
Osteopontin	P10451	Ex	Cell adhesion	A	No
Paralemmin-1	O75781	Mem	Synapse maturation	R	Yes
PDZ and LIM domain protein 7	Q9NR12	Cy	Differentiation	A	No
Peptide deformylase	Q9HBH1	Mit	Protein biosynthesis	R	No
Peptidyl-prolyl isomerase	P62937	Cy, Ex	Protein processing	All	Yes
Peptidyl-tRNA hydrolase ICT1	Q14197	Mit	Protein biosynthesis	R	No
Perilipin-3	O60664	Cy	Transport	R, C	Yes
Peroxiredoxin	Q06830	Cy	Redox homeostasis	All	Yes
PHD finger protein 24	Q9UPV7	-	Neurotransmission	R, C	Yes
Phosphate carrier protein	Q00325	Mit	Transport	A	No
Phosphatidylethanolamine-binding protein 1	P30086	Cy	Regulation of neurotransmission	R, C	Yes
Phosphoglucomutase-1	P36871	Cy	Carbohydrate metabolism	A	No
Phosphoglycerate kinase 1	P00558	Cy	Carbohydrate metabolism	A, C	Yes
Phosphoglycerate mutase 1	P18669	Cy, Ex	Carbohydrate metabolism	R, C	Yes
Phosphoserine aminotransferase	Q9Y617	Cy	Amino-acid biosynthesis	A	No
PITH domain-containing protein	Q9GZP4	Nu	-	A, C	No
Platelet-activating factor acetylhydrolase IB subunit beta	P68402	Cy	Lipid metabolism	R	Yes
Plectin	Q15149	Cysk	Cysk regulation	R, C	Yes
Poly(rC)-binding protein	Q15365	Nu, Cy	mRNA Splicing	A	Yes
Polyadenylate-binding protein 2	Q86U42	Nu	mRNA processing	R	Yes
Prefoldin subunit 3	P61758	Nu	Chaperone	A,R	No
Prelamin	P02545	Nu	Regulation of chaperone genes	All	Yes
Profilin	P07737	Cysk	Protein processing	R	Yes
Prohibitin	P35232	Mit	DNA synthesis	A,R	Yes
Prolactin-inducible protein	P12273	Ex	Protein processing	C	No

Propionyl-CoA carboxylase	P05165	Mit	Biotin metabolic process	A, R	Yes
ProSAAS	Q9UHG2	Golgi	neuropeptide signaling pathway	C	Yes
Prosaposin	P07602	Ly	Lipid metabolism	A	Yes
Proteasome subunit beta type-4	P28070	Nu	Protein processing	R	No
Protein ABHD14B	Q96IU4	Nu	Transcription regulation	All	No
Protein AMBP	P02760	Ex	Protein metabolism	A	No
Protein disulfide-isomerase	P07237	ER	Chaperone	All	Yes
Protein kinase C	Q9BY11	Cy	Endocytosis	R, C	Yes
Protein NDRG1	Q92597	Nu, Cy	Signal transduction	R	Yes
Protein RUFY3	Q7L099	Cy	Differentiation, Neurogenesis	R	Yes
Protein S100-A7	P31151	Cy, Ex	Immune response	A	No
Protein S100-A8	P05109	Ex	Immune response	A, R	Yes
Protein SET	Q01105	Nu, Cy, ER	Chaperone	A	No
Protein SOGA3	Q5TF21	Mem	Autophagy	R	No
Protein unc-119 homolog B	A6NIH7	Cy	Transport	R	No
Protein/nucleic acid deglycase DJ-1	Q99497	Mit, Mem, Nu	Stress response, Chaperone	A, R	No
Protein-L-isoaspartate(D-aspartate) O-methyltransferase	P22061	Cy	Protein processing	All	Yes
Proteolipid protein 2	Q04941	Mem	Transport	A	No
Pyruvate dehydrogenase E1 component subunit alpha	P08559	Mit	Carbohydrate metabolism	A, R	Yes
Ras GTPase-activating protein-binding protein 2	Q9UN86	Cy	Stress granule assembly	R	Yes
Ras-related protein Rab-7a	P51149	Ly	Autophagy, Transport	A	Yes
Ras-related protein Ral-A	P11233	Mem	Cell cycle, Exocytosis	R	Yes
Reticulocalbin-1	Q15293	ER	Protein metabolism	A	Yes
Reticulon-4	Q9NQC3	ER, Mem	Neurogenesis	A, R	Yes*
Ribosome-recycling factor	Q96E11	Mit	Protein biosynthesis	R	No
RNA-binding motif protein	P38159	Nu	mRNA processing, Transcription	A, R	No
RNA-binding protein Raly	Q9UKM9	Nu	mRNA processing	A	Yes
RuvB-like 1	Q9Y265	Nu	DNA repair	A, R	Yes
Sarcalumenin	Q86TD4	ER	Transport	A	Yes
Sarcoplasmic/ER calcium ATPase	P16615	ER	Transport	A, R	Yes
Secretoglobin family 1D member 2	O95969	Ex	Transcriptional regulation	A	No
Septin	Q9NVA2	Cysk	Cell cycle	All	Yes
Serine hydroxymethyltransferase	P34897	Nu, Mit, Cy	One-carbon metabolism	A, R	No
Serine protease HTRA1	Q92743	Cy, Ex	Protein processing	R	No
Serine/arginine-rich splicing factor	O75494	Nu	mRNA processing	A, R	Yes

Serine/threonine-protein phosphatase	P30153	Mem	Chromosome partition	A, R	Yes
Serine-threonine kinase receptor-associated protein	Q9Y3F4	Nu	mRNA processing	A	Yes
Shootin-1	A0MZ66	Cysk	Developmental protein	R, C	No
Single-stranded DNA-binding protein	Q04837	Mit	DNA replication	R	Yes
Sodium/potassium-transporting ATPase subunits	P05023	Mem	Transport	A, R	Yes
Solute-carrier family 12 member 5	Q9H2X9	Mem	Transport	R	Yes
SPARC-related modular calcium-binding protein 1	Q9H4F8	Ex	Differentiation	R	No
Spliceosome RNA helicase	Q13838	Nu	mRNA processing, Transport	A	No
Splicing factor	Q12874	Nu	mRNA splicing	R	Yes
Stomatin-like protein 2	Q9UJZ1	Mit, Mem	Mitochondrial fusion	R	Yes
Stress-70 protein	P38646	Nu, Mit	Chaperone	A,R	Yes
Submaxillary gland androgen-regulated protein 3B	P02814	Ex	Pain perception	R	No
Succinate--CoA ligase subunit β	Q9P2R7	Mit	Carbohydrate metabolism	R	Yes
Succinate-semialdehyde dehydrogenase	P51649	Mit	GABA metabolism	R, C	Yes
Succinyl-CoA:3-ketoacid coenzyme A transferase 1	P55809	Mit	Protein processing	A, R	Yes
Sulfite oxidase	P51687	Mit	Nitrate assimilation	R	No
Superoxide dismutase [Mn]	P04179	Mit	Superoxide metabolism	R, C	Yes
Suprabasin	Q6UWP8	Ex	-	R, C	No
Synapsin	P17600	Golgi	Neurotransmitter secretion	R	Yes
Syntaxin-binding protein	P61764	Cy	Transport	R, C	Yes
T-complex protein 1	P17987	Cy	Chaperone	A, R	Yes
TGF-beta-activated kinase 1	Q15750	Nu, Cy	Protein processing	R	No
Thioredoxin	P10599	Nu, Sec	Transcription regulation	A	No
Thioredoxin domain-containing protein 5	Q8NBS9	ER	Cell survival	R	No
THO complex subunit 4	Q86V81	Cy	Chaperone	R	No
Thymidine phosphorylase	P19971	Cy	Angiogenesis	A	No
Thymidylate kinase	P23919	Nu, Cy, Mit	Nucleotide biosynthesis	C	No
Transaldolase	P37837	Cy	Carbohydrate metabolism	A	No
Transcription factor A	Q00059	Mit	Transcription regulation	R	No
Transcriptional activator protein Pur-alpha	Q00577	Nu	Transcription regulation	R, C	No
Transformer-2 protein homolog beta	P62995	Nu	mRNA processing	A	Yes
Transforming protein RhoA	P61586	Mem	Cell cycle	A, R	No
Transgelin-3	Q9UI15	Nu, Cy	Development	R	Yes
Transitional ER ATPase	P55072	Nu, Cy, ER	Transport, protein processing	R	Yes

Transketolase	P29401	Nu, Ex, Cy	Carbohydrate metabolism	A	Yes
Transmembrane emp24 domain-containing protein 10	P49755	ER, Golgi	Protein transport	A	Yes
Trifunctional enzyme subunit α	P40939	Mit	Fatty acid metabolism	A	Yes
Triosephosphate isomerase	P60174	Cy	Gluconeogenesis, Glycolysis	All	Yes
Tripeptidyl-peptidase 1	O14773	Ly	Protein processing	R, C	Yes
tRNA-splicing ligase RtcB homolog	Q9Y3I0	Nu	tRNA processing	A, C	Yes
Tropomodulin-2	Q9NZR1	Cysk	synaptic transmission	R, C	Yes
Tubulin polymerization-promoting protein	O94811	Cy, Nu	microtubule bundle formation	R	Yes
Tubulin polymerization-promoting protein family member	Q9BW30	Cy	microtubule bundle formation	R	No
Tubulin-specific chaperone C	Q15814	Cy	Chaperone	R	No
Tubulin-specific chaperone cofactor E-like protein	Q5QJ74	Cysk	regulator of tubulin stability.	R	No
Ubiquitin carboxyl-terminal hydrolase	P54578	Mem	Immunity	A, R	Yes
Ubiquitin domain-containing protein	O14562	-	NF-kappa-B regulator.	R	No
Ubiquitin-60S ribosomal protein L40	P62987	Nu	Protein processing	A, R	Yes
UBX domain-containing protein	Q04323	Cy	Protein processing	R	Yes
UMP-CMP kinase	P30085	Nu	Pyrimidine biosynthesis	A, R	Yes
Uromodulin	P07911	CM, Sec	Ion homeostasis	A	No
Uroporphyrinogen-III synthase	P10746	Cy, Mit	Heme biosynthesis	R	No
UTP--glucose-1-phosphate uridylyltrans-ferase	Q16851	Cy	Carbohydrate metabolism	A, R	No
Vacuolar protein sorting-associated protein 4A	Q9UN37	Cy	Cell cycle, Transport	R	Yes
Versican core protein	P13611	Ex	Protein processing	All	Yes
Very long-chain specific acyl-CoA dehydro-genase	P49748	Mit	Fatty acid metabolism	A	Yes
Vesicle-fusing ATPase	P46459	Cy	Transport	R	Yes
Voltage-dependent anion-selective channel protein	P21796	Mem, Mit	Apoptosis, Transport	All	Yes
V-type proton ATPase subunit E	P36543	Cy	Transport	R, C	Yes
WAS protein family homolog 2	Q6VEQ5	Cy	Transport	R	No
WD repeat-containing protein	O75083	Cy	Actin filament depolymeriza-tion	A, R	Yes
Zinc finger C3H1 domain-containing pro-tein	O60293	Nu	RNA processing	A	No
Zinc-alpha-2-glycoprotein	P25311	Ex	Transport	All	No
Zymogen granule protein 16 homolog B	Q96DA0	Ex	Homeostasis	C	No

7. References

Abu-Rumeileh, S., Capellari, S., & Parchi, P. (2018). Rapidly progressive Alzheimer's disease: contributions to clinical-pathological definition and diagnosis. *Journal of Alzheimer's Disease*, *63*(3), 887-897.

Ahn, H. J., Zamolodchikov, D., Cortes-Canteli, M., Norris, E. H., Glickman, J. F., & Strickland, S. (2010). Alzheimer's disease peptide β-amyloid interacts with fibrinogen and induces its oligomerization. *Proceedings of the National Academy of Sciences, 107*(50), 21812-21817.

Alzheimer, A. (1907). Über eine eigenartige Erkrankung der Hirnrinde. *Allgemeine Zeitschrift für Psychiatrie und Psychisch-gerichtliche Medizin, 64*, 146-148.

Amano, N., Yagishita, S., Yokoi, S., Itoh, Y., Kinoshita, J., Mizutani, T., & Matsuishi, T. (1992). Gerstmann-Sträussler syndrome - a variant type: amyloid plaques and Alzheimer's neurofibrillary tangles in cerebral cortex. *Acta Neuropathologica*, *84*(1), 15-23.

Angulo, E., Noé, V., Casadó, V., Mallol, J., Gomez-Isla, T., Lluis, C., Ferrer, I., Ciudad, C.J. & Franco, R. (2004). Up-regulation of the Kv3. 4 potassium channel subunit in early stages of Alzheimer's disease. *Journal of Neurochemistry, 91*(3), 547-557.

Araman, C., van Gent, M. E., Meeuwenoord, N. J., Heijmans, N., Marqvorsen, M. H., Doelman, W., Faber, B.W., 't Hart, B.A. & Van Kasteren, S. I. (2018). Amyloid-like behavior of site-specifically citrullinated myelin oligodendrocyte protein (MOG) peptide fragments inside EBV-infected B-cells influences their cytotoxicity and autoimmunogenicity. *Biochemistry*, *58*(6), 763-775.

Ardura, J. A., & Friedman, P. A. (2011). Regulation of G protein-coupled receptor function by Na^+/H^+ exchange regulatory factors. *Pharmacological Reviews, 63*(4), 882-900.

Awada, A. A. (2015). Early and late-onset Alzheimer's disease: What are the differences? *Journal of Neurosciences in Rural Practice*, *6*(3), 455-456.

Ba, M., Li, X., Ng, K. P., Pascoal, T. A., Mathotaarachchi, S., Rosa-Neto, P., Gauthier, S. & Alzheimer's Disease Neuroimaging Initiative. (2017). The prevalence and biomarkers' characteristic of rapidly progressive Alzheimer's disease from the Alzheimer's Disease Neuroimaging Initiative

database. *Alzheimer's & Dementia: Translational Research & Clinical Interventions, 3*(1), 107-113.

Baiardi, S., Abu-Rumeileh, S., Rossi, M., Zenesini, C., Bartoletti-Stella, A., Polischi, B., Capellari, S. & Parchi, P. (2019). Antemortem CSF Aβ42/Aβ40 ratio predicts Alzheimer's disease pathology better than Aβ42 in rapidly progressive dementias. *Annals of Clinical and Translational Neurology, 6*(2), 263-273.

Balejčíková, L., Petrenko, V. I., Baťková, M., Šipošová, K., Garamus, V. M., Bulavin, L. A., Avdeev, M.V., Almásy, L. & Kopčanský, P. (2019). Disruption of amyloid aggregates by artificial ferritins. *Journal of Magnetism and Magnetic Materials, 473*, 215-220.

Bamburg, J. R., & Bloom, G. S. (2009). Cytoskeletal pathologies of Alzheimer disease. *Cell Motility and the Cytoskeleton, 66*(8), 635.

Baranello, J. R., Bharani, L. K., Padmaraju, V., Chopra, N., Lahiri, K. D., Greig, H. N., A Pappolla, M. & Sambamurti, K. (2015). Amyloid-beta protein clearance and degradation (ABCD) pathways and their role in Alzheimer's disease. *Current Alzheimer Research, 12*(1), 32-46.

Barcikowska, M., Kwiecinski, H., Liberski, P. P., Kowalski, J., Brown, P., & Gajdusek, D. C. (1995). Creutzfeldt-Jakob disease with Alzheimer-type Aβ-reactive amyloid plaques. *Histopathology, 26*(5), 445-450.

Barritt, J. D., & Viles, J. H. (2015). Truncated amyloid-β (11–40/42) from Alzheimer disease binds Cu^{2+} with a femtomolar affinity and influences fiber assembly. *Journal of Biological Chemistry, 290*(46), 27791-27802.

Barritt, J. D., Younan, N. D., & Viles, J. H. (2017). N-Terminally Truncated Amyloid-β (11–40/42) Cofibrillizes with its Full-Length Counterpart: Implications for Alzheimer's Disease. *Angewandte Chemie, 129*(33), 9948-9951.

Bibl, M., Mollenhauer, B., Esselmann, H., Lewczuk, P., Klafki, H. W., Sparbier, K., Smirnov, A., Cepek, L., Trenkwalder, C., Rüther, E. & Kornhuber, J. (2006). CSF amyloid-β-peptides in Alzheimer's disease, dementia with Lewy bodies and Parkinson's disease dementia. *Brain*, 129(5), 1177-1187.

Boluda, S., Toledo, J. B., Irwin, D. J., Raible, K. M., Byrne, M. D., Lee, E. B., Lee, V.M.Y & Trojanowski, J. Q. (2014). A comparison of Aβ amyloid pathology staging systems and correlation with clinical diagnosis. *Acta Neuropathologica, 128*(4), 543-550.

Bonito-Oliva, A., Barbash, S., Sakmar, T. P., & Graham, W. V. (2017). Nucleobindin 1 binds to multiple types of pre-fibrillar amyloid and inhibits fibrillization. *Scientific reports, 7*, 42880.

Bouter, Y., Dietrich, K., Wittnam, J. L., Rezaei-Ghaleh, N., Pillot, T., Papot-Couturier, S., Lefebvre, T., Sprenger, F., Wirths, O., Zweckstetter, M. & Bayer, T. A. (2013). N-truncated amyloid β (Aβ) 4-42 forms stable aggregates and induces acute and long-lasting behavioral deficits. *Acta Neuropathologica, 126*(2), 189-205.

Braak, H., & Braak, E. (1991). Neuropathological stageing of Alzheimer-related changes. *Acta Neuropathologica, 82*(4), 239-259.

Bradford, M. M. (1976). A rapid and sensitive method for the quantitation of microgram quantities of protein utilizing the principle of protein-dye binding. *Analytical Biochemistry, 72*(1-2), 248-254.

Bronfman, F. C., Alvarez, A., Morgan, C., & Inestrosa, N. C. (1998). Laminin blocks the assembly of wild-type Aβ and the Dutch variant peptide into Alzheimer's fibrils. *Amyloid, 5*(1), 16-23.

Brothers, H. M., Gosztyla, M. L., & Robinson, S. R. (2018). The physiological roles of amyloid-β peptide hint at new ways to treat Alzheimer's disease. *Frontiers in Aging Neuroscience, 10*, 118.

Burdick, D., Soreghan, B., Kwon, M., Kosmoski, J., Knauer, M., Henschen, A., Yates, J., Cotman, C. & Glabe, C. (1992). Assembly and aggregation properties of synthetic Alzheimer's A4/beta amyloid peptide analogs. *Journal of Biological Chemistry, 267*(1), 546-554.

Cam, J. A., Zerbinatti, C. V., Knisely, J. M., Hecimovic, S., Li, Y., & Bu, G. (2004). The low density lipoprotein receptor-related protein 1B retains β-amyloid precursor protein at the cell surface and reduces amyloid-β peptide production. *Journal of Biological Chemistry, 279*(28), 29639-29646.

Candelise, N., Schmitz, M., Llorens, F., Villar-Piqué, A., Cramm, M., Thom, T., da Silva Correia, S.M., da Cunha, J.E.G., Möbius, W., Outeiro, T.F., Álvarez, V. G., Banchelli, M., D'Andrea, C.,

de Angelis, M., Zafar, S., Rabano, A., Matteini, P. & Zerr, I. (2019). Seeding variability of different alpha synuclein strains in synucleinopathies. *Annals of Neurology, 85*(5), 691-703.

Chakraborty, S., & Das, P. (2017). Emergence of alternative structures in amyloid beta 1-42 monomeric landscape by N-terminal hexapeptide amyloid inhibitors. *Scientific Reports, 7*(1), 9941.

Cheignon, C., Tomas, M., Bonnefont-Rousselot, D., Faller, P., Hureau, C., & Collin, F. (2018). Oxidative stress and the amyloid beta peptide in Alzheimer's disease. *Redox Biology, 14*, 450-464.

Chen, G. F., Xu, T. H., Yan, Y., Zhou, Y. R., Jiang, Y., Melcher, K., & Xu, H. E. (2017). Amyloid beta: structure, biology and structure-based therapeutic development. *Acta Pharmacologica Sinica, 38*(9), 1205.

Chen, K., Maley, J., & Yu, P. H. (2006). Potential implications of endogenous aldehydes in β-amyloid misfolding, oligomerization and fibrillogenesis. *Journal of Neurochemistry, 99*(5), 1413-1424.

Chow, V. W., Mattson, M. P., Wong, P. C., & Gleichmann, M. (2010). An overview of APP processing enzymes and products. *Neuromolecular Medicine, 12*(1), 1-12.

Ciechanover, A., & Kwon, Y. T. (2015). Degradation of misfolded proteins in neurodegenerative diseases: therapeutic targets and strategies. *Experimental and Molecular Medicine, 47*(3), e147.

Citron, M., Vigo-Pelfrey, C., Teplow, D. B., Miller, C., Schenk, D., Johnston, J., Winblad, B., Venizelos, N., Lannfelt, L. & Selkoe, D. J. (1994). Excessive production of amyloid beta-protein by peripheral cells of symptomatic and presymptomatic patients carrying the Swedish familial Alzheimer disease mutation. *Proceedings of the National Academy of Sciences, 91*(25), 11993-11997.

Clarris, H. J., Key, B., Beyreuther, K., Masters, C. L., & Small, D. H. (1995). Expression of the amyloid protein precursor of Alzheimer's disease in the developing rat olfactory system. *Developmental Brain Research, 88*(1), 87-95.

Cohen, M. L., Kim, C., Haldiman, T., ElHag, M., Mehndiratta, P., Pichet, T., Lissemore, F., Shea, M., Cohen, Y., Chen, W. & Blevins, J. (2015). Rapidly progressive Alzheimer's disease features distinct structures of amyloid-β. *Brain, 138*(4), 1009-1022.

Colciaghi, F., Borroni, B., Pastorino, L., Marcello, E., Zimmermann, M., Cattabeni, F., Padovani, A. & Di Luca, M. (2002). α-Secretase ADAM10 as well as αAPPs is reduced in platelets and CSF of Alzheimer disease patients. *Molecular Medicine, 8*(2), 67-74.

Collinge, J. (2001). Prion diseases of humans and animals: their causes and molecular basis. *Annual Review of Neuroscience, 24*(1), 519-550.

Condello, C., Lemmin, T., Stöhr, J., Nick, M., Wu, Y., Maxwell, A. M., Watts, J.C., Caro, C.D., Oehler, A., Keene, C.D. & Bird, T. D. (2018). Structural heterogeneity and intersubject variability of Aβ in familial and sporadic Alzheimer's disease. *Proceedings of the National Academy of Sciences, 115*(4), E782-E791.

Cotman, S. L., Halfter, W. and Cole, G.J. (2000). Agrin binds to beta-amyloid (Aβ), accelerates Aβ fibril formation, and is localized to Aβ deposits in Alzheimer's disease brain. *Molecular and Cellular Neurosciences, 15*(2), 183-98.

Crous-Bou, M., Minguillón, C., Gramunt, N., & Molinuevo, J. L. (2017). Alzheimer's disease prevention: from risk factors to early intervention. *Alzheimer's Research & Therapy, 9*(1), 71.

Das, S., & Mukhopadhyay, D. (2011). Intrinsically unstructured proteins and neurodegenerative diseases: conformational promiscuity at its best. *IUBMB Life, 63*(7), 478-488.

Davis-Salinas, J., & Van Nostrand, W. E. (1995). Amyloid β-protein aggregation nullifies its pathologic properties in cultured cerebrovascular smooth muscle cells. *Journal of Biological Chemistry, 270*(36), 20887-20890.

De, S., Whiten, D. R., Ruggeri, F. S., Hughes, C., Rodrigues, M., Sideris, D. I., Taylor, C.G., Aprile, F.A., Muyldermans, S., Knowles, T.P. & Vendruscolo, M. (2019). Soluble aggregates present in cerebrospinal fluid change in size and mechanism of toxicity during Alzheimer's disease progression. *Acta Neuropathologica Communications, 7*(1), 120.

Demetrius, L. A., & Driver, J. (2013). Alzheimer's as a metabolic disease. *Biogerontology, 14*(6), 641-649.

Di Domenico, F., Barone, E., Perluigi, M., & Butterfield, D. A. (2017). The triangle of death in Alzheimer's disease brain: the aberrant cross-talk among energy metabolism, mammalian target of

rapamycin signaling, and protein homeostasis revealed by redox proteomics. *Antioxidants & Redox Signaling*, 26(8), 364-387.

Di Fede, G., Catania, M., Maderna, E., Ghidoni, R., Benussi, L., Tonoli, E., Giaccone, G., Moda, F., Paterlini, A., Campagnani, I. & Sorrentino, S. (2018). Molecular subtypes of Alzheimer's disease. *Scientific Reports, 8*(1), 3269.

Di Giovanni, S., Eleuteri, S., Paleologou, K. E., Yin, G., Zweckstetter, M., Carrupt, P. A., & Lashuel, H. A. (2010). Entacapone and tolcapone, two catechol O-methyltransferase inhibitors, block fibril formation of α-synuclein and β-amyloid and protect against amyloid-induced toxicity. *Journal of Biological Chemistry, 285*(20), 14941-14954.

Ding, Q., Markesbery, W. R., Chen, Q., Li, F., & Keller, J. N. (2005). Ribosome dysfunction is an early event in Alzheimer's disease. *Journal of Neuroscience, 25*(40), 9171-9175.

Drüeke, T.B. (2000). Beta2-microglobulin and amyloidosis. *Nephrology, Dialysis and Transplantation, 15* (1), 17-24.

Drummond, E., Nayak, S., Faustin, A., Pires, G., Hickman, R. A., Askenazi, M., Cohen, M., Haldiman, T., Kim, C., Han, X., Shao, Y., Safar J.G., Ueberheide, B. & Wisniewski T. (2017). Proteomic differences in amyloid plaques in rapidly progressive and sporadic Alzheimer's disease. *Acta Neuropathologica*, *133*(6), 933-954.

Du, X., Wang, X., & Geng, M. (2018). Alzheimer's disease hypothesis and related therapies. *Translational Neurodegeneration*, *7*(1), 2.

Duce, J. A., Smith, D. P., Blake, R. E., Crouch, P. J., Li, Q. X., Masters, C. L., & Trounce, I. A. (2006). Linker histone H1 binds to disease associated amyloid-like fibrils. *Journal of Molecular Biology, 361*(3), 493-505.

Dunys, J., Valverde, A., & Checler, F. (2018). Are N- and C-terminally truncated Aβ species key pathological triggers in Alzheimer's disease? *Journal of Biological Chemistry, 293*(40), 15419-15428.

Dykens, J. A. (1994). Isolated cerebral and cerebellar mitochondria produce free radicals when exposed to elevated Ca^{2+} and Na^{+}: implications for neurodegeneration. *Journal of Neurochemistry, 63*(2), 584-591.

Dykens, J. A. (2007). Redox enzymes. *Comprehensive Medicinal Chemistry II. 2*. 1053-1087

Eckman, E. A., & Eckman, C. B. (2005). Aβ-degrading enzymes: modulators of Alzheimer's disease pathogenesis and targets for therapeutic intervention. *Biochemical Society Transactions*, *33*(5), 1101-1105.

Endo, Y., Hasegawa, K., Nomura, R., Arishima, H., Kikuta, K. I., Yamashita, T., Inoue, Y., Ueda, M., Ando, Y., Wilson, M.R. & Hamano, T. (2019). Apolipoprotein E and clusterin inhibit the early phase of amyloid-β aggregation in an *in vitro* model of cerebral amyloid angiopathy. *Acta Neuropathologica Communications, 7*(1), 12.

Eriksson, S., Janciauskiene, S., & Lannfelt, L. (1995). Alpha 1-antichymotrypsin regulates Alzheimer beta-amyloid peptide fibril formation. *Proceedings of the National Academy of Sciences*, *92*(6), 2313-2317.

Esposito, Z., Belli, L., Toniolo, S., Sancesario, G., Bianconi, C., & Martorana, A. (2013). Amyloid β, glutamate, excitotoxicity in Alzheimer's disease: are we on the right track? *CNS Neuroscience & Therapeutics*, *19*(8), 549-555.

Etcheberrigaray, R., Ito, E., Kim, C. S., & Alkon, D. L. (1994). Soluble beta-amyloid induction of Alzheimer's phenotype for human fibroblast K^+ channels. *Science*, *264*(5156), 276-279.

Fang, Y. S., Tsai, K. J., Chang, Y. J., Kao, P., Woods, R., Kuo, P. H., Wu, C.C., Liao, J.Y., Chou, S.C., Lin, V. & Jin, L. W. (2014). Full-length TDP-43 forms toxic amyloid oligomers that are present in frontotemporal lobar dementia-TDP patients. *Nature Communications, 5*, 4824.

Fichou, Y., Lin, Y., Rauch, J. N., Vigers, M., Zeng, Z., Srivastava, M., Keller, T.J., Freed, J.H., Kosik, K.S. & Han, S. (2018). Cofactors are essential constituents of stable and seeding-active tau fibrils. *Proceedings of the National Academy of Sciences, 115*(52), 13234-13239.

Finn, T. E., Nunez, A. C., Sunde, M., & Easterbrook-Smith, S. B. (2012). Serum albumin prevents protein aggregation and amyloid formation and retains chaperone-like activity in the presence of physiological ligands. *Journal of Biological Chemistry*, *287*(25), 21530-21540.

Forman, M. S., Farmer, J., Johnson, J. K., Clark, C. M., Arnold, S. E., Coslett, H. B., Chatterjee, A., Hurtig, H. I., Karlawish, J. H., Rosen, H. J., Van Deerlin, V. Lee, V. M., Miller, B. L., Trojanowski, J. Q. , & Grossman, M. (2006). Frontotemporal dementia: clinicopathological correlations. *Annals of Neurology*, *59*(6), 952-962.

Froese, D. S., Michaeli, A., McCorvie, T. J., Krojer, T., Sasi, M., Melaev, E., Goldblum, A., Zatsepin, M., Lossos, A., Álvarez, R. & Escribá, P. V. (2015). Structural basis of glycogen branching enzyme deficiency and pharmacologic rescue by rational peptide design. *Human Molecular Genetics*, *24*(20), 5667-5676.

Furukawa, Y., Kaneko, K., Matsumoto, G., Kurosawa, M., & Nukina, N. (2009). Cross-seeding fibrillation of Q/N-rich proteins offers new pathomechanism of polyglutamine diseases. *Journal of Neuroscience*, *29*(16), 5153-5162.

Gabbita, S. P., Lovell, M. A., & Markesbery, W. R. (1998). Increased nuclear DNA oxidation in the brain in Alzheimer's disease. *Journal of Neurochemistry*, *71*(5), 2034-2040.

Garcia-Esparcia, P., Sideris-Lampretsas, G., Hernandez-Ortega, K., Grau-Rivera, O., Sklaviadis, T., Gelpi, E., & Ferrer, I. (2017). Altered mechanisms of protein synthesis in frontal cortex in Alzheimer disease and a mouse model. *American Journal of Neurodegenerative Disease*, *6*(2), 15.

Gaugler, J., James, B., Johnson, T., Marin, A., & Weuve, J. (2019). 2019 Alzheimer's disease facts and figures. *Alzheimers & Dementia*, *15*(3), 321-387.

Gelfanova, V., Higgs, R. E., Dean, R. A., Holtzman, D. M., Farlow, M. R., Siemers, E. R., Boodhoo, A., Qian, Y.W., He, X., Jin, Z. & Fisher, D. L. (2007). Quantitative analysis of amyloid-β peptides in cerebrospinal fluid using immunoprecipitation and MALDI-Tof mass spectrometry. *Briefings in Functional Genomics and Proteomics*, *6*(2), 149-158.

Geut, H., Vergouw, L. J. M., Galis, Y., Ingrassia, A., de Jong, F. J., Quadri, M., Bonifati, V., Lemstra, A.W., Rozemuller, A.J.M. & van de Berg, W. D. J. (2019). Neuropathological and genetic characteristics of a post-mortem series of cases with dementia with Lewy bodies clinically suspected of Creutzfeldt-Jakob's disease. *Parkinsonism & Related Disorders*, *63*:162-168.

Gillam, J. E., & MacPhee, C. E. (2013). Modelling amyloid fibril formation kinetics: mechanisms of nucleation and growth. *Journal of Physics: Condensed Matter*, 25(37), 373101.

Gkanatsiou, E., Portelius, E., Toomey, C. E., Blennow, K., Zetterberg, H., Lashley, T., & Brinkmalm, G. (2019). A distinct brain beta amyloid signature in cerebral amyloid angiopathy compared to Alzheimer's disease. *Neuroscience Letters, 701,* 125-131.

Glenner, G. G., & Wong, C. W. (1984). Alzheimer's disease: initial report of the purification and characterization of a novel cerebrovascular amyloid protein. *Biochemical and Biophysical Research Communications*, *120*(3), 885-890.

Goate, A., Chartier-Harlin, M. C., Mullan, M., Brown, J., Crawford, F., Fidani, L., Giuffra, L. Haynes, A. Irving, N. James, L. & Mant, R. (1991). Segregation of a missense mutation in the amyloid precursor protein gene with familial Alzheimer's disease. *Nature*, *349*(6311), 704-706.

Gosztyla, M. L., Brothers, H. M., & Robinson, S. R. (2018). Alzheimer's amyloid-β is an antimicrobial peptide: a review of the evidence. *Journal of Alzheimer's Disease*, 62(4), 1495-1506.

Granold, M., Moosmann, B., Staib-Lasarzik, I., Arendt, T., del Rey, A., Engelhard, K., Behl, C. & Hajieva, P. (2015). High membrane protein oxidation in the human cerebral cortex. *Redox Biology, 4*, 200-207.

Grignaschi, E., Cereghetti, G., Grigolato, F., Kopp, M. R., Caimi, S., Faltova, L., Saad, S., Peter, M. & Arosio, P. (2018). A hydrophobic low-complexity region regulates aggregation of the yeast pyruvate kinase Cdc19 into amyloid-like aggregates *in vitro*. *Journal of Biological Chemistry*, *293*(29), 11424-11432.

Grimm, M. O., Grimm, H. S., & Hartmann, T. (2007). Amyloid beta as a regulator of lipid homeostasis. *Trends in Molecular Medicine*, *13*(8), 337-344.

Groh, N., Bühler, A., Huang, C., Li, K. W., van Nierop, P., Smit, A. B., Fändrich, M., Baumann, F. & David, D. C. (2017). Age-dependent protein aggregation initiates amyloid-β aggregation. *Frontiers in Aging Neuroscience*, 9, 138.

Gunn, A. P., Wong, B. X., Johanssen, T., Griffith, J. C., Masters, C. L., Bush, A. I., Barnham, K.J., Duce, J.A. & Cherny, R. A. (2016). Amyloid-β peptide Aβ3pE-42 induces lipid peroxidation, membrane permeabilization, and calcium influx in neurons. *Journal of Biological Chemistry*, *291*(12), 6134-6145.

Haass, C. (1996). Presenile because of presenilin: the presenilin genes and early onset Alzheimer's disease. *Current Opinion in Neurology*, *9*(4), 254-259.

Haass, C., Kaether, C., Thinakaran, G., & Sisodia, S. (2012). Trafficking and proteolytic processing of APP. *Cold Spring Harbor Perspectives in Medicine*, *2*(5), a006270.

Haltia, M., Ghiso, J., Wisniewski, T., Kiuru, S., Miller, D., & Frangione, B. (1991). Gelsolin variant and β-amyloid co-occur in a case of Alzheimer's with Lewy bodies. *Neurobiology of Aging*, *12*(4), 313-316.

Han, X. J., Hu, Y. Y., Yang, Z. J., Jiang, L. P., Shi, S. L., Li, Y. R., Guo, M.Y., Wu, H.L. & Wan, Y. Y. (2017). Amyloid β-42 induces neuronal apoptosis by targeting mitochondria. *Molecular Medicine Reports*, *16*(4), 4521-4528.

Hardas, S. S., Sultana, R., Clark, A. M., Beckett, T. L., Szweda, L. I., Murphy, M. P., & Butterfield, D. A. (2013). Oxidative modification of lipoic acid by HNE in Alzheimer disease brain. *Redox Biology*, *1*(1), 80-85.

Harris, M. E., Carney, J. M., Cole, P. S., Hensley, K., Howard, B. J., Martin, L., Bummer, P., Wang, Y., Pedigo, J.N. & Butterfield, D. A. (1995). β-Amyloid peptide-derived, oxygen-dependent free radicals inhibit glutamate uptake in cultured astrocytes: implications for Alzheimer's disease. *Neuroreport*, *6*(14), 1875-1879.

Hendriks, L., Thinakaran, G., Harris, C. L., De Jonghe, C., Martin, J. J., Sisodia, S. S., & Van Broeckhoven, C. (1997). Processing of presenilin 1 in brains of patients with Alzheimer's disease and controls. *Neuroreport*, *8*(7), 1717-1721.

Henriques, A. G., Vieira, S. I., Da Cruz e Silva, E. F., & Da Cruz e Silva, O. A. (2010). Aβ promotes Alzheimer's disease-like cytoskeleton abnormalities with consequences to APP processing in neurons. *Journal of Neurochemistry*, *113*(3), 761-771.

Hermes, M., Eichhoff, G., & Garaschuk, O. (2010). Intracellular calcium signaling in Alzheimer's disease. *Journal of Cellular and Molecular Medicine*, *14*(1-2), 30-41.

Hernandez-Zimbron, L. F., Luna-Muñoz, J., Mena, R., Vazquez-Ramirez, R., Kubli-Garfias, C., Cribbs, D. H., Manoutcharian, K. & Gevorkian, G. (2012). Amyloid-β peptide binds to cytochrome C oxidase subunit 1. *PloS One*, *7*(8), e42344.

Honda, R. (2018). Amyloid-β peptide induces prion protein amyloid formation: evidence for its widespread amyloidogenic effect. *Angewandte Chemie International Edition*, *57*(21), 6086-6089.

Horn, M., Bertling, A., Brodde, M. F., Müller, A., Roth, J., Van Aken, H., Jurk, K., Heilmann, C., Peters, G. & Kehrel, B. E. (2012). Human neutrophil alpha-defensins induce formation of fibrinogen and thrombospondin-1 amyloid-like structures and activate platelets via glycoprotein IIb/IIIa. *Journal of Thrombosis and Haemostasis*, *10*(4), 647-661.

Huang, C. C., Faber, P. W., Persichetti, F., Mittal, V., Vonsattel, J. P., MacDonald, M. E., & Gusella, J. F. (1998). Amyloid formation by mutant huntingtin: threshold, progressivity and recruitment of normal polyglutamine proteins. *Somatic Cell and Molecular Genetics*, *24*(4), 217-233.

Inouye, H., Fraser, P. E., & Kirschner, D. A. (1993). Structure of beta-crystallite assemblies formed by Alzheimer beta-amyloid protein analogues: analysis by x-ray diffraction. *Biophysical Journal*, *64*(2), 502-519.

Ito, M., Johansson, J., Strömberg, R., & Nilsson, L. (2011). Unfolding of the amyloid β-peptide central helix: mechanistic insights from molecular dynamics simulations. *PloS One*, *6*(3), e17587.

Jack, C. R., Bennett, D. A., Blennow, K., Carrillo, M. C., Dunn, B., Haeberlein, S. B., Holtzman, D.M., Jagust, W., Jessen, F., Karlawish, J. & Liu, E. (2018). NIA-AA Research Framework: Toward a biological definition of Alzheimer's disease. *Alzheimer's & Dementia*, *14*(4), 535-562.

Jarvela, T. S., Lam, H. A., Helwig, M., Lorenzen, N., Otzen, D. E., McLean, P. J. & Lindberg, I. (2016). The neural chaperone proSAAS blocks α-synuclein fibrillation and neurotoxicity. *Proceedings of the National Academy of Sciences*, *113*(32), E4708-E4715.

Jaunmuktane, Z., & Brandner, S. (2018). Transmissible human proteopathies: an expanding field. *Diagnostic Histopathology, 25*(1), 16-22.

Jayawardena, N., Kaur, M., Nair, S., Malmstrom, J., Goldstone, D., Negron, L., Gerrard, J. & Domigan, L. (2017). Amyloid fibrils from hemoglobin. *Biomolecules, 7*(2), 37.

Joachim, C. L., Mori, H., & Selkoe, D. J. (1989). Amyloid β-protein deposition in tissues other than brain in Alzheimer's disease. *Nature, 341*(6239), 226.

Kang, J., Lemaire, H. G., Unterbeck, A., Salbaum, J. M., Masters, C. L., Grzeschik, K. H., Multhaup, G., Beyreuther, K. & Müller-Hill, B. (1987). The precursor of Alzheimer's disease amyloid A4 protein resembles a cell-surface receptor. *Nature*, *325*(6106), 733.

Karch, A., Llorens, F., Schmitz, M., Arora, A. S., Zafar, S., Lange, P., Schmidt, C. & Zerr, I. (2016). Stratification by genetic and demographic characteristics improves diagnostic accuracy of cerebrospinal fluid biomarkers in rapidly progressive dementia. *Journal of Alzheimer's Disease*, *54*(4), 1385-1393.

Keefer, K. M., Stein, K. C., & True, H. L. (2017). Heterologous prion-forming proteins interact to cross-seed aggregation in Saccharomyces cerevisiae. *Scientific Reports*, *7*(1), 5853.

Khan, M. A. I., Respondek, M., Kjellström, S., Deep, S., Linse, S., & Akke, M. (2017). Cu/Zn superoxide dismutase forms amyloid fibrils under near-physiological quiescent conditions: The roles of disulfide bonds and effects of denaturant. *ACS Chemical Neuroscience*, *8*(9), 2019-2026.

Khandelwal, P. J., & Moussa, C. (2010). The relationship between Parkin and protein aggregation in neurodegenerative diseases. *Frontiers in Psychiatry, 1*, 15.

Khurana, R., Ionescu-Zanetti, C., Pope, M., Li, J., Nielson, L., Ramírez-Alvarado, M., Regan, L., Fink, A.L. & Carter, S. A. (2003). A general model for amyloid fibril assembly based on morphological studies using atomic force microscopy. *Biophysical Journal*, *85*(2), 1135-1144.

Kim, B., Park, J., Chang, K. T., & Lee, D. S. (2016). Peroxiredoxin 5 prevents amyloid-beta oligomer-induced neuronal cell death by inhibiting ERK–Drp1-mediated mitochondrial fragmentation. *Free Radical Biology and Medicine, 90*, 184-194.

Kinney, J. W., Bemiller, S. M., Murtishaw, A. S., Leisgang, A. M., Salazar, A. M., & Lamb, B. T. (2018). Inflammation as a central mechanism in Alzheimer's disease. *Alzheimer's & Dementia: Translational Research & Clinical Interventions*, *4*, 575-590.

Kitazawa, M., Medeiros, R., & M LaFerla, F. (2012). Transgenic mouse models of Alzheimer disease: developing a better model as a tool for therapeutic interventions. *Current Pharmaceutical Design*, *18*(8), 1131-1147.

Knowles, T. P., Vendruscolo, M., & Dobson, C. M. (2014). The amyloid state and its association with protein misfolding diseases. *Nature Reviews Molecular Cell biology*, *15*(6), 384-396.

Komatsu, H., Shinotani, N., Kimori, Y., Tokuoka, J. I., Kaseda, K., Nakagawa, H., & Kodama, T. (2006). Aggregation of partially unfolded myosin subfragment-1 into spherical oligomers with amyloid-like dye-binding properties. *Journal of Biochemistry*, *139*(6), 989-996.

Kuhn, P. H., Wang, H., Dislich, B., Colombo, A., Zeitschel, U., Ellwart, J. W., Kremmer, E., Roßner, S. & Lichtenthaler, S. F. (2010). ADAM10 is the physiologically relevant, constitutive α-secretase of the amyloid precursor protein in primary neurons. *The EMBO Journal*, *29*(17), 3020-3032.

Kummer, M. P., & Heneka, M. T. (2014). Truncated and modified amyloid-beta species. *Alzheimer's Research & Therapy*, *6*(3), 28.

Laemmli, U. K. (1970). Cleavage of structural proteins during the assembly of the head of bacteriophage T4. *Nature, 227*(5259), 680.

Ledesma, M. D., Da Silva, J. S., Crassaerts, K., Delacourte, A., De Strooper, B. & Dotti C. G (2000). Brain plasmin enhances APP alpha-cleavage and Aβ degradation and is reduced in Alzheimer's disease brains. *EMBO Reports, 1*(6):530-5.

Lewis, P. A., Tattum, M. H., Jones, S., Bhelt, D., Batchelor, M., Clarke, A. R., Collinge, J. & Jackson, G. S. (2006). Codon 129 polymorphism of the human prion protein influences the kinetics of amyloid formation. *Journal of General Virology, 87*(8), 2443-2449.

Lim, K. H. (2019). Diverse Misfolded conformational strains and cross-seeding of misfolded proteins implicated in neurodegenerative diseases. *Frontiers in Molecular Neuroscience, 12*, 158.

Lin, H., & Schlaepfer, W. W. (2006). Role of neurofilament aggregation in motor neuron disease. *Annals of Neurology*, *60*(4), 399-406.

Lin, Y., Kardos, J., Imai, M., Ikenoue, T., Kinoshita, M., Sugiki, T., Ishimori, K., Goto, Y. & Lee, Y. H. (2016). Amorphous aggregation of cytochrome c with inherently low amyloidogenicity is characterized by the metastability of supersaturation and the phase diagram. *Langmuir*, *32*(8), 2010-2022.

Liu, C. C., Zhao, N., Yamaguchi, Y., Cirrito, J. R., Kanekiyo, T., Holtzman, D. M., & Bu, G. (2016). Neuronal heparan sulfates promote amyloid pathology by modulating brain amyloid-β

clearance and aggregation in Alzheimer's disease. *Science Translational Medicine, 8*(332), 332ra44-332ra44.

Liu, J., Bang, A. G., Kintner, C., Orth, A. P., Chanda, S. K., Ding, S., & Schultz, P. G. (2005). Identification of the Wnt signaling activator leucine-rich repeat in flightless interaction protein 2 by a genome-wide functional analysis. *Proceedings of the National Academy of Sciences, 102*(6), 1927-1932.

Liu, W., Xing, F., Iiizumi-Gairani, M., Okuda, H., Watabe, M., Pai, S. K., Pandey, P.R., Hirota, S., Kobayashi, A., Mo, Y.Y. & Fukuda, K. (2012). N-myc downstream regulated gene 1 modulates Wnt-β-catenin signalling and pleiotropically suppresses metastasis. *EMBO Molecular Medicine, 4*(2), 93-108.

Llorens, F., Schmitz, M., Karch, A., Cramm, M., Lange, P., Gherib, K., Varges, D., Schmidt, C., Zerr, I. & Stoeck, K. (2016). Comparative analysis of cerebrospinal fluid biomarkers in the differential diagnosis of neurodegenerative dementia. *Alzheimer's & Dementia, 12*(5), 577-589.

Lloret, A., Badia, M. C., Giraldo, E., Ermak, G., Alonso, M. D., Pallardó, F. V., Davies, K.J. & Viña, J. (2011). Amyloid-β toxicity and tau hyperphosphorylation are linked via RCAN1 in Alzheimer's disease. *Journal of Alzheimer's Disease, 27*(4), 701-709.

Lu, J. X., Qiang, W., Yau, W. M., Schwieters, C. D., Meredith, S. C., & Tycko, R. (2013). Molecular structure of β-amyloid fibrils in Alzheimer's disease brain tissue. *Cell, 154*(6), 1257-1268.

Luo, J., Wärmländer, S. K., Gräslund, A., & Abrahams, J. P. (2014). Non-chaperone proteins can inhibit aggregation and cytotoxicity of Alzheimer amyloid β peptide. *Journal of Biological Chemistry, 289*(40), 27766-27775.

Ma, J. (2012). The role of cofactors in prion propagation and infectivity. *PLoS Pathogens, 8*(4), e1002589.

Maler, J. M., Klafki, H. W., Paul, S., Spitzer, P., Groemer, T. W., Henkel, A. W., Esselmann, H., Lewczuk, P., Kornhuber, J. & Wiltfang, J. (2007). Urea-based two-dimensional electrophoresis of beta-amyloid peptides in human plasma: Evidence for novel Aβ species. *Proteomics, 7*(20), 3815-3820.

Mann, U. M., Mohr, E., & Chase, T. N. (1989). Rapidly progressive Alzheimer's disease. *The Lancet*, *334*(8666), 799.

Martel, C. L., Mackic, J. B., McComb, J. G., Ghiso, J., & Zlokovic, B. V. (1996). Blood-brain barrier uptake of the 40 and 42 amino acid sequences of circulating Alzheimer's amyloid β in guinea pigs. *Neuroscience Letters, 206*(2-3), 157-160.

Mastaglia, F. L., Masters, C. L., Beyreuther, K., & Kakulas, B. A. (1989). Deposition of Alzheimer's disease amyloid (A4) protein in the cerebral cortex in Parkinson's disease. *Progress in Clinical and Biological Research*, *317*, 475-484.

Mattson, M. P., Cheng, B., Davis, D., Bryant, K., Lieberburg, I., & Rydel, R. E. (1992). β-Amyloid peptides destabilize calcium homeostasis and render human cortical neurons vulnerable to excitotoxicity. *Journal of Neuroscience, 12*(2), 376-389.

Mattson, M. P., Tomaselli, K. J., & Rydel, R. E. (1993). Calcium-destabilizing and neurodegenerative effects of aggregated β-amyloid peptide are attenuated by basic FGF. *Brain Research*, *621*(1), 35-49.

Miravalle, L., Calero, M., Takao, M., Roher, A. E., Ghetti, B., & Vidal, R. (2005). Amino-terminally truncated Aβ peptide species are the main component of cotton wool plaques. *Biochemistry*, *44*(32), 10810-10821.

Mizuno, S., Iijima, R., Ogishima, S., Kikuchi, M., Matsuoka, Y., Ghosh, S., Miyamoto, T., Miyashita, A., Kuwano, R. & Tanaka, H. (2012). AlzPathway: a comprehensive map of signaling pathways of Alzheimer's disease. *BMC Systems Biology*, *6*(1), 52.

Moh, C., Kubiak, J. Z., Bajic, V. P., Zhu, X., Smith, M. A., & Lee, H. G. (2011). Cell cycle deregulation in the neurons of Alzheimer's disease. *In: Cell Cycle in Development* (pp. 565-576). Springer, Berlin, Heidelberg.

Moir, R. D., Lathe, R., & Tanzi, R. E. (2018). The antimicrobial protection hypothesis of Alzheimer's disease. *Alzheimer's & Dementia*, *14*(12), 1602-1614.

Moore, B. D., Martin, J., de Mena, L., Sanchez, J., Cruz, P. E., Ceballos-Diaz, C., Ladd, T.B., Ran, Y., Levites, Y., Kukar, T.L. & Kurian, J. J. (2018). Short Aβ peptides attenuate Aβ42 toxicity *in vivo*. *Journal of Experimental Medicine, 215*(1), 283-301.

Morales, R. (2017). Prion strains in mammals: Different conformations leading to disease. *PLOS Pathogens*, *13*(7), e1006323.

Morel, B., Casares, S., & Conejero-Lara, F. (2006). A Single mutation induces amyloid aggregation in the α-spectrin SH3 domain: analysis of the early stages of fibril formation. *Journal of Molecular Biology*, *356*(2), 453-468.

Mosser, S., Alattia, J. R., Dimitrov, M., Matz, A., Pascual, J., Schneider, B. L., & Fraering, P. C. (2014). The adipocyte differentiation protein APMAP is an endogenous suppressor of Aβ production in the brain. *Human Molecular Genetics*, *24*(2), 371-382.

Moustafa, A. A., Hassan, M., Hewedi, D. H., Hewedi, I., Garami, J. K., Al Ashwal, H., Zaki, N., Seo, S.Y., Cutsuridis, V., Angulo, S.L. & Natesh, J. Y. (2017). Genetic underpinnings in Alzheimer's disease–a review. *Reviews in the Neurosciences*, *29*(1), 21-38.

Mu, Y., & Gage, F. H. (2011). Adult hippocampal neurogenesis and its role in Alzheimer's disease. *Molecular Neurodegeneration*, *6*(1), 85.

Muronetz, V. I., Barinova, K. V., Stroylova, Y. Y., Semenyuk, P. I., & Schmalhausen, E. V. (2017). Glyceraldehyde-3-phosphate dehydrogenase: Aggregation mechanisms and impact on amyloid neurodegenerative diseases. *International Journal of Biological Macromolecules*, *100*, 55-66.

Neto, S. A., Neto, S. H., Simabukuro, M. M., Solla, D. J., Gonçalves, M. R., Fortini, I., Castro, L.H., & Nitrini, R. (2017). Rapidly progressive dementia: prevalence and causes in a neurologic unit of a tertiary hospital in Brazil. *Alzheimer Disease & Associated Disorders*, *31*(3), 239-243.

Newton, J. R., Parkinson, D., & Clench, M. R. (2006). Strategies for examination of Alzheimer's disease amyloid precursor protein isoforms. *Analytical and bioanalytical chemistry*, *385*(4), 692-699.

Nguyen, P. T., Andraka, N., De Carufel, C. A., & Bourgault, S. (2015). Mechanistic contributions of biological cofactors in islet amyloid polypeptide amyloidogenesis. *Journal of Diabetes Research*, 2015.

Nizynski, B., Dzwolak, W., & Nieznanski, K. (2017). Amyloidogenesis of Tau protein. *Protein Science*, *26*(11), 2126-2150.

Nizynski, B., Nieznanska, H., Dec, R., Boyko, S., Dzwolak, W., & Nieznanski, K. (2018). Amyloidogenic cross-seeding of tau protein: transient emergence of structural variants of fibrils. *PloS one*, *13*(7), e0201182.

Novo, M., Freire, S., & Al-Soufi, W. (2018). Critical aggregation concentration for the formation of early Amyloid-β (1–42) oligomers. *Scientific Reports*, *8*(1), 1783.

Oddo, S. (2012). The role of mTOR signaling in Alzheimer disease. *Frontiers in Bioscience (Scholar edition)*, *4*, 941.

Öhrfelt, A., Brinkmalm, A., Dumurgier, J., Brinkmalm, G., Hansson, O., Zetterberg, H., Bouaziz-Amar, E., Hugon, J., Paquet, C. & Blennow, K. (2016). The pre-synaptic vesicle protein synaptotagmin is a novel biomarker for Alzheimer's disease. *Alzheimer's Research & Therapy*, *8*(1), 41.

Olsson, F., Schmidt, S., Althoff, V., Munter, L. M., Jin, S., Rosqvist, S., Lendahl, U., Multhaup, G. & Lundkvist, J. (2014). Characterization of intermediate steps in amyloid beta (Aβ) production under near-native conditions. *Journal of Biological Chemistry*, *289*(3), 1540-1550.

Ortore, M. G., Macedo, J. N., Araujo, A. P. U., Ferrero, C., Mariani, P., Spinozzi, F., & Itri, R. (2015). Structural and thermodynamic properties of septin 3 investigated by small-angle X-ray scattering. *Biophysical Journal*, *108*(12), 2896-2902.

Ovsepian, S. V., O'Leary, V. B., Zaborszky, L., Ntziachristos, V., & Dolly, J. O. (2018). Synaptic vesicle cycle and amyloid β: biting the hand that feeds. *Alzheimer's & Dementia*, *14*(4), 502-513.

Palmqvist, S., Schöll, M., Strandberg, O., Mattsson, N., Stomrud, E., Zetterberg, H., Blennow, K., Landau, S., Jagust, W. & Hansson, O. (2017). Earliest accumulation of β-amyloid occurs within the default-mode network and concurrently affects brain connectivity. *Nature Communications*, *8*(1), 1214.

Palomer, E., Buechler, J., & Salinas, P. C. (2019). Wnt signalling deregulation in the ageing and Alzheimer´ s brain. *Frontiers in Cellular Neuroscience*, *13*, 227.

Papageorgiou, S. G., Kontaxis, T., Bonakis, A., Karahalios, G., Kalfakis, N., & Vassilopoulos, D. (2009). Rapidly progressive dementia: causes found in a Greek tertiary referral center in Athens. *Alzheimer Disease & Associated Disorders*, *23*(4), 337-346.

Pardo, J. V. (2019). Fact, Fiction, or Evolution: Mechanism Hypothesis of Alzheimer's Disease. In Alzheimer's Dementia and Korsakoff's Disease-Linking Memory Pathology to the Autobiographical Self. *IntechOpen*.

Park, J., Kim, B., Chae, U., Lee, D. G., Kam, M. K., Lee, S. R., Lee, H.S., Park, J.W & Lee, D. S. (2017). Peroxiredoxin 5 decreases beta-amyloid-mediated cyclin-dependent kinase 5 activation through regulation of Ca^{2+}-mediated calpain activation. *Antioxidants & Redox Signaling*, *27*(11), 715-726.

Parodi, J., Sepúlveda, F. J., Roa, J., Opazo, C., Inestrosa, N. C., & Aguayo, L. G. (2010). β-amyloid causes depletion of synaptic vesicles leading to neurotransmission failure. *Journal of Biological Chemistry*, *285*(4), 2506-2514.

Paterson, R. W., Takada, L. T., & Geschwind, M. D. (2012). Diagnosis and treatment of rapidly progressive dementias. *Neurology: Clinical Practice*, *2*(3), 187-200.

Pathak, B. K., Mondal, S., Banerjee, S., Ghosh, A. N., & Barat, C. (2017). Sequestration of ribosome during protein aggregate formation: contribution of ribosomal RNA. *Scientific Reports*, *7*, 42017.

Petersen, C., Nolan, A. L., Resende, E. D. P. F., Ehrenberg, A. J., Spina, S., Miller, B., LSeelay, W., Miller, Z. & Grinberg, L. (2019). Alzheimer's disease clinical variants show distinct regional patterns of neurofibrillary tangle accumulation. *Acta Neuropathologica*, *138*(4) 1-16.

Pfefferkorn, C. M., McGlinchey, R. P., & Lee, J. C. (2010). Effects of pH on aggregation kinetics of the repeat domain of a functional amyloid, Pmel17. *Proceedings of the National Academy of Sciences*, *107*(50), 21447-21452.

Pike, C. J., Overman, M. J., & Cotman, C. W. (1995). Amino-terminal deletions enhance aggregation of β-amyloid peptides *in vitro*. *Journal of Biological Chemistry*, *270*(41), 23895-23898.

Pillai, J. A., Appleby, B. S., Safar, J., & Leverenz, J. B. (2018). Rapidly progressive Alzheimer's disease in two distinct autopsy cohorts. *Journal of Alzheimer's Disease*, *64*(3), 973-980.

Plassman, B. L., & Breitner, J. C. (1996). Recent advances in the genetics of Alzheimer's disease and vascular dementia with an emphasis on gene-environment interactions. *Journal of the American Geriatrics Society*, *44*(10), 1242-1250.

Pollard, H. B., Rojas, E., & Arispe, N. (1993). A new hypothesis for the mechanism of amyloid toxicity, based on the calcium channel activity of amyloid β protein (AβP) in phospholipid bilayer membranes. *Annals of the New York Academy of Sciences, 695*(1), 165-168.

Portelius, E., Andreasson, U., Ringman, J. M., Buerger, K., Daborg, J., Buchhave, P., Hansson, O., Harmsen, A., Gustavsson, M. K., Hanse, E. & Galasko, D. (2010). Distinct cerebrospinal fluid amyloid β peptide signatures in sporadic and PSEN1 A431E-associated familial Alzheimer's disease. *Molecular Neurodegeneration, 5*(1), 2.

Portelius, E., Bogdanovic, N., Gustavsson, M. K., Volkmann, I., Brinkmalm, G., Zetterberg, H., Winblad, B. & Blennow, K. (2010). Mass spectrometric characterization of brain amyloid beta isoform signatures in familial and sporadic Alzheimer's disease. *Acta Neuropathologica, 120*(2), 185-193.

Portelius, E., Lashley, T., Westerlund, A., Persson, R., Fox, N. C., Blennow, K., Revesz, T. & Zetterberg, H. (2015). Brain amyloid-beta fragment signatures in pathological ageing and Alzheimer's disease by hybrid immunoprecipitation mass spectrometry. *Neurodegenerative Diseases, 15*(1), 50-57.

Poser, S., Mollenhauer, B., Krauβ, A., Zerr, I., Steinhoff, B. J., Schroeter, A., Finkenstaedt, M., Schulz-Schaeffer, W.J., Kretzschmar, H.A. & Felgenhauer, K. (1999). How to improve the clinical diagnosis of Creutzfeldt–Jakob disease. *Brain, 122*(12), 2345-2351.

Posey, A. E., Ruff, K. M., Harmon, T. S., Crick, S. L., Li, A., Diamond, M. I., & Pappu, R. V. (2018). Profilin reduces aggregation and phase separation of huntingtin N-terminal fragments by preferentially binding to soluble monomers and oligomers. *Journal of Biological Chemistry, 293*(10), 3734-3746.

Pujol-Pina, R., Vilaprinyó-Pascual, S., Mazzucato, R., Arcella, A., Vilaseca, M., Orozco, M. & Carulla, N. (2015). SDS-PAGE analysis of Aβ oligomers is disserving research into Alzheimer s disease: appealing for ESI-IM-MS. *Scientific Reports, 5*, p.14809.

Qiang, W., Yau, W. M., Lu, J. X., Collinge, J., Tycko, R. (2017). Structural variation in amyloid-β fibrils from Alzheimer's disease clinical subtypes. *Nature, 541*(7636), 217.

Rajmohan, R., & Reddy, P. H. (2017). Amyloid-beta and phosphorylated tau accumulations cause abnormalities at synapses of Alzheimer's disease neurons. *Journal of Alzheimer's Disease*, *57*(4), 975-999.

Raman, B., Ban, T., Sakai, M., Pasta, S. Y., Ramakrishna, T., Naiki, H., Goto, Y. & Rao, C. M. (2005). αB-Crystallin, a small heat-shock protein, prevents the amyloid fibril growth of an amyloid β-peptide and β2-microglobulin. *Biochemical Journal, 392*(3), 573-581.

Rana, A., Gupta, T. P., Bansal, S., & Kundu, B. (2008). Formation of amyloid fibrils by bovine carbonic anhydrase. *Biochimica et Biophysica Acta (BBA)-Proteins and Proteomics, 1784*(6), 930-935.

Rasmussen, J., Jucker, M., & Walker, L. C. (2017). Aβ seeds and prions: how close the fit? *Prion, 11*(4), 215-225.

Rasmussen, J., Mahler, J., Beschorner, N., Kaeser, S. A., Häsler, L. M., Baumann, F., Sofie, N., Portelius, E., Blennoe, K., Lashley, T., Fox, N. C., Falla, D.S., Glatzel, M., Oblak, A.L., Ghetti, B., Nilsson, P.R., Hammarstrom, P., Staufenbiel, M., Walker, L.C. & Jucker, M. (2017). Amyloid polymorphisms constitute distinct clouds of conformational variants in different etiological subtypes of Alzheimer's disease. *Proceedings of the National Academy of Sciences*, *114*(49), 13018-13023.

Reinwald, S., Westner, I. M., & Niedermaier, N. (2004). Rapidly progressive Alzheimer's disease mimicking Creutzfeldt–Jakob disease. *Journal of Neurology*, *251*(8), 1020-1022.

Reiss, A. B., Arain, H. A., Stecker, M. M., Siegart, N. M., & Kasselman, L. J. (2018). Amyloid toxicity in Alzheimer's disease. *Reviews in the Neurosciences*, *29*(6), 613-627.

Ries, M., Loiola, R., Shah, U. N., Gentleman, S. M., Solito, E., & Sastre, M. (2016). The anti-inflammatory annexin A1 induces the clearance and degradation of the amyloid-β peptide. *Journal of Neuroinflammation*, *13*(1), 234.

Rival, T., Page, R. M., Chandraratna, D. S., Sendall, T. J., Ryder, E., Liu, B., Lewis, H., Rosahl, T., Hider, R., Camargo, L.M. & Shearman, M. S. (2009). Fenton chemistry and oxidative stress mediate the toxicity of the β-amyloid peptide in a Drosophila model of Alzheimer's disease. *European Journal of Neuroscience*, *29*(7), 1335-1347.

Rodrigue, K. M., Kennedy, K. M., & Park, D. C. (2009). Beta-amyloid deposition and the aging brain. *Neuropsychology Review*, *19*(4), 436.

Rossi, M., Kai, H., Baiardi, S., Bartoletti-Stella, A., Carlà, B., Zenesini, C., Capellari, S., Kitamoto, T. & Parchi, P. (2019). The characterization of AD/PART co-pathology in CJD suggests independent pathogenic mechanisms and no cross-seeding between misfolded Aβ and prion proteins. *Acta Neuropathologica Communications, 7*(1), 53.

Rubinsztein, D. C. (2006). The roles of intracellular protein-degradation pathways in neurodegeneration. *Nature, 443*(7113), 780-786.

Ruiz-Riquelme, A., Lau, H. H., Stuart, E., Goczi, A. N., Wang, Z., Schmitt-Ulms, G., & Watts, J. C. (2018). Prion-like propagation of β-amyloid aggregates in the absence of APP overexpression. *Acta Neuropathologica Communications*, *6*(1), 26.

Rush, D. K., Aschmies, S., & Merriman, M. C. (1992). Intracerebral/β-amyloid (25–35) produces tissue damage: is it neurotoxic? *Neurobiology of Aging, 13*(5), 591-594.

Russell, C. L., Semerdjieva, S., Empson, R. M., Austen, B. M., Beesley, P. W., & Alifragis, P. (2012). Amyloid-β acts as a regulator of neurotransmitter release disrupting the interaction between synaptophysin and VAMP2. *PloS One*, *7*(8), e43201.

Rusten, T. E., Filimonenko, M., Rodahl, L. M., Stenmark, H., & Simonsen, A. (2008). ESCRTing autophagic clearance of aggregating proteins. *Autophagy*, *4*(2), 233-236.

Ryan, N. S., Nicholas, J. M., Weston, P. S., Liang, Y., Lashley, T., Guerreiro, R., Adamson, G., Kenny, J., Beck, J., Chavez-Gutierrez, L., de Strooper, B., Revesz, T., Holton, J., Mead, S., Rossor, M. N., & Fox, N. C. (2016). Clinical phenotype and genetic associations in autosomal dominant familial Alzheimer's disease: a case series. *The Lancet Neurology*, *15*(13), 1326-1335.

Saijo, E., Metrick, M. A., Koga, S., Parchi, P., Litvan, I., Spina, S., Boxer, A., Rojas, J.C., Galasko, D., Kraus, A., Rossi, M. & Caughey B (2019). 4-Repeat tau seeds and templating subtypes as brain and CSF biomarkers of frontotemporal lobar degeneration. *Acta Neuropathologica*, *139*(1):63-77.

Sakamoto, T., Saito, H., Ishii, K., Takahashi, H., Tanabe, S., & Ogasawara, Y. (2006). Aluminum inhibits proteolytic degradation of amyloid β peptide by cathepsin D: a potential link between aluminum accumulation and neuritic plaque deposition. *FEBS letters*, *580*(28-29), 6543-6549.

Scheidt, T., Łapińska, U., Kumita, J. R., Whiten, D. R., Klenerman, D., Wilson, M. R., Cohen, S.I., Linse, S., Vendruscolo, M., Dobson, C.M. & Knowles, T. P. (2019). Secondary nucleation and elongation occur at different sites on Alzheimer's amyloid-β aggregates. *Science Advances*, *5*(4), eaau3112.

Schieb, H., Kratzin, H., Jahn, O., Möbius, W., Rabe, S., Staufenbiel, M., Wiltfang, J. & Klafki, H. W. (2011). β-Amyloid peptide variants in brains and cerebrospinal fluid from amyloid precursor protein (APP) transgenic mice comparison with human Alzheimer amyloid. *Journal of Biological Chemistry*, *286*(39), 33747-33758.

Schilling, S., Lauber, T., Schaupp, M., Manhart, S., Scheel, E., Böhm, G., & Demuth, H. U. (2006). On the seeding and oligomerization of pGlu-amyloid peptides (*in vitro*). *Biochemistry*, *45*(41), 12393-12399.

Schmidt, C., Haïk, S., Satoh, K., Rábano, A., Martinez-Martin, P., Roeber, S., Brandel, J.P., Calero-Lara, M., de Pedro-Cuesta, J., Laplanche, J.L. & Hauw, J. J. (2012). Rapidly progressive Alzheimer's disease: a multicenter update. *Journal of Alzheimer's Disease*, *30*(4), 751-756.

Schmidt, C., Redyk, K., Meissner, B., Krack, L., Von Ahsen, N., Roeber, S., Kretzschmar, H. & Zerr, I. (2010). Clinical features of rapidly progressive Alzheimer's disease. *Dementia and Geriatric Cognitive Disorders*, *29*(4), 371-378.

Scopa, C., Marrocco, F., Latina, V., Ruggeri, F., Corvaglia, V., La Regina, F., Ammassari-Teule, M., Middei, S., Amadoro, G., Meli, G. & Scardigli, R. (2019). Impaired adult neurogenesis is an early event in Alzheimer's disease neurodegeneration, mediated by intracellular Aβ oligomers. *Cell Death & Differentiation*, 1-15.

Sergeant, N., Bombois, S., Ghestem, A., Drobecq, H., Kostanjevecki, V., Missiaen, C., Wattez, A., David, J.P., Vanmechelen, E., Sergheraert, C. & Delacourte, A. (2003). Truncated beta-amyloid peptide species in pre-clinical Alzheimer's disease as new targets for the vaccination approach. *Journal of Neurochemistry*, *85*(6), 1581-1591.

Serpell, L. C. (2000). Alzheimer's amyloid fibrils: structure and assembly. *Biochimica et Biophysica Acta (BBA)-Molecular Basis of Disease*, *1502*(1), 16-30.

Sgourakis, N. G., Yan, Y., McCallum, S. A., Wang, C., & Garcia, A. E. (2007). The Alzheimer's peptides Aβ40 and 42 adopt distinct conformations in water: a combined MD/NMR study. *Journal of Molecular Biology*, *368*(5), 1448-1457.

Shao, Z. Q. (2015). Comparison of the efficacy of four cholinesterase inhibitors in combination with memantine for the treatment of Alzheimer's disease. *International Journal of Clinical and Experimental Medicine*, *8*(2), 2944-2948.

Shea, D., Hsu, C. C., Bi, T. M., Paranjapye, N., Childers, M. C., Cochran, J., Tomberlin, C.P., Wang, L., Paris, D., Zonderman, J. & Varani, G. (2019). α-Sheet secondary structure in amyloid β-peptide drives aggregation and toxicity in Alzheimer's disease. *Proceedings of the National Academy of Sciences*, *116*(18), 8895-8900.

Shimada, T., Fournier, A. E., & Yamagata, K. (2013). Neuroprotective function of 14-3-3 proteins in neurodegeneration. *BioMed Research International*, *2013*: 564534.

Shirwany, N. A., Payette, D., Xie, J., & Guo, Q. (2007). The amyloid beta ion channel hypothesis of Alzheimer's disease. *Neuropsychiatric Disease and Treatment*, *3*(5), 597.

Sikkink, L. A., & Ramirez-Alvarado, M. (2008). Salts enhance both protein stability and amyloid formation of an immunoglobulin light chain. *Biophysical Chemistry*, *135*(1-3), 25-31.

Singh, S. M., Molas, J. F., Kongari, N., Bandi, S., Armstrong, G. S., Winder, S. J., & Mallela, K. M. (2012). Thermodynamic stability, unfolding kinetics, and aggregation of the N-terminal actin-binding domains of utrophin and dystrophin. *Proteins: Structure, Function, and Bioinformatics*, *80*(5), 1377-1392.

Sinha, M. S., Ansell-Schultz, A., Civitelli, L., Hildesjö, C., Larsson, M., Lannfelt, L., Ingelsson, M. & Hallbeck, M. (2018). Alzheimer's disease pathology propagation by exosomes containing toxic amyloid-beta oligomers. *Acta Neuropathologica*, *136*(1), 41-56.

Smith, L. M., & Strittmatter, S. M. (2017). Binding sites for amyloid-β oligomers and synaptic toxicity. *Cold Spring Harbor Perspectives in Medicine*, 7(5), 024075.

Sofola-Adesakin, O., Khericha, M., Snoeren, I., Tsuda, L., & Partridge, L. (2016). pGluAβ increases accumulation of Aβ *in vivo* and exacerbates its toxicity. *Acta Neuropathologica Communications*, *4*(1), 109.

Sogorb-Esteve, A., García-Ayllón, M. S., Gobom, J., Alom, J., Zetterberg, H., Blennow, K., & Sáez-Valero, J. (2018). Levels of ADAM10 are reduced in Alzheimer's disease CSF. *Journal of Neuroinflammation, 15*(1), 213.

Sohma, Y., Yamasaki, M., Kawashima, H., Taniguchi, A., Yamashita, M., Akaji, K., Mukai, H. & Kiso, Y. (2013). Comparative properties of Aβ1–42, Aβ11–42, and [Pyr11] Aβ11–42 generated from O-acyl isopeptides. *Bioorganic & Medicinal Chemistry Letters, 23*(5), 1326-1329.

Solé-Domènech, S., Rojas, A. V., Maisuradze, G. G., Scheraga, H. A., Lobel, P., & Maxfield, F. R. (2018). Lysosomal enzyme tripeptidyl peptidase 1 destabilizes fibrillar Aβ by multiple endo-proteolytic cleavages within the β-sheet domain. *Proceedings of the National Academy of Sciences, 115*(7), 1493-1498.

Stanley, M., Macauley, S. L., & Holtzman, D. M. (2016). Changes in insulin and insulin signaling in Alzheimer's disease: cause or consequence? *Journal of Experimental Medicine*, *213*(8), 1375-1385.

Stockley, J. H., & O'Neill, C. (2007). The proteins BACE1 and BACE2 and β-secretase activity in normal and Alzheimer's disease brain. *Biochemical Society Transactions, 35*(3), 574 – 576.

Südhof, T. C. (2012). Calcium control of neurotransmitter release. *Cold Spring Harbor Perspectives in Biology*, *4*(1), a011353.

Tang-Wei, D.F., Josephs, K.A. and Peterson R.C. (2005). Alzheimer's disease – Overview. In Beal, M.F., Lang, A.E. and Ludolph, A.C. (Eds.), In: *Neurodegenerative diseases: Neurobiology, Pathogenesis and Therapeutics* (pp. 416-432). Thailand: Cambridge University Press.

Tanneberger, K., Pfister, A. S., Kriz, V., Bryja, V., Schambony, A., & Behrens, J. (2011). Structural and functional characterization of the Wnt inhibitor APC membrane recruitment 1 (Amer1). *Journal of Biological Chemistry*, *286*(22), 19204-19214.

Tao, C. C., Cheng, K. M., Ma, Y. L., Hsu, W. L., Chen, Y. C., Fuh, J. L., W.J., Chao, C.C. & Lee, E. H. (2020). Galectin-3 promotes Aβ oligomerization and Aβ toxicity in a mouse model of Alzheimer's disease. *Cell Death & Differentiation, 27*(1), 192-209.

Toyota, Y., Ikeda, M., Shinagawa, S., Matsumoto, T., Matsumoto, N., Hokoishi, K., Fukuhara, R., Ishikawa, T., Mori, T., Adachi, H. & Komori, K. (2007). Comparison of behavioral and psychological symptoms in early-onset and late-onset Alzheimer's disease. *International Journal of Geriatric Psychiatry, 22*(9), 896-901.

Tracy, T. E., & Gan, L. (2018). Tau-mediated synaptic and neuronal dysfunction in neurodegenerative disease. *Current Opinion in Neurobiology, 51*, 134-138.

Valls-Comamala, V., Guivernau, B., Bonet, J., Puig, M., Perálvarez-Marín, A., Palomer, E., Fernàndez-Busquets, X., Altafaj, X., Tajes, M., Puig-Pijoan, A. & Vicente, R. (2017). The antigen-binding fragment of human gamma immunoglobulin prevents amyloid β-peptide folding into β-sheet to form oligomers. *Oncotarget, 8*(25), 41154.

Vandersteen, A., Hubin, E., Sarroukh, R., De Baets, G., Schymkowitz, J., Rousseau, F., Subramaniam, V., Raussens, V., Wenschuh, H., Wildemann, D. & Broersen, K. (2012). A comparative analysis of the aggregation behavior of amyloid-β peptide variants. *FEBS Letters, 586*(23), 4088-4093.

Virok, D. P., Simon, D., Bozsó, Z., Rajkó, R., Datki, Z., Bálint, É., Szegedi, V., Janáky, T., Penke, B. & Fülöp, L. (2011). Protein array based interactome analysis of amyloid-β indicates an inhibition of protein translation. *Journal of Proteome Research, 10*(4), 1538-1547.

Wang, J. S. H., Whitehead, S. N., & Yeung, K. K. C. (2018). Detection of Amyloid Beta (Aβ) Oligomeric Composition Using Matrix-Assisted Laser Desorption Ionization Mass Spectrometry (MALDI MS). *Journal of the American Society for Mass Spectrometry, 29*(4), 786-795.

Wang, Q., Wang, C., Ji, B., Zhou, J., Yang, C., & Chen, J. (2019). Hapln2 in Neurological Diseases and Its Potential as Therapeutic Target. *Frontiers in Aging Neuroscience, 11*.

Wang, S., Wang, R., Chen, L., Bennett, D. A., Dickson, D. W., & Wang, D. S. (2010). Expression and functional profiling of neprilysin, insulin-degrading enzyme, and endothelin-converting enzyme in prospectively studied elderly and Alzheimer's brain. *Journal of Neurochemistry, 115*(1), 47-57.

Wang, Z., Jiang, H., Chen, S., Du, F., & Wang, X. (2012). The mitochondrial phosphatase PGAM5 functions at the convergence point of multiple necrotic death pathways. *Cell, 148*(1-2), 228-243.

Watt, A. D., Perez, K. A., Rembach, A., Sherrat, N. A., Hung, L. W., Johanssen, T., McLean, C.A., Kok, W.M., Hutton, C.A., Fodero-Tavoletti, M. & Masters, C. L. (2013). Oligomers, fact or artefact? SDS-PAGE induces dimerization of β-amyloid in human brain samples. *Acta Neuropathologica, 125*(4), 549-564.

Webster, J. M., Darling, A. L., Uversky, V. N., & Blair, L. J. (2019). Small heat Shock proteins, big impact on protein aggregation in neurodegenerative disease. *Frontiers in Pharmacology, 10*.

Weiffert, T., Meisl, G., Flagmeier, P., De, S., Dunning, C. J., Frohm, B., Zetterberg, H., Blennow, K., Portelius, E., Klenerman, D. & Dobson, C. M. (2019). Increased Secondary Nucleation Underlies Accelerated Aggregation of the Four-Residue N-Terminally Truncated Aβ42 Species Aβ5–42. *ACS Chemical Neuroscience, 10*(5), 2374-2384.

Weihl, C., & Bieschke, J. (2017). Prion-like protein aggregation of desmin myofibrillar myopathies. *Neuromuscular Disorders, 27,* S247-S248.

Wildburger, N. C., Esparza, T. J., LeDuc, R. D., Fellers, R. T., Thomas, P. M., Cairns, N. J., Kelleher, N. L., Bateman, R. J. & Brody, D. L. (2017). Diversity of amyloid-beta proteoforms in the Alzheimer's disease brain. *Scientific Reports, 7*(1), 9520.

Wilham, J. M., Orrú, C. D., Bessen, R. A., Atarashi, R., Sano, K., Race, B., Meade-White, K.D., Taubner, L.M., Timmes, A. & Caughey, B. (2010). Rapid end-point quantitation of prion seeding activity with sensitivity comparable to bioassays. *PLoS Pathogens, 6*(12), e1001217.

Wilhelmus, M. M., de Waal, R. M., & Verbeek, M. M. (2007). Heat shock proteins and amateur chaperones in amyloid-Beta accumulation and clearance in Alzheimer's disease. *Molecular Neurobiology*, 35(3), 203-216.

Wittnam, J. L., Portelius, E., Zetterberg, H., Gustavsson, M. K., Schilling, S., Koch, B., Demuth, H.U., Blennow, K., Wirths, O. & Bayer, T. A. (2012). Pyroglutamate amyloid β (Aβ) aggravates behavioral deficits in transgenic amyloid mouse model for Alzheimer disease. *Journal of Biological Chemistry, 287*(11), 8154-8162.

Woo, H. N., Park, J. S., Gwon, A. R., Arumugam, T. V., & Jo, D. G. (2009). Alzheimer's disease and Notch signaling. *Biochemical and Biophysical Research Communications, 390*(4), 1093-1097.

Wujek, J. R., Dority, M. D., Frederickson, R. C., & Brunden, K. R. (1996). Deposits of Aβ fibrils are not toxic to cortical and hippocampal neurons *in vitro*. *Neurobiology of Aging, 17*(1), 107-113.

Xiao, Y., Ma, B., McElheny, D., Parthasarathy, S., Long, F., Hoshi, M., Nussinov, R. & Ishii, Y. (2015). Aβ (1–42) fibril structure illuminates self-recognition and replication of amyloid in Alzheimer's disease. *Nature Structural & Molecular Biology, 22*(6), 499.

Xu, G., Stevens Jr, S. M., Moore, B. D., McClung, S., & Borchelt, D. R. (2013). Cytosolic proteins lose solubility as amyloid deposits in a transgenic mouse model of Alzheimer-type amyloidosis. *Human Molecular Genetics, 22*(14), 2765-2774.

Yatin, S. M., Varadarajan, S., Link, C. D., & Butterfield, D. A. (1999). *In vitro* and *in vivo* oxidative stress associated with Alzheimer's amyloid ß-peptide (1–42). *Neurobiology of Aging, 20*(3), 325-330.

Ye, J., Xu, J., Li, Y., Huang, Q., Huang, J., Wang, J., Zhong, W., Lin, X., Chen, W. & Lin, X. (2017). DDAH1 mediates gastric cancer cell invasion and metastasis via Wnt/β-catenin signaling pathway. *Molecular Oncology, 11*(9), 1208-1224.

Yoo, B. C., Kim, S. H., Cairns, N., Fountoulakis, M., & Lubec, G. (2001). Deranged expression of molecular chaperones in brains of patients with Alzheimer's disease. *Biochemical and Biophysical Research Communications*, *280*(1), 249-258.

Younan, N. D., Chen, K. F., Rose, R. S., Crowther, D. C., & Viles, J. H. (2018). Prion protein stabilizes amyloid-β (Aβ) oligomers and enhances Aβ neurotoxicity in a Drosophila model of Alzheimer's disease. *Journal of Biological Chemistry, 293*(34), 13090-13099.

Young, K. F., Pasternak, S. H., & Rylett, R. J. (2009). Oligomeric aggregates of amyloid β peptide 1–42 activate ERK/MAPK in SH-SY5Y cells via the α7 nicotinic receptor. *Neurochemistry International*, *55*(8), 796-801.

Zaarur, N., Xu, X., Lestienne, P., Meriin, A. B., McComb, M., Costello, C. E., Newnam, G.P., Ganti, R., Romanova, N.V., Shanmugasundaram, M. & Silva, S. T. (2015). RuvbL1 and RuvbL2 enhance aggresome formation and disaggregate amyloid fibrils. *The EMBO journal, 34*(18), 2363-2382.

Zafar, S., Shafiq, M., Younas, N., Schmitz, M., Ferrer, I., & Zerr, I. (2017). Prion protein interactome: Identifying novel targets in slowly and rapidly progressive forms of Alzheimer's disease. *Journal of Alzheimer's Disease*, *59*(1), 265-275.

Zapadka, K. L., Becher, F. J., Gomes dos Santos, A. L., & Jackson, S. E. (2017). Factors affecting the physical stability (aggregation) of peptide therapeutics. *Interface Focus*, *7*(6), 20170030.

Zempel, H., Thies, E., Mandelkow, E., & Mandelkow, E. M. (2010). Aβ oligomers cause localized Ca^{2+} elevation, missorting of endogenous Tau into dendrites, Tau phosphorylation, and destruction of microtubules and spines. *Journal of Neuroscience*, *30*(36), 11938-11950.

Zerr, I., Kallenberg, K., Summers, D. M., Romero, C., Taratuto, A., Heinemann, U., Breithaupt, M., Varges, D., Meissner, B., Ladogana, A. & Schuur, M. (2009). Updated clinical diagnostic criteria for sporadic Creutzfeldt-Jakob disease. *Brain*, *132*(10), 2659-2668.

Zhang, X., & Song, W. (2013). The role of APP and BACE1 trafficking in APP processing and amyloid-β generation. *Alzheimer's Research & Therapy*, *5*(5), 46.

Zhao, W. Q., De Felice, F. G., Fernandez, S., Chen, H., Lambert, M. P., Quon, M. J., Krafft, G.A. & Klein, W. L. (2008). Amyloid beta oligomers induce impairment of neuronal insulin receptors. *The FASEB Journal*, *22*(1), 246-260.

Zheng, Y., Tian, S., Peng, X., Yang, J., Fu, Y., Jiao, Y., Zhao, J., He, J. & Hong, T. (2016). Kinesin-1 inhibits the aggregation of amyloid-β peptide as detected by fluorescence cross-correlation spectroscopy. *FEBS Letters*, 590(7), 1028-1037.

Zhu, L., Zhong, M., Zhao, J., Rhee, H., Caesar, I., Knight, E. M., Volpicelli-Daley, L., Bustos, V., Netzer, W., Liu, L. & Lucast, L. (2013). Reduction of synaptojanin 1 accelerates Aβ clearance and attenuates cognitive deterioration in an Alzheimer mouse model. *Journal of Biological Chemistry*, *288*(44), 32050-32063.

Zoltowska, K. M., Maesako, M., Lushnikova, I., Takeda, S., Keller, L. J., Skibo, G., Hyman, B.T. & Berezovska, O. (2017). Dynamic presenilin 1 and synaptotagmin 1 interaction modulates exocytosis and amyloid β production. *Molecular Neurodegeneration*, *12*(1), 15.

Publications:

1. Zafar, S, **Noor, A.** and Zerr, I., 2019. Therapies for prion diseases. In: *Handbook of Clinical Neurology* (pp. 47-58) Elsevier B.V.
2. **Noor, A.***, Laaldin, N*., Baloch, S.R*., Aziz, A., Gul, A., Rajput, T.A. and Babar, M.M., 2019. Animal Models: bridging cross-species variation through animal biotechnology In: *Genomics and Biotechnological Advances in Veterinary, Poultry and Fisheries* (pp. 183-207) Academic Press, Elsevier Inc. **equal contribution.*
3. Nizami, S.B., Kazmi, S.H., Abid, F., Babar, M.M., **Noor, A**., Najam-us-Sahar, S.Z, Khan, S.U., Hasan, H., Ali, M. and Gul, A., 2017. Omics Approaches in Forensic Biotechnology: Looking for Ancestry to Offence. In: *Omics Technologies and Bio-engineering: Volume 1: Towards Improving Quality of Life* (pp. 111-129) Academic Press, Elsevier Inc.
4. Babar, M.M., Ali, Z., Siddiqui, H., Fatima, M., Abid, F., Nizami, S.B., **Noor, A.**, Khan, A.N., Faisal, S. and Gul, A., 2017. Transport and Metabolism of Nitrogen in Legume Nodules Under Phosphorus Deficiency. In: *Legume Nitrogen Fixation in Soils with Low Phosphorus Availability* (pp. 111-134). Springer, Cham.
5. **Noor, A.** and Zahid, S., 2017. Alterations in adult hippocampal neurogenesis, aberrant protein S-nitrosylation, and associated spatial memory loss in streptozotocin-induced diabetes mellitus type 2 mice. *Iranian journal of basic medical sciences*, 20(10), pp.1159.
6. **Noor, A.** and Zahid, S., 2017. A review of the role of synaptosomal-associated protein 25 (SNAP-25) in neurological disorders. *International Journal of Neuroscience*, 127(9), pp.805-811.

Oral Talks:

1. **Amyloid-β strain specific profiling in Alzheimer's disease.**
   Physics to Medicine Mini-Symposium, Göttingen, Germany.
2. **Aberrations of Amyloid-β in clinical subtypes of Alzheimer's Disease.**
   Annual Research Conference, Department of Neurology, Göttingen, Germany.
3. **Amyloid-ß strain specific profiling in Alzheimer´s disease: functional and clinical signature.**
   Annual Research Conference, Department of Neurology, Göttingen, Germany.

Poster Presentations:

1. **Amyloid-β strain specific profiling in Alzheimer's disease.**
   Molecular Medicine retreat, Wernigerode, Germany.
2. **Distinct interactions of Amyloid-β in clinical subtypes of Alzheimer's disease.**
   Biomedical Student Symposium, Göttingen, Germany.
3. **Distinct interactions of Amyloid-β in clinical subtypes of Alzheimer's disease.**
   DZNE PhD retreat, Essen, Germany.
4. **Amyloid-ß strain specific profiling in Alzheimer´s disease: functional and clinical signature.**
   PRION 2018, Santiago, Spain.
5. **Aberrations of Amyloid-beta in slow and rapidly progressive dementias.**
   PRION 2019, Edmonton, Canada.

Acknowledgements:

I am grateful to Allah for presenting me with an opportunity to further my knowledge in a field that I have always been passionate about and bringing in so many people to help me make the most it. First of all, I would like to thank **Prof. Dr. Inga Zerr** for hosting me in her group for almost four years and giving me an opportunity to learn and grow as a scientist. Her positive comments were always a source of great encouragement and pushed me to do better every day. I am also grateful to **Dr. Saima Zafar** for her enlightening ideas, helpful feedback and continuous support that have played an immense role in polishing my professional and personal capabilities. I would like to acknowledge the organizers of **Physics-to-Medicine Initiative Göttingen** (LM der Niedersächsischen Vorab) for partly funding my PhD studies.

There are so many people who have helped me with my project over the last few semesters. I would like to acknowledge my thesis committee members, **Prof. Dr. mult. Thomas Meyer** and **Prof. Dr. Tiago Fleming Outeiro** for always making time to hear me out and providing valuable advice for improving my project and skills. I am also thankful to **Prof. Dr. Hassan Dihazi** and **Sandra Hoffmeister** for teaching me MALDI-MS and allowing me to work in their lab. I am especially thankful to **Florian Alexander Mann** for sparing time out of his otherwise hectic days to help me with atomic force microscopy and **Dr. Tayyaba Noor** for providing me with the opportunity to perform FTIR spectroscopy. I am grateful to **Prof. Dr. Michael Hoppert** for letting me use his facilities for electron microscopy. I would like to acknowledge **Dr. Christof Lenz** for making time to have helpful discussions with me about various proteomic techniques. I would also like to thanks **Prof. Dr. Abdul Rehman Asif** and **Dr. Sidra Shahid** for always having the doors of their lab open for me and providing me with whatever that I needed on short notice. I would not have finished my project without all these people.

All my labmates have been an immense source of knowledge, positivity and encouragement throughout my PhD. I would express my gratitude to **Dr. Neelam, Dr. Mohsin, Dr. Matthias, Tobias, Nicco, Katrin, Angela, Susana, Vivi, Sebastian, Uzma, Anna-Lisa** and **Anna Siegart** for helping me with everything from settling in a new culture to handling data and surviving bad lab days. I would also like to thank **Jolanata** and **Maya** for always being there to help me with smiles on their faces.

I would like to express my heartfelt gratitude to my family and friends that have always been there for me. I would like to thank my parents, who gave me all the confidence I needed to chase my dreams and continue to be the light in the darkest of my days. I am grateful to my husband, who has been more patient with me than I could have ever imagined and supported me through all the tantrums. I would like to thank my siblings, Hammad and Fareya, for always being there to hear me complain in the event of slightest inconveniences. I would also like to acknowledge my friends Hira and Ayesha for keeping me sane through this journey and making me feel at home away from home.

Aneeqa